Mathematical Biosciences 375 (2024) 109243

Contents lists available at ScienceDirect

Mathematical Biosciences

journal homepage: www.elsevier.com/locate/mbs

Original Research Article

Spatial heterogeneity analysis for the transmission of syphilis disease in China via a data-validated reaction–diffusion model

Peng Wu [a], Xiunan Wang [b], Hao Wang [c,*]

[a] School of Sciences, Hangzhou Dianzi University, Hangzhou 310018, China
[b] Department of Mathematics, University of Tennessee at Chattanooga, Chattanooga, TN 37403, USA
[c] Department of Mathematical and Statistical Sciences, University of Alberta, Edmonton, AB T6G 2G1, Canada

ARTICLE INFO

MSC:
92D30
35B40
58Z05

Keywords:
Syphilis
Spatial heterogeneity
Diffusion
Patch model
Global dynamics
Markov Chain Monte Carlo (MCMC)

ABSTRACT

Based on the distinctive spatial diffusion characteristics observed in syphilis transmission patterns, this paper introduces a novel reaction–diffusion model for syphilis disease dynamics, incorporating general incidence functions within a heterogeneous environment. We derive the basic reproduction number essential for threshold dynamics and investigate the uniform persistence of the model. We validate the model and estimate its parameters by employing the multi-objective Markov Chain Monte Carlo (MCMC) method, using real syphilis data from the years 2004 to 2018 in China. Furthermore, we explore the impact of spatial heterogeneity and intervention measures on syphilis transmission. Our findings reveal several key insights: (1) In addition to the original high-incidence areas of syphilis, Xinjiang, Guizhou, Hunan and Northeast China have also emerged as high-incidence regions for syphilis in China. (2) The latent syphilis cases represent the highest proportion of newly reported cases, highlighting the critical importance of considering their role in transmission dynamics to avoid underestimation of syphilis outbreaks. (3) Neglecting spatial heterogeneity results in an underestimation of disease prevalence and the number of syphilis-infected individuals, undermining effective disease prevention and control strategies. (4) The initial conditions have minimal impact on the long-term spatial distribution of syphilis-infected individuals in scenarios of varying diffusion rates. This study underscores the significance of spatial dynamics and intervention measures in assessing and managing syphilis transmission, which offers insights for public health policymakers.

1. Introduction

Among the myriad sexually transmitted diseases, syphilis stands out due to its extensive reach and the significant threat it poses to both the physical and mental well-being of those affected. Before the discovery of penicillin, syphilis was a formidable and often fatal affliction, listed alongside tuberculosis and leprosy as one of the world's three major chronic diseases in the history of medicine [1]. During the 1980s and 1990s, the incidence of syphilis saw a decline, attributed in part to increased awareness campaigns promoting safe sex and the emergence of the HIV epidemic. However, since the turn of the 21st century, the prevalence of syphilis has experienced a dramatic resurgence, with some countries witnessing a surge of more than 300% in reported cases [2]. For instance, data from the China Center for Disease Control and Prevention reveals a staggering 464,435 newly reported cases of syphilis in China in 2020, while Fig. 1.1 illustrates the trend in newly reported cases from 2004 to 2018. Similarly, statistics from the Tokyo Infectious Disease Information Center indicate that Japan reported over 10,000 confirmed cases of syphilis in 2020, totaling 10,141 cases [3].

Syphilis infection in the human body is caused by Treponema pallidum, also known as Spirochaeta pallidum. This bacterium adheres to cell surface receptors using its own surface mucopolysaccharide enzyme and then spreads within the body with the assistance of hyaluronidase. This process leads to tissue necrosis and the formation of ulcers [5]. Syphilis can be transmitted through various routes, primarily including direct contact transmission, transplacental infection, birth canal infection, blood transfusion, or medical device-related infections [6]. The course of syphilis is typically divided into several stages: (1) Incubation Period: Treponema pallidum enters the lymph nodes, and within 2–3 days, it invades the bloodstream, spreading throughout the body. During this stage, there are no noticeable symptoms. (2) Primary Stage: After an incubation period of 2–4 weeks (averaging around 3 weeks), the body initiates an inflammatory response to the initial Treponema pallidum invasion, resulting in the development of characteristic primary syphilis symptoms, including infiltration nodules and ulcers. (3) Secondary Stage: Approximately three weeks after the appearance of

* Corresponding author.
E-mail addresses: hzpengwu89@hdu.edu.cn (P. Wu), xiunan-wang@utc.edu (X. Wang), hao8@ualberta.ca (H. Wang).

https://doi.org/10.1016/j.mbs.2024.109243
Received 2 February 2024; Received in revised form 5 May 2024; Accepted 22 June 2024
Available online 2 July 2024

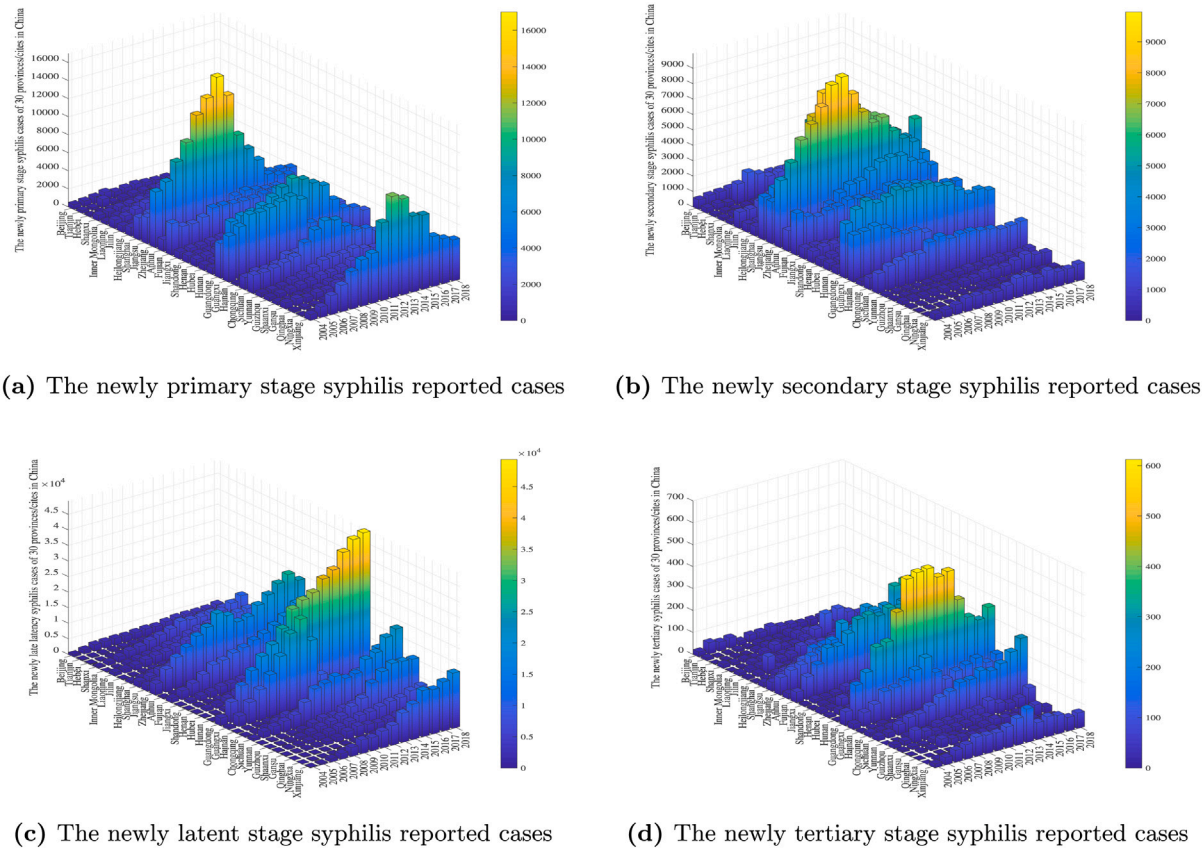

(a) The newly primary stage syphilis reported cases

(b) The newly secondary stage syphilis reported cases

(c) The newly latent stage syphilis reported cases

(d) The newly tertiary stage syphilis reported cases

Fig. 1.1. The newly primary, secondary, latent and tertiary stage syphilis reported cases of 30 provinces/cities in China from 2004 to 2018. *Source:* Data from [4].

the chancre, the systemic lymph nodes begin to swell. Within 4–12 weeks after that, individuals experience systemic symptoms, skin damage, as well as symptoms affecting the bones, eyes, and nervous system. This marks the progression to secondary syphilis. (4) Latent Stage: Following Treponema pallidum infection, approximately 30% of infected individuals do not experience initial or secondary symptoms, referred to as early latent syphilis. After 2 to 15 years or more, the infection progresses to the late latent stage. (5) Tertiary Stage: During this late stage, the disease can result in irreversible damage, such as tissue ulceration and neurosyphilis [7]. Additional classifications of syphilis, such as King and Nocil's (1975), WHO's (1981), Petting's (1986), and CDC's (1997) classifications, can be explored in more detail in reference materials [8].

Syphilis prevention and control strategies have been implemented globally to curb the spread of the disease and mitigate its impact on public health. These efforts encompass a multifaceted approach, including education and awareness campaigns [9], routine screening [10], and comprehensive healthcare services [11]. Condom promotion and distribution programs play a crucial role in preventing sexual transmission, particularly in high-risk populations [12]. Partner notification and treatment initiatives aim to identify and treat individuals who may have been exposed to syphilis, reducing the likelihood of further transmission [13]. Antenatal screening programs are pivotal in preventing mother-to-child transmission [14]. Additionally, targeted interventions focus on key populations, such as men who have sex with men and sex workers, acknowledging the heightened vulnerability within these groups. Beyond traditional approaches, some regions have explored innovative strategies, including the use of technology for outreach and testing services [15]. The success of these interventions often relies on collaboration between healthcare providers, public health agencies, and community organizations, emphasizing the importance of a comprehensive and adaptable approach to syphilis prevention and control on a global scale.

Advancements in our understanding of syphilis transmission dynamics have been propelled by the essential role played by mathematical modeling and analysis. The intricate nature of syphilis spread, marked by distinct spatial diffusion patterns and varying incidence rates, necessitates a rigorous quantitative approach to unravel its complexities. Mathematical frameworks have proven instrumental in unveiling the interplay of factors governing syphilis transmission. These models not only elucidate the dynamics of the disease but also offer invaluable insights crucial for formulating targeted intervention strategies. By quantifying the impact of spatial heterogeneity, population mobility, and intervention measures, mathematical modeling becomes an indispensable tool in the ongoing efforts to combat and mitigate the consequences of syphilis outbreaks. Since the seminal works on syphilis modeling by [16,17], numerous mathematical frameworks have emerged to delve into the intricate transmission dynamics of this disease. Grassly et al. [18] conducted a comprehensive study, fitting real-life data to an SIRS syphilis model using information collected by the US CDC from 1941 to 2002 across 68 cities in the United States. Their work stands as a crucial reference point. Iboi and Okuonghae [19] delved into the population dynamics of a mathematical model for syphilis. Their findings suggest that high treatment rates for individuals in the

primary and secondary stages of syphilis have a positive impact on the overall population of syphilis-infected individuals in the later stages of infection. Saad-Roy et al. [20] formulated a mathematical model to investigate the transmission dynamics of syphilis within the MSM (Men Who Have Sex with Men) population. Their research underscores the importance of early treatment in the control of syphilis. Gumel et al. [21] presented a novel 2-group sex-structured model for assessing the community-level impact of treatment and condom use on the transmission dynamics and control of syphilis. Nwankwo and Okuonghae [22] established a mathematical model to examine the dynamic behavior of HIV and syphilis co-infection in the presence of syphilis therapy. Omame et al. [23] developed a co-infection model for HPV and syphilis, performing an in-depth analysis of optimal control strategies and cost-effectiveness.

While various mathematical models have been developed to explore syphilis transmission, encompassing factors such as treatment, condom use, severity heterogeneity, and regional lockdowns, many of these analyses have primarily relied on ordinary differential equations (ODEs) to explore the temporal dynamics of syphilis transmission within homogeneous populations. Biologically, spatial diffusion is a significant aspect often overlooked in disease spread [24,25]. In reality, syphilis exhibits distinctive spatial diffusion characteristics [26]. While some studies have highlighted the pronounced impact of spatial heterogeneity on syphilis transmission in China, little attention has been paid to the effects of spatial diffusion in a heterogeneous environment through mathematical modeling. This stems from the considerable challenge of incorporating real reported data into numerical simulations of reaction–diffusion models, particularly when dealing with data from diverse regions within a country. This paper addresses this challenge by proposing a novel approach that transforms the reaction–diffusion model into a patch model within a discrete space framework. We then employ a multi-objective MCMC (Markov Chain Monte Carlo) method to fit the model with actual case data. Subsequently, we use the parameter values obtained from the patch model to inform the space-dependent parameter values of the continuous-space reaction–diffusion model, ensuring the model's validity. Finally, we explore the impact of various spatial factors on syphilis transmission.

The structure of this paper is organized as follows: In Section 2, we present a reaction–diffusion syphilis compartment model with general incidence functions within a heterogeneous environment. In Section 3, we establish the well-posedness of the system and derive the functional expression for the basic reproduction number. Section 4 delves into the threshold dynamics of the system. In Section 5, we conduct numerical simulations using the data-validated reaction–diffusion model to investigate the influence of spatial heterogeneity on syphilis transmission. Finally, we conclude the paper with a discussion and summary in Section 6.

2. Model formulation

In this section, drawing upon prior research in mathematical modeling of syphilis transmission [19,20], we focus on the fundamental compartments representing different stages of individuals in the context of syphilis infection. These compartments include susceptible individuals (S), exposed individuals (E), primary stage infected individuals (I_1), secondary stage infected individuals (I_2), early latent stage infected individuals (L_1), late latent stage infected individuals (L_2), and tertiary stage infected individuals (I_3).

To investigate the spatial diffusion of syphilis within a heterogeneous environment, we introduce distribution functions denoted as $S(x,t)$, $E(x,t)$, $I_1(x,t)$, $I_2(x,t)$, $L_1(x,t)$, $L_2(x,t)$, and $I_3(x,t)$. These functions represent the spatial distribution of susceptible, exposed, primary, secondary, and latent (both early and late) infected individuals, as well as individuals in the tertiary stage, at location x and time t. Following the introduction of these concepts, we can proceed to discuss the proposed model as depicted in Fig. 2.2:

$$
\begin{cases}
\dfrac{\partial S(x,t)}{\partial t} = \nabla\cdot\big(d_1(x)\nabla S(x,t)\big) + \lambda(S(x,t)) \\
\qquad - \alpha(x) f_1(I_1(x,t),S(x,t)) - \beta(x) f_2(I_2(x,t),S(x,t)) \\
\qquad - \gamma(x) f_3(L_1(x,t),S(x,t)) - \mu(x) S(x,t), \\
\dfrac{\partial E(x,t)}{\partial t} = \nabla\cdot\big(d_2(x)\nabla E(x,t)\big) \\
\qquad + \alpha(x) f_1(I_1(x,t),S(x,t)) + \beta(x) f_2(I_2(x,t),S(x,t)) \\
\qquad + \gamma(x) f_3(L_1(x,t),S(x,t)) - (\mu(x)+\delta(x)) E(x,t), \\
\dfrac{\partial I_1(x,t)}{\partial t} = \nabla\cdot\big(d_3(x)\nabla I_1(x,t)\big) + \delta(x) E(x,t) \\
\qquad + (1-\epsilon(x))\omega(x) L_1(x,t) - (\mu(x)+\zeta_1(x)) I_1(x,t), \\
\dfrac{\partial I_2(x,t)}{\partial t} = \nabla\cdot\big(d_4(x)\nabla I_2(x,t)\big) + \zeta_1(x) I_1(x,t) \\
\qquad + \epsilon(x)\omega(x) L_1(x,t) - (\mu(x)+\zeta_2(x)+\sigma(x)) I_2(x,t), \\
\dfrac{\partial L_1(x,t)}{\partial t} = \nabla\cdot\big(d_5(x)\nabla L_1(x,t)\big) \\
\qquad + \zeta_2(x) I_2(x,t) - (\mu(x)+\omega(x)+\eta_1(x)) L_1(x,t), \\
\dfrac{\partial L_2(x,t)}{\partial t} = \nabla\cdot\big(d_6(x)\nabla L_2(x,t)\big) + \eta_1(x) L_1(x,t) - (\mu(x)+\eta_2(x)) L_2(x,t), \\
\dfrac{\partial I_3(x,t)}{\partial t} = \nabla\cdot\big(d_7(x)\nabla I_3(x,t)\big) \\
\qquad + \eta_2(x) L_2(x,t) + \sigma(x) I_2(x,t) - (\mu(x)+d(x)) I_3(x,t),
\end{cases}
\tag{2.1}
$$

with the following initial and boundary conditions:

$$
\begin{aligned}
&S(x,0)=\phi_1(x), \quad E(x,0)=\phi_2(x), \quad I_1(x,0)=\phi_3(x), \\
&I_2(x,0)=\phi_4(x), \quad L_1(x,0)=\phi_5(x), \\
&L_2(x,0)=\phi_6(x), \quad I_3(x,0)=\phi_7(x), \quad x\in\overline{\Omega}, \\
&\frac{\partial S(x,t)}{\partial \nu}=0, \quad \frac{\partial E(x,t)}{\partial \nu}=0, \quad \frac{\partial I_1(x,t)}{\partial \nu}=0, \quad \frac{\partial I_2(x,t)}{\partial \nu}=0, \\
&\frac{\partial L_1(x,t)}{\partial \nu}=0, \frac{\partial L_2(x,t)}{\partial \nu}=0, \quad \frac{\partial I_3(x,t)}{\partial \nu}=0, \quad x\in\partial\Omega.
\end{aligned}
$$

Here Ω is a spatial bounded domain with the smooth boundary $\partial\Omega$ and ν is the unit normal vector on $\partial\Omega$. Parameter $d_i(x)$ is the space-dependent diffusion rate, $i=1,2,3,4,5,6,7$. We denote $\lambda(S(x,t))$ the recruitment rate of the susceptible and denote by $\alpha(x)f_1(I_1(x,t),S(x,t))+\beta(x)f_2(I_2(x,t),S(x,t))+\gamma(x)f_3(L_1(x,t),S(x,t))$ the distribution of the newly infected individuals, where $\alpha(x),\beta(x),\gamma(x)$ and $f_j(j=1,2,3)$ represent the space-dependent infection rates and general incidence functions, respectively. The parameters $\mu(x)$ and $d(x)$ represent the natural and disease-induced death rates, respectively. The parameter $\omega(x)$ represents the removal rate at which infected individuals in the early latent stage of infection revert to either the primary or the secondary stage of infection, and the parameter $\epsilon(x)$ is the fraction of infected individuals in the early latent stage in this reversion. The parameters $\delta(x)$, $\zeta_1(x)$, $\zeta_2(x)$, $\eta_1(x)$, $\eta_2(x)$, and $\sigma(x)$ represent the progression rates from a previous stage to some later stage of the disease.

Throughout the paper, we make the hypothesis as follows:

Hypothesis 2.1. We assume that

- **(H1)** Function $\lambda(S(x,t)) \in C^1(\Omega\times\mathbb{R})$ and $\partial_S\lambda(S(x,t)) < 0$ for $x\in\Omega, S(x,t)\geq 0$. There exists a unique $\tilde{S}(x)>0$ in $C(\Omega\times\mathbb{R})$ such that $\lambda(\tilde{S}(x))=0$.
- **(H2)** Functions $f_1(I_1(x,t),S(x,t))$, $f_2(I_2(x,t),S(x,t))$, $f_3(L_1(x,t),S(x,t))\in C^1(\Omega\times\mathbb{R}\times\mathbb{R})$, $\partial_{I_1}f_1(I_1,S)$, $\partial_S f_1(I_1,S)$, $\partial_{I_2}f_2(I_2,S)$, $\partial_S f_2(I_2,S)$, $\partial_{L_1}f_3(L_1,S)$ and $\partial_S f_3(L_1,S)$ are all positive for $x\in\Omega$, $I_1>0, I_2>0, L_1>0$ and $S>0$ and $\partial f_i(0,S)/\partial S=0, i=1,2,3$. Furthermore, $f_1(I_1,S)=0$, $f_2(I_2,S)=0$, and $f_3(L_1,S)=0$ hold iff $I_1S=0$, $I_2S=0$ and $L_1S=0$, respectively. Suppose that $\partial^2 f_1(I_1,S)/\partial(I_1)^2\leq 0$, $\partial^2 f_2(I_2,S)/\partial(I_2)^2\leq 0$ and

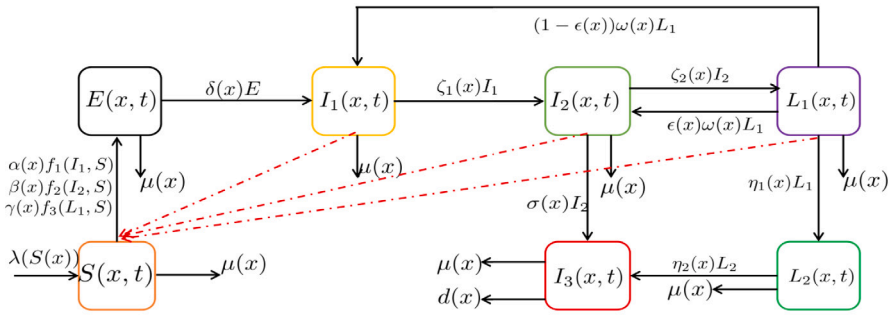

Fig. 2.2. Schematic diagram of the syphilis transmission model (2.1).

$\partial^2 f_3(L_1,S)/\partial(L_1)^2 \le 0$ for $S \ge 0, I_1 \ge 0, I_2 \ge 0, L_1 \ge 0$. There exist constants $N_1 > 0$, $N_2 > 0$, $N_3 > 0$ such that $f_j(\cdot,S) \le N_j S$, $j = 1,2,3$.

3. Well-posedness of system (2.1)

In this section, we are devoted to studying the global existence and uniqueness of the solution of system (2.1). To this end, we first define $\underline{u} = \min_{x\in\overline{\Omega}}\{u(x)\}, \overline{u} = \max_{x\in\overline{\Omega}}\{u(x)\}$. From Hypothesis 2.1, we know that $\lambda(S(x,t)) \le \Lambda - \hat{\mu}S(x,t)$, where $\Lambda > 0, \hat{\mu} > 0$.

Let space $\mathbb{Q} = C(\overline{\Omega},\mathbb{R})$ be equipped with the supremum norm $\|\cdot\|_{\mathbb{Q}}$ and $\mathbb{Q}_+ = C(\overline{\Omega},\mathbb{R}_+)$ be the positive cone of $\mathbb{Q}$. It is easy to obtain that $(\mathbb{Q},\mathbb{Q}_+)$ is an ordered Banach space. We set $\mathbb{M} = \mathbb{Q}^7$ equipped with norm $\|\phi\|_{\mathbb{M}} = \max\{\|\phi_1\|_{\mathbb{Q}}, \|\phi_2\|_{\mathbb{Q}}, \|\phi_3\|_{\mathbb{Q}}, \|\phi_4\|_{\mathbb{Q}}, \|\phi_5\|_{\mathbb{Q}}, \|\phi_6\|_{\mathbb{Q}}, \|\phi_7\|_{\mathbb{Q}}\}$, where $\phi = (\phi_1,\phi_2,\cdots,\phi_7) \in \mathbb{M}, \phi_i \in \mathbb{Q}, i = 1,2,\cdots,7$. Set the following C_0 semigroup $\mathcal{T}_i(t) : \mathbb{Q} \to \mathbb{Q}$

$$(\mathcal{T}_i(t)\phi)(x) = \int_\Omega H_i(x,y,t)\phi(y)\mathrm{d}y, \phi \in \mathbb{Q}, \quad t \ge 0, \ i = 1,2,\cdots,7,$$

where $H_i(x,y,t)(i = 1,2,\cdots,7)$ are the Green functions associated with $\nabla\cdot\big(d_1(\cdot)\nabla S(\cdot,t)\big) - \mu(\cdot)S(\cdot,t)$, $\nabla\cdot\big(d_2(\cdot)\nabla E(\cdot,t)\big) - (\mu(\cdot)+\delta(\cdot))E(\cdot,t)$, $\nabla\cdot\big(d_3(\cdot)\nabla I_1(\cdot,t)\big) - (\mu(\cdot)+\zeta_1(\cdot))I_1(\cdot,t)$, $\nabla\cdot\big(d_4(\cdot)\nabla I_2(\cdot,t)\big) - (\mu(\cdot)+\zeta_2(\cdot)+\sigma(\cdot))I_2(\cdot,t)$, $\nabla\cdot\big(d_5(\cdot)\nabla L_1(\cdot,t)\big) - (\mu(\cdot)+\omega(\cdot)+\eta_1(\cdot))L_1(\cdot,t)$, $\nabla\cdot\big(d_6(\cdot)\nabla L_2(\cdot,t)\big) - (\mu(\cdot)+\eta_2(\cdot))L_2(\cdot,t)$, $\nabla\cdot\big(d_7(\cdot)\nabla I_3(\cdot,t)\big) - (\mu(\cdot)+d(\cdot))I_3(\cdot,t)$, respectively. In view of Neumann boundary condition, we can obtain that $\mathcal{T}_i(t)$ are compact and strongly positive from [27, Corollary 7.2.3]. Hence, we can verify that there exist some positive constants a_i such that $\|\mathcal{T}_i(t)\| \le a_i e^{\psi_i t}$ for $t \ge 0$, where ψ_i are the principle eigenvalue of $\nabla\cdot\big(d_i(\cdot)\nabla\cdot\big) - b_i(\cdot)$ subject to Neumann boundary condition. Let $u(\phi,\cdot,t) = (S(\phi,\cdot,t), E(\phi,\cdot,t), I_1(\phi,\cdot,t),$
$I_2(\phi,\cdot,t), L_1(\phi,\cdot,t), L_2(\phi,\cdot,t), I_3(\phi,\cdot,t))^T$ be the solution of system (2.1) with the initial condition $\phi \in \mathbb{M}$, then we can rewrite system (2.1) as follows:

$$u(\phi,\cdot,t) = \mathcal{T}\phi + \int_0^t \mathcal{T}(t-s)\mathcal{A}(u(\phi,\cdot,t))\mathrm{d}s, \quad t > 0, \tag{3.2}$$

where $\mathcal{T} = \mathrm{diag}\{\mathcal{T}_1,\mathcal{T}_2,\cdots,\mathcal{T}_7\}$ and $\mathcal{A} = (\mathcal{A}_1,\mathcal{A}_2,\cdots,\mathcal{A}_7)^T$ with

$$\mathcal{A}_1(\phi)(x) = \lambda(\phi_1(x)) - (\alpha(x)\phi_3(x) + \beta(x)\phi_4(x) + \gamma(x)\phi_5(x)),$$

$$\mathcal{A}_2(\phi)(x) = (\alpha(x)\phi_3(x) + \beta(x)\phi_4(x) + \gamma(x)\phi_5(x)),$$

$$\mathcal{A}_3(\phi)(x) = \delta(x)\phi_2(x) + (1-\epsilon(x))\omega(x)\phi_5(x),$$

$$\mathcal{A}_4(\phi)(x) = \zeta_1(x)\phi_3(x) + \epsilon(x)\omega(x)\phi_5(x),$$

$$\mathcal{A}_5(x) = \zeta_2(x)\phi_4(x), \mathcal{A}_6(x) = \eta_1(x)\phi_5(x), \mathcal{A}_7(x) = \eta_2(x)\phi_6(x) + \sigma(x)\phi_4(x).$$

Based on the conclusion in [28, Corollary 4], we can obtain the following lemma:

Lemma 3.1. *For system (3.2) with the initial condition $\phi \in \mathbb{M}$, there exists a unique non-negative mild solution $u(\phi,\cdot,t) \in \mathbb{M}_+ \times [0,t_f), t_f \le +\infty$. Furthermore, the solution $u(\phi,\cdot,t)$ is a classical solution of system (3.2).*

Theorem 3.2. *If $u(\phi,\cdot,t)$ is the solution of system (3.2) with the initial condition $\phi \in \mathbb{M}_+$ for $t \in [0,+\infty)$, then $u(\phi,\cdot,t)$ is ultimately bounded.*

Proof. Let $u(\phi,\cdot,t)$ be a nonnegative solution of system (3.2) for $t \in [0,t_f)$ in Lemma 3.1. We assume that $t_f < \infty$, then we have $\|u(\phi,\cdot,t)\|_{\mathbb{M}} \to \infty (t \to t_f)$. According to Hypothesis 2.1 (**H1**), one has

$$\frac{\partial S(x,t)}{\partial t} \le \nabla\cdot\big(d_1(\cdot)\nabla S(\cdot,t)\big) + \Lambda - \hat{\mu}S(x,t), \quad x \in \overline{\Omega}, \ t \in [0,t_f).$$

Applying the comparison principle for parabolic equations, we immediately have that there admits a constant M_1 such that $S(x,t) \le M_1$ for $(x,t) \in (\overline{\Omega}\times[0,t_f)$. Based on Hypothesis 2.1 (**H2**), we can further obtain that

$$\begin{aligned}\frac{\partial E(x,t)}{\partial t} &\le \nabla\cdot\big(d_2(\cdot)\nabla E(\cdot,t)\big) + \overline{\alpha}M_1N_1 + \overline{\beta}M_1N_2 \\ &\quad + \overline{\gamma}M_1N_3 - (\underline{\mu}+\underline{\delta})E(x,t), \quad (x,t) \in \overline{\Omega}\times[0,t_f).\end{aligned}$$

We consider the following comparison system

$$\begin{cases}\dfrac{\partial v(x,t)}{\partial t} = \nabla\cdot\big(d_2(\cdot)\nabla v(\cdot,t)\big) + \overline{\alpha}M_1N_1 + \overline{\beta}M_1N_2 \\ \qquad\qquad + \overline{\gamma}M_1N_3 - (\underline{\mu}+\underline{\delta})v(x,t), \quad t > 0, \ x \in \Omega, \\ \dfrac{\partial v(\cdot,t)}{\partial \nu} = 0, \quad x \in \partial\Omega.\end{cases} \tag{3.3}$$

It is obvious that the eigenvalue problem with respect to system (3.3) has one principle eigenvalue ψ_0 associated with a strongly positive eigenfunction $\varphi = (\varphi_1,\cdots,\varphi_n)$. Then we can obtain that system (3.3) admits a solution $\lambda_0 e^{\psi_0}\varphi(x), t \ge 0$, where $\lambda_0 > 0, \lambda_0\varphi(x) \ge E(x,0), x \in \overline{\Omega}$. Further, there exists an $N_2 > 0$ such that $E(x,t) \le N_2$ for $x \in \overline{\Omega}, t \in [0,t_f)$. Similarly, we can verify that there exists an N^* such that $I_1(x,t) \le N^*, I_2(x,t) \le N^*, L_1(x,t) \le N^*, L_2(x,t) \le N^*$ and $I_3(x,t) \le N^*$ for $x \in \overline{\Omega}, t \in]0,t_f)$. This contradicts $\|u(\phi,\cdot,t)\|_{\mathbb{M}} \to \infty (t \to t_f)$. Thus, we can verify that $t_f = \infty$. To prove the global existence of $u(\phi,\cdot,t)$, it suffices to prove that the solution $u(\phi,\cdot,t)$ of system (3.2) is ultimate bounded. Obviously, it follows from Lemma 3.1 that the ultimate boundedness of $E(x,t)$ holds for $t \ge t_1$, i.e., $E(x,t) \le N_2$. Next, we set $U(t) = \int_\Omega (S(x,t)+I_1(x,t)+I_2(x,t)+L_1(x,t)+L_2(x,t)+I_3(x,t))dx$,

then we can obtain

$$\begin{aligned}\frac{dU(t)}{dt}\Big|_{(2.1)} \le& \int_\Omega [\lambda(S(x,t)) - \mu(x)E(x,t) - \mu(x)I_1(x,t) - \mu(x)I_2(x,t)\\ &- \mu(x)L_1(x,t) - \mu(x)L_2(x,t) - (\mu(x)+d(x))I_3(x,t)]\mathrm{d}x\\ \le& \overline{\lambda}|\Omega| - \underline{\mu}U(t), \quad t \ge 0.\end{aligned}$$

Applying the comparison principle, we have that there exist constants $N_3 > 0$ and $t_2 > 0$ such that $U(t) \le N_3$ for $t > t_2$. Let ψ_j be the eigenvalue of $\nabla\left(d_2(\cdot)\nabla E(\cdot,t)\right) - (\mu(\cdot)+\delta(\cdot))E(\cdot,t)$ subject to Neumann boundary condition. Then $\psi_1 \ge \psi_2 \ge \cdots \ge \psi_j \ge \cdots$. It further follows from [29, Theorem 2.4.7] that there exists a positive constant c_1 such that $H_2(x,y,t) \le c_1\sum_{j\ge1} e^{\psi_j t} \le c_1 e^{\psi_j t} \le u_2 e^{-\underline{\delta}t}$ for $t > 0$. Based on Hypothesis 2.1 (**H**2), we can obtain that

$$\begin{aligned}E(x,t) =& \mathcal{T}_2(t)E(x,t) + \int_{t_3}^t \mathcal{T}_2(t-s)(\alpha(x)f_1(I_1(x,s),S(x,s))\\ &+ \beta(x)f_2(I_2(x,s),S(x,s))\\ &+ \gamma(x)(L_1(x,s),S(x,s)))\mathrm{d}s\\ \le& N_2 e^{\psi_2(t-t_3)}\|E(\cdot,t_3)\|_{\mathbb{Q}} + \int_{t_3}^t H_2(x,y,t-s)(\alpha(x)f_1(I_1(x,s),S(x,s))\\ &+ \beta(x)f_2(I_2(x,s),S(x,s))\\ &+ \gamma(x)(L_1(x,s),S(x,s)))\mathrm{d}s\\ \le& N_2 e^{\psi_2(t-t_3)}\|E(\cdot,t_3)\|_{\mathbb{Q}} + \int_{t_3}^t c_1(\overline{\alpha}e^{-\underline{\zeta}_1(t-s)}MN_1\\ &+ \overline{\beta}e^{-(\underline{\zeta}_2+\underline{\sigma})(t-s)}N_2 + \overline{\gamma}e^{-(\underline{\eta}_1+\underline{\omega})(t-s)}N_3)M_1\mathrm{d}s\\ \le& N_3 e^{\psi_2(t-t_3)}\|E(\cdot,t_3)\|_{\mathbb{Q}}\\ &+ c_1N_1\left(\frac{\overline{\alpha}M_1}{\underline{\zeta}_1} + \frac{\overline{\beta}M_2}{\underline{\zeta}_2+\underline{\sigma}} + \frac{\overline{\gamma}N_2}{\underline{\eta}_1+\underline{\omega}}\right), \quad t > t_3,\ t_3 = \max\{t_1,t_2\},\end{aligned}$$

which implies that $\limsup_{t\to\infty}\|E(\cdot,t)\|_{\mathbb{Q}} \le c_2N_1\left(\frac{\overline{\alpha}M_1}{\underline{\zeta}_1} + \frac{\overline{\beta}M_2}{\underline{\zeta}_2+\underline{\sigma}} + \frac{\overline{\gamma}M_3}{\underline{\eta}_1+\underline{\omega}}\right)$. Similarly, we can show that $I_1(x,t), I_2(x,t), L_1(x,t), L_2(x,t), I_3(x,t)$ are all ultimately bounded. This completes the proof. □

From Theorem 3.2 we know that the solution semiflow $\Phi(t) = u(\cdot,t) : \mathbb{M}_+ \to \mathbb{M}_+$ is point dissipative on $\mathbb{M}_+$. Moreover, based on [29, Theorem 2.6] and [30, Theorem 3.4.8], we have the following result:

Theorem 3.3. *The solution semiflow of system (2.1) $\Phi(t) = u(\cdot,t) : \mathbb{M}_+ \to \mathbb{M}_+$ has a global attractor.*

4. The basic reproduction number and dynamical behaviors of system (2.1)

This section is devoted to deriving the functional expression of the basic reproduction number and discussing the dynamical behaviors of system (2.1). To this end, we first consider the following parabolic system:

$$\begin{cases}\dfrac{\partial S(x,t)}{\partial t} = \nabla\cdot\left(d_1(x)\nabla S(x,t)\right) + \lambda(S(x,t)), & t > 0,\\ \dfrac{\partial S(x,t)}{\partial \nu} = 0, & t > 0,\ x \in \partial\Omega.\end{cases} \tag{4.4}$$

From [24, Lemma 1], we obtain the following lemma:

Lemma 4.1. *System (4.4) has a unique positive steady state $S^*(x)$, which is globally attractive in $C(\overline{\Omega},\mathbb{R}_+)$.*

It follows from Lemma 4.1 that system (2.1) has a disease-free steady state $E_0(x) = (S^*(x),0,0,0,0,0,0)$, where $S^*(x)$ is the solution of parabolic system (4.4). Thus, the linearized system at $E_0(x)$ of the four compartments E, I_1, I_2, L_1 is as follows:

$$\begin{cases}\dfrac{\partial E(x,t)}{\partial t} =& \nabla\cdot\left(d_2(x)\nabla E(x,t)\right) + \alpha(x)\dfrac{\partial f_1(0,S^*(x))}{\partial I_1}I_1(x,t)\\ &+ \beta(x)\dfrac{\partial f_2(0,S^*(x))}{\partial I_2}I_2(x,t)\\ &+ \gamma(x)\dfrac{\partial f_3(0,S^*(x))}{\partial L_1}L_1(x,t)\\ &- (\mu(x)+\delta(x))E(x,t),\\ \dfrac{\partial I_1(x,t)}{\partial t} =& \nabla\cdot\left(d_3(x)\nabla I_1(x,t)\right) + \delta(x)E(x,t) + (1-\epsilon(x))\omega(x)L_1(x,t)\\ &- (\mu(x)+\zeta_1(x))I_1(x,t),\\ \dfrac{\partial I_2(x,t)}{\partial t} =& \nabla\cdot\left(d_4(x)\nabla I_2(x,t)\right) + \zeta_1(x)I_1(x,t) + \epsilon(x)\omega(x)L_1(x,t)\\ &- (\mu(x)+\zeta_2(x)+\sigma(x))I_2(x,t),\\ \dfrac{\partial L_1(x,t)}{\partial t} =& \nabla\cdot\left(d_5(x)\nabla L_1(x,t)\right) + \zeta_2(x)I_2(x,t)\\ &- (\mu(x)+\omega(x)+\eta_1(x))L_1(x,t),\\ \dfrac{\partial E(x,t)}{\partial \nu} =& 0, \quad \dfrac{\partial I_1(x,t)}{\partial \nu} = 0, \quad \dfrac{\partial I_2(x,t)}{\partial \nu} = 0, \quad \dfrac{\partial L_1(x,t)}{\partial \nu} = 0, \quad x \in \partial\Omega.\end{cases} \tag{4.5}$$

Let $(E,I_1,I_2,L_1) = e^{\omega t}(\phi_2(x),\phi_3(x),\phi_4(x),\phi_5(x))$, then we can rewrite system (4.5) as follows:

$$\begin{cases}\omega\phi_2(x) =& \nabla\cdot\left(d_2(x)\nabla\phi_2(x)\right) + \alpha(x)\dfrac{\partial f_1(0,S^*(x))}{\partial I_1}\phi_3(x)\\ &+ \beta(x)\dfrac{\partial f_2(0,S^*(x))}{\partial I_2}\phi_4(x)\\ &+ \gamma(x)\dfrac{\partial f_3(0,S^*(x))}{\partial L_1}\phi_5(x) - (\mu(x)+\delta(x))\phi_2(x),\\ \omega\phi_3(x) =& \nabla\cdot\left(d_3(x)\nabla\phi_3(x)\right) + \delta(x)\phi_2(x) + (1-\epsilon(x))\omega(x)\phi_5(x)\\ &- (\mu(x)+\zeta_1(x))\phi_3(x),\\ \omega\phi_4(x) =& \nabla\cdot\left(d_4(x)\nabla\phi_4(x)\right) + \zeta_1(x)\phi_3(x) + \epsilon(x)\omega(x)\phi_5(x)\\ &- (\mu(x)+\zeta_2(x)+\sigma(x))\phi_4(x),\\ \omega\phi_5(x) =& \nabla\cdot\left(d_5(x)\nabla\phi_5(x)\right) + \zeta_2(x)\phi_4(x) - (\mu(x)+\omega(x)+\eta_1(x))\phi_5(x),\\ \dfrac{\partial\phi_2(x)}{\partial\nu} =& 0, \dfrac{\partial\phi_3(x)}{\partial\nu} = 0, \quad \dfrac{\partial\phi_4(x)}{\partial\nu} = 0, \quad \dfrac{\partial\phi_5(x)}{\partial\nu} = 0, \quad x \in \partial\Omega.\end{cases} \tag{4.6}$$

It is easy to see that system (4.6) is a cooperative system. Based on Krein–Rutman theorem, we can verify that system (4.6) admits a unique principle eigenvalue $\omega_0(S^*)$ associated with a strongly positive eigenfunction $(\sigma_2,\sigma_3,\sigma_4,\sigma_5)$. Let $\Psi(t) : C(\overline{\Omega},\mathbb{R}^4) \to C(\overline{\Omega},\mathbb{R}^4)$ be the solution semigroup of system (4.5) and define

$$\mathbb{F} = \begin{pmatrix} 0 & \alpha(x)\frac{\partial f_1(0,S^*(x))}{\partial I_1} & \beta(x)\frac{\partial f_2(0,S^*(x))}{\partial I_2} & \gamma(x)\frac{\partial f_3(0,S^*(x))}{\partial L_1}\\ 0 & 0 & 0 & 0\\ 0 & 0 & 0 & 0\\ 0 & 0 & 0 & 0\end{pmatrix},$$

Thus, the total number of the newly infected individuals can be expressed as

$$\mathbb{L}(\phi)(x) = \int_0^{+\infty}\mathbb{F}(x)\Psi(t)\phi\mathrm{d}t.$$

According to the definition of the next generation operator, we have the following basic reproduction number of system (2.1):

$$\mathcal{R}_0 = r(\mathbb{L}), \quad \text{where } r \text{ is the spectral radius of } \mathbb{L}.$$

Based on the result of [24, Lemma 1], we have the following lemma:

Lemma 4.2. *$\mathcal{R}_0 - 1$ has the same sign as the principle eigenvalue ω_0 of system (4.6). Furthermore, the local asymptotic stability of the disease-free steady state $E_0(x)$ holds for $\mathcal{R}_0 < 1$. If $\mathcal{R}_0 > 1$, then it is unstable.*

Theorem 4.3. *The global asymptotic stability of the disease-free steady state $E_0(x)$ holds for $\mathcal{R}_0 < 1$.*

Proof. Applying the comparison principle of parabolic equations, we obtain that $\limsup_{t\to\infty} S(x,t) \le S^*(x)$ uniformly for $x \in \overline{\Omega}$. Then we assume that $S(x,t) \le S^*(x)+\eta, t > t^* > 0, x \in \overline{\Omega}$. Based on Lemma 4.2, we know that $\omega_0(S^*(x)) < 0$ when $R_0 < 1$. Since $\lim_{\eta\to 0}\omega_0(S^*(x)+\eta) = \omega_0(S^*(x)) < 0$, it follows that there exists an $\eta > 0$ such that $\omega_0(S^*(x)+\eta) < 0$. Then it follows from Hypothesis 2.1 that

$$\begin{cases}
\frac{\partial E(x,t)}{\partial x} \le \nabla\cdot\left(d_2(x)\nabla E(x,t)\right) + \alpha(x)\frac{\partial f_1(0,S^*(x)+\eta)}{\partial I_1}I_1(x,t) \\
\qquad + \beta(x)\frac{\partial f_2(0,S^*(x)+\eta)}{\partial I_2}I_2(x,t) \\
\qquad + \gamma(x)\frac{\partial f_3(0,S^*(x)+\eta)}{\partial L_1}L_1(x,t) - (\mu(x)+\delta(x))E(x,t), \quad t > t^* \\
\frac{\partial I_1(x,t)}{\partial x} = \nabla\cdot\left(d_3(x)\nabla I_1(x,t)\right) + \delta(x)E(x,t) + (1-\epsilon(x))\omega(x)L_1(x,t) \\
\qquad - (\mu(x)+\zeta_1(x))I_1(x,t), \quad t > t^* \\
\frac{\partial I_2(x,t)}{\partial x} = \nabla\cdot\left(d_4(x)\nabla I_2(X,t)\right) + \zeta_1(x)I_1(x,t) + \epsilon(x)\omega(x)L_1(x,t) \\
\qquad - (\mu(x)+\zeta_2(x)+\sigma(x))I_2(x,t), \quad t > t^* \\
\frac{\partial L(x,t)}{\partial x} = \nabla\cdot\left(d_5(x)\nabla L_1(x,t)\right) + \zeta_2(x)I_2(x,t) \\
\qquad - (\mu(x)+\omega(x)+\eta_1(x))L_1(x,t), \quad t > t^* \\
\frac{\partial E(x,t)}{\partial \nu} = 0, \frac{\partial I_1(x,t)}{\partial \nu} = 0, \frac{\partial I_2(x,t)}{\partial \nu} = 0, \frac{\partial L_1(x,t)}{\partial \nu} = 0, \quad x \in \partial\Omega,\ t > t^*.
\end{cases}$$

Then we can verify that $\omega_0(S^*+\eta) < 0$ is the principle eigenvalue of the following eigenvalue problem

$$\begin{cases}
\omega\phi_2(x) = \nabla\cdot\left(d_2(x)\nabla\phi_2(x)\right) + \alpha(x)\frac{\partial f_1(0,S^*(x)+\eta)}{\partial I_1}\phi_3(x) \\
\qquad + \beta(x)\frac{\partial f_2(0,S^*(x)+\eta)}{\partial I_2}\phi_4(x) \\
\qquad + \gamma(x)\frac{\partial f_3(0,S^*(x)+\eta)}{\partial L_1}\phi_5(x) - (\mu(x)+\delta(x))\phi_2(x), \quad t > t^* \\
\omega\phi_3(x) = \nabla\cdot\left(d_3(x)\nabla\phi_3(x)\right) + \delta(x)\phi_2(x) + (1-\epsilon(x))\omega(x)\phi_5(x) \\
\qquad - (\mu(x)+\zeta_1(x))\phi_3(x), \quad t > t^* \\
\omega\phi_4(x) = \nabla\cdot\left(d_4(x)\nabla\phi_4(x)\right) + \zeta_1(x)\phi_3(x) + \epsilon(x)\omega(x)\phi_5(x) \\
\qquad - (\mu(x)+\zeta_2(x)+\sigma(x))\phi_4(x), \quad t > t^* \\
\omega\phi_5(x) = \nabla\cdot\left(d_5(x)\nabla\phi_5(x)\right) + \zeta_2(x)\phi_4(x) \\
\qquad - (\mu(x)+\omega(x)+\eta_1(x))\phi_5(x), \quad t > t^* \\
\frac{\partial\phi_2(x)}{\partial\nu} = 0, \frac{\partial\phi_3(x)}{\partial\nu} = 0, \frac{\partial\phi_4(x)}{\partial\nu} = 0, \frac{\partial\phi_5(x)}{\partial\nu} = 0, \quad x \in \partial\Omega,\ t > t^*.
\end{cases} \tag{4.7}$$

Define $\tilde{\phi}(x) = (\tilde{\phi}_2(x), \tilde{\phi}_3(x), \tilde{\phi}_4(x), \tilde{\phi}_5(x))$ as the positive eigenfucntion associated with eigenvalue problem (4.7). Applying the comparison principle, one has

$$\begin{aligned}
&(E(x,t), I_1(x,t), I_2(x,t), L_1(x,t)) \\
&\quad \le c_2(\tilde{\phi}_2(x), \tilde{\phi}_3(x), \tilde{\phi}_4(x), \tilde{\phi}_5(x))e^{\omega_0(S^*+\eta)(t-t^*)}, \quad t > t^*,
\end{aligned}$$

which implies that $\lim_{t\to\infty}(E, I_1, I_2, L_1) = 0$. In addition, it follows from the theory of asymptotically autonomous semiflows [31] that $\lim_{t\to\infty} S(x,t) = S^*(x)$. Thus, combined with Lemma 4.2, the global asymptotic stability of $E_0(x)$ holds. This completes the proof. □

Theorem 4.4. *For the solution $u(\phi,\cdot,t)$ of system (2.1) with the initial value $\phi \in \mathbb{M}_+$ and $\phi_n \not\equiv 0, n = 2,3,4,5$, if $\mathcal{R}_0 > 1$, then there exists a constant $\xi > 0$ such that*

$$\liminf_{t\to\infty} \|u(\phi,\cdot,t) - E_0(x)\|_{\mathbb{M}} \ge \xi. \tag{4.8}$$

Furthermore, system (2.1) has at least one positive steady state.

Proof. We first introduce the following notations which will be used later.

$\mathbb{Y}_0 = \{\phi = (S,E,I_1,I_2,L_1,L_2,I_3) \in \mathbb{M}_+ : E \not\equiv 0, I_1 \not\equiv 0, I_2 \not\equiv 0, L_1 \not\equiv 0\}$,

$\partial\mathbb{Y}_0 = \{(E,I_1,I_2,L_1,L_2,I_3) \in \mathbb{M},\ E \equiv 0 \text{ or } I_1 \equiv 0 \text{ or } I_2 \equiv 0 \text{ or } L_1 \equiv 0\}$,

$\mathbb{Y}_\partial = \{\phi \in \partial\mathbb{Y}_0, \Phi(t)\phi \in \partial\mathbb{Y}_0,\ t \ge 0\}$,

$\omega(\phi)$ be the omega limit set of forward orbit $\gamma^+(\phi) = \{\Phi(t)(\phi) : t \ge 0\}$.

We divide the process of proof into three steps:

Step 1: We prove $\cup_{\phi\in\mathbb{Y}_\partial}\omega(\phi) = E_0(x)$. In fact, if $\phi \in \mathbb{Y}_\partial$, then $E \equiv 0$ or $I_1 \equiv 0$ or $I_2 \equiv 0$ or $L_1 \equiv 0$. Without loss of generality, we assume that $L_1(x,t) = 0$, then $I_2(x,t) = 0$ from the fifth equation of system (2.1), $I_1(x,t) = 0$ from the fourth equation of system (2.1), and $E(x,t) = 0$ from the second equation of system (2.1) and Hypothesis 2.1 (**H1**). Then $S(x,t) \to S^*(x)(t\to\infty)$ uniformly for $x \in \overline{\Omega}$ by the asymptotically autonomous semiflows theory.

Step 2: We show that there exists a constant $\eta > 0$ such that $\limsup_{t\to\infty}\|\Psi(t)(\phi) - E_0(x)\|_{\mathbb{M}} \ge \eta$ when $R_0 > 1$. From Lemma 4.1, we know that there admits a $\eta > 0$ such that $\omega_0(S^*(x)-\eta) > 0$. If it is not true, then there exists a $\phi_0 \in \mathbb{Y}_0$ such that $\limsup_{t\to\infty}\|\Psi(t)(\phi) - E_0(x)\|_{\mathbb{M}} < \eta$. This means that there admits a $t_1^* > 0$ such that $S(x,t,\phi_0) > S^*(x) - \eta$ for $t > t_1^*$, then we obtain

$$\begin{cases}
\frac{\partial E(x,t)}{\partial x} \ge \nabla\cdot\left(d_2(x)\nabla E(x,t)\right) + \alpha(x)\frac{\partial f_1(0,S^*(x)+\eta)}{\partial I_1}I_1(x,t) \\
\qquad + \beta(x)\frac{\partial f_2(0,S^*(x)-\eta)}{\partial I_2}I_2(x,t) \\
\qquad + \gamma(x)\frac{\partial f_3(0,S^*(x)-\eta)}{\partial L_1}L_1(x,t) - (\mu(x)+\delta(x))E(x,t), t > t^*, \\
\frac{\partial I_1(x,t)}{\partial x} = \nabla\cdot\left(d_3(x)\nabla I_1(x,t)\right) + \delta(x)E(x,t) + (1-\epsilon(x))\omega(x)L_1(x,t) \\
\qquad - (\mu(x)+\zeta_1(x))I_1(x,t), t > t^*, \\
\frac{\partial I_2(x,t)}{\partial x} = \nabla\cdot\left(d_4(x)\nabla I_2(X,t)\right) + \zeta_1(x)I_1(x,t) + \epsilon(x)\omega(x)L_1(x,t) \\
\qquad - (\mu(x)+\zeta_2(x)+\sigma(x))I_2(x,t), t > t^*, \\
\frac{\partial L(x,t)}{\partial x} = \nabla\cdot\left(d_5(x)\nabla L_1(x,t)\right) + \zeta_2(x)I_2(x,t) \\
\qquad - (\mu(x)+\omega(x)+\eta_1(x))L_1(x,t), t > t^*, \\
\frac{\partial E(x,t)}{\partial \nu} = 0, \frac{\partial I_1(x,t)}{\partial \nu} = 0, \frac{\partial I_2(x,t)}{\partial \nu} = 0, \frac{\partial L_1(x,t)}{\partial \nu} = 0, \quad x \in \partial\Omega, t > t^*.
\end{cases}$$

Then we can verify that $\omega_0(S^*-\eta) > 0$ is the principle eigenvalue of the following eigenvalue problem

$$\begin{cases}
\omega\phi_2(x) = \nabla\cdot\left(d_2(x)\nabla\phi_2(x)\right) + \alpha(x)\frac{\partial f_1(0,S^*(x)-\eta)}{\partial I_1}\phi_3(x) \\
\qquad + \beta(x)\frac{\partial f_2(0,S^*(x)-\eta)}{\partial I_2}\phi_4(x) \\
\qquad + \gamma(x)\frac{\partial f_3(0,S^*(x)-\eta)}{\partial L_1}\phi_5(x) - (\mu(x)+\delta(x))\phi_2(x), \quad t > t_1^* \\
\omega\phi_3(x) = \nabla\cdot\left(d_3(x)\nabla\phi_3(x)\right) + \delta(x)\phi_2(x) + (1-\epsilon(x))\omega(x)\phi_5(x) \\
\qquad - (\mu(x)+\zeta_1(x))\phi_3(x), \quad t > t_1^* \\
\omega\phi_4(x) = \nabla\cdot\left(d_4(x)\nabla\phi_4(x)\right) + \zeta_1(x)\phi_3(x) + \epsilon(x)\omega(x)\phi_5(x) \\
\qquad - (\mu(x)+\zeta_2(x)+\sigma(x))\phi_4(x), \quad t > t^* \\
\omega\phi_5(x) = \nabla\cdot\left(d_5(x)\nabla\phi_5(x)\right) + \zeta_2(x)\phi_4(x) \\
\qquad - (\mu(x)+\omega(x)+\eta_1(x))\phi_5(x), \quad t > t_1^* \\
\frac{\partial\phi_2(x)}{\partial\nu} = 0, \frac{\partial\phi_3(x)}{\partial\nu} = 0, \frac{\partial\phi_4(x)}{\partial\nu} = 0, \frac{\partial\phi_5(x)}{\partial\nu} = 0, \quad x \in \partial\Omega,\ t > t^*.
\end{cases} \tag{4.9}$$

Let $\hat{\phi} = (\hat{\phi}_2, \hat{\phi}_3, \hat{\phi}_4, \hat{\phi}_5)$ be the eigenfunction of eigenvalue problem (4.9) with the principle eigenvalue $\omega_0(S^*-\eta) > 0$. Suppose that there is $c > 0$ and $t_2^* > 0$ such that $c(\hat{\phi}_2, \hat{\phi}_3, \hat{\phi}_4, \hat{\phi}_5) \le (E(x,t_2^*), I_1(x,t_2^*), I_2(x,t_2^*), L_1(x,t_2^*))$, then we have $(E(x,t), I_1(x,t), I_2(x,t), L_1(x,t)) \ge c(\hat{\phi}_2, \hat{\phi}_3, \hat{\phi}_4, \hat{\phi}_5)e^{\omega_0(S^*-\eta)(t-t_2^*)}, t > t_2^*$, which implies that $\lim_{t\to\infty}(E(x,t), I_1(x,t), I_2(x,t),$

$L_1(x,t)) = +\infty$. This leads to a contradiction with the dissipativeness of system (2.1).

Step 3: If $R_0 > 1$, then there exists a $\eta_0 > 0$ such that $\liminf_{t\to\infty} u(x,t,\phi) \geq \eta_0, \phi \in \mathbb{Y}_0$. We define a continuous function $\theta : \mathbb{M}_+ \to [0,\infty)$ by $\theta(\phi) = \min\{\min_{x\in\overline{\Omega}} \phi_2, \min_{x\in\overline{\Omega}} \phi_3, \min_{x\in\overline{\Omega}} \phi_4, \min_{x\in\overline{\Omega}} \phi_5\}$, $\phi \in \mathbb{M}_+$. It is obvious that $\theta^{-1}[0,\infty) \subset \mathbb{Y}_0$ and $\theta(\phi) = 0$, or $\theta(\phi) > 0$, $\phi \in \mathbb{Y}_0$. Then $\theta(\Psi(t)(\phi)) > 0$. Hence, we can obtain that γ^+ of the solution semiflow $\Psi(t)$ in $\mathbb{Y}_\partial$ converges to $E_0(x)$ and $W^s(E_0(x)) \cap \mathbb{Y}_0 = \emptyset$. Furthermore, it is easy to obtain that $\{E_0(x)\}$ does not form any cycle in $\partial\mathbb{Y}_0$ and it is isolated in $\mathbb{M}_+$. Based on [32, Theorem 3.4], we can verify that there exists a $\eta^* > 0$ such that

$$\liminf_{t\to\infty} E(x,t) \geq \eta^*,\ \liminf_{t\to\infty} I_1(x,t) \geq \eta^*,\ \liminf_{t\to\infty} I_2(x,t) \geq \eta^*,$$
$$\liminf_{t\to\infty} L_1(x,t) \geq \eta^*,\ \liminf_{t\to\infty} L_2(x,t) \geq \eta^*,\ \liminf_{t\to\infty} I_3(x,t) \geq \eta^*.$$

Due to the dissipativeness of system (2.1), we have $\partial S(x,t)/\partial t \geq \nabla\cdot\big(d_1(x)\nabla S(x,t)\big) + \underline{\lambda} - (\overline{\mu} + \overline{\alpha}N_1 + \overline{\beta}N_2 + \overline{\gamma}N_3)S(x,t)$, then $\liminf_{t\to\infty} S(x,t,\phi) \geq \eta_1^* := \underline{\lambda}/(\overline{\mu} + \overline{\alpha}N_1 + \overline{\beta}N_2 + \overline{\gamma}N_3)$. We set $\eta = \min\{\eta^*, \eta_1^*\}$. Thus, we can verify that system (2.1) is uniformly persistent. In view of the uniform persistence of system (2.1), we can further conclude that system (2.1) has at least one positive steady state according to [24, Theorem 3]. This completes the proof. □

5. Numerical simulation

5.1. Numerical simulations for model (2.1) in space-discrete environment

In this section, we aim to conduct some numerical simulation of system (2.1). For this purpose, we choose $\lambda(S) = \lambda(x) - \mu(x)S$, $f_1(S,I_1) = SI_1$, $f_2(S,I_2) = SI_2$, $f_3(S,L_1) = SL_1$, and consider the environment of discrete diffusion in space. According to [33,34], when the discrete-space diffusion is concerned, the reaction–diffusion PDE model (2.1) can be transformed into the following patch model:

$$\begin{cases}
\frac{dS_k(t)}{dt} = d_1\sum_{l\in\Gamma} M^S_{kl}S_l(t) \\
\quad + \lambda_k - S_k(t)(\alpha_k(I_{1k}(t) + \beta_k I_{2k}(t) + \gamma_k L_{1k}(t))) - \mu_k S_k(t), \\
\frac{dE_k(t)}{dt} = d_2\sum_{l\in\Gamma} M^E_{kl}E_l(t) \\
\quad + S_k(t)(\alpha_k(I_{1k}(t) + \beta_k I_{2k}(t) + \gamma_k L_{1k}(t))) - (\mu_k + \delta_k)E_k(t), \\
\frac{dI_{1k}(t)}{dt} = d_3\sum_{l\in\Gamma} M^{I_1}_{kl}I_{1l}(t) \\
\quad + \delta_k E_k(t) + (1-\epsilon_k)\omega_k L_{1k}(t) - (\mu_k + \zeta_{1k})I_{1k}(t), \\
\frac{dI_{2k}(t)}{dt} = d_4\sum_{l\in\Gamma} M^{I_2}_{kl}I_{2l}(t) + \zeta_{1k}I_{1k}(t) \\
\quad + \epsilon_k\omega_k L_{1k}(t) - (\mu_k + \zeta_{2k} + \sigma_k)I_{2k}(t), \\
\frac{dL_{1k}(t)}{dt} = d_5\sum_{l\in\Gamma} M^{L_1}_{kl}L_{1l}(t) \\
\quad + \zeta_{2k}I_{2k}(t) - (\mu_k + \omega_k + \eta_{1k})L_{1k}(t), \\
\frac{dL_{2k}(t)}{dt} = d_6\sum_{l\in\Gamma} M^{L_2}_{kl}L_{2l}(t) \\
\quad + \eta_{1k}L_{1k}(t) - (\mu_k + \eta_{2k})L_{2k}(t), \\
\frac{dI_{3k}(t)}{dt} = d_7\sum_{l\in\Gamma} M^{I_3}_{kl}I_{3l}(t) \\
\quad + \eta_{2k}L_{2k}(t) + \sigma_k I_{2k}(t) - (\mu_k + d_k)I_{3k}(t)
\end{cases} \tag{5.10}$$

for $k \in \Gamma = \{1,\dots,30\}$, where the kth-patch respectively represents Heilongjiang, Xinjiang, Jilin, Liaoning, Inner Mongolia, Beijing, Tianjin, Ningxia, Hebei, Shanxi, Shandong, Qinghai, Gansu, Henan, Shaanxi, Jiangsu, Anhui, Shanghai, Sichuan, Hubei, Zhejiang, Chongqing, Jiangxi, Hunan, Guizhou, Fujian, Yunnan, Guangdong, Guangxi, Hainan Province/City in China. $M^\upsilon = (M^\upsilon_{kl})$ is the migration matrix of $\upsilon = \{S, E, I_1, I_2, L_1, L_2, I_3\}$, where M^υ_{kl} is the degree of incoming movement from patch l to k for $k \neq l$ and $M^\upsilon_{kk} = -\sum_{l\neq k} M_{lk}$ is the degree of outgoing movement from patch k to the other patches. The biological meanings of the other parameters are the same as those in model (2.1).

Table 1
The initial values of model (5.10).
Source: Data from [33].

Initial value	$I_{1k}(0)$	$I_{2k}(0)$	$L_{1k}(0)$	$L_{2k}(0)$	$I_{3k}(0)$
1(Heilongjiang)	973	622	617	154	5
2(Xinjiang)	654	403	114	28	18
3(Jilin)	701	550	148	37	8
4(Liaoning)	939	1060	884	221	13
5(InnerMongolia)	365	187	68	17	3
6(Beijing)	510	612	518	130	22
7(Tianjin)	281	340	173	43	12
8(Ningxia)	131	57	19	5	0
9(Hebei)	186	157	160	40	2
10(Shanxi)	622	189	353	88	18
11(Shandong)	805	751	141	35	6
12(Qinghai)	233	57	18	5	1
13(Gansu)	686	106	133	33	2
14(Henan)	837	482	217	54	18
15(Shaanxi)	351	242	206	52	8
16(Jiangsu)	2918	2716	1516	379	41
17(Anhui)	1281	1351	292	732	24
18(Shanghai)	2459	2776	1543	383	22
19(Sichuan)	2040	1288	622	156	21
20(Hubei)	632	487	110	27	10
21(Zhejiang)	6162	4344	2858	715	79
22(Chongqing)	1370	763	264	66	20
23(Jiangxi)	787	708	154	38	7
24(Hunan)	699	414	108	27	4
25(Guizhou)	483	159	591	15	0
26(Fujian)	3508	2718	1178	295	48
27(Yunnan)	431	128	65	16	17
28(Guangdong)	3833	3522	1986	497	63
29(Guangxi)	5070	3045	500	126	25
30(Hainan)	259	303	100	25	6

5.2. The initial values and parameter estimation

We take 2004 as the initial time ($t = 0$). The syphilis newly reported cases are listed in Tables 12–15. The corresponding collection of syphilis reported cases is given in "Appendix A". It is necessary to mention that all data listed in Tables 12–15 can be obtain from [35]. Due to the low proportion of infection cases in the total population, we can assume that $S_k(0) = N_k$ and the initial values are given in Table 1. Moreover, the values of $E_k(0), k \in \Gamma$ are obtained by data fitting.

Next, we estimate the values of some parameters of model (5.10) as follows: (1) The natural death rate of the population of the kth patch: Based on China Statistical Yearbook in 2004 [35], we list the value of the natural death rate (μ_k) of the kth patch in Table 2.

(2) The value of $\lambda_k, k \in \Gamma = \{1,2,\dots,30\}$. Similar to [36], we assume $\lambda_k = \mu_k N_k$, where N_k represents the total number of population in the kth patch and its values are listed in Table 3.

(3) Based on the data from [37], we can assume that $\frac{1}{\zeta_{1k}} = \frac{46}{365}$years, $\frac{1}{\zeta_{2k}} = \frac{108}{365}$years, $\frac{1}{\delta_k} = \frac{28}{365}$years.

(4) Disease-related death rate of $I_{3k}(t)$ in the kth patch. Based on the statistical data in [38], the values of d_k are listed in Table 4.

(5) The migration matrices $M^\upsilon, \upsilon = \{S, I_1, I_2, L_1, L_2, I_3\}$. In Figure A2 of [39], the authors collected Φ, the number of daily travelers in 30 provinces of China (except Tibet), and obtained the daily migration rate of the kth province, i.e., $\eta_k(t) = \frac{\Phi(t)}{N_k}$ with N_k representing the total population of the kth patch, which are shown in Figs. 6.17–6.19 in "Appendix B". Considering the annual data and the symmetry of M^υ in our simulation, we assume that the degree of incoming movement

Table 2
The natural death rate of population in the kth patch.
Source: Data from [35].

μ_k	μ_1	μ_2	μ_3	μ_4	μ_5	μ_6	μ_7	μ_8	μ_9	μ_{10}
Value(‰)	5.45	5.23	5.64	5.83	6.17	5.20	6.04	4.73	6.27	6.04
μ_k	μ_{11}	μ_{12}	μ_{13}	μ_{14}	μ_{15}	μ_{16}	μ_{17}	μ_{18}	μ_{19}	μ_{20}
Value(‰)	6.64	6.09	6.46	6.46	6.38	7.03	5.20	6.20	6.06	5.94
μ_k	μ_{21}	μ_{22}	μ_{23}	μ_{24}	μ_{25}	μ_{26}	μ_{27}	μ_{28}	μ_{29}	μ_{30}
Value(‰)	6.38	6.30	7.20	5.98	6.87	6.87	5.58	7.20	5.31	6.57

Table 3
The total number of population in the kth patch.
Source: Data from [35].

N_k	N_1	N_2	N_3	N_4	N_5	N_6	N_7	N_8	N_9	N_{10}
Value(thousand)	38 150	19 340	27 040	42 100	23 800	14 560	10 110	5800	67 690	33 140
N_k	N_{11}	N_{12}	N_{13}	N_{14}	N_{15}	N_{16}	N_{17}	N_{18}	N_{19}	N_{20}
Value(thousand)	91 250	5340	2603	96 670	36 900	74 060	64 100	17 110	87 000	60 020
N_k	N_{21}	N_{22}	N_{23}	N_{24}	N_{25}	N_{26}	N_{27}	N_{28}	N_{29}	N_{30}
Value(thousand)	46 800	31 300	42 540	66 630	38 700	34 880	43 760	79 540	48 570	8110

Table 4
The death rate d_k of population in the kth patch.
Source: Data from [35].

d_k	d_1	d_2	d_3	d_4	d_5	d_6	d_7	d_8	d_9	d_{10}
Value(‰)	5.3	28.6	3.5	4.0	1.2	1.3	14.7	1.3	4.7	3.1
d_k	d_{11}	d_{12}	d_{13}	d_{14}	d_{15}	d_{16}	d_{17}	d_{18}	d_{19}	d_{20}
Value(‰)	3.1	16.7	3.8	3.1	2.6	1.2	1.6	1.4	3.6	1.7
d_k	d_{21}	d_{22}	d_{23}	d_{24}	d_{25}	d_{26}	d_{27}	d_{28}	d_{29}	d_{30}
Value(‰)	2.0	3.3	1.5	1.5	5.6	10.2	3.3	2.4	2.0	1.2

$M^v_{kl} = M^v_{lk} = 360\bar{\eta}_k(t)$ with $\bar{\eta}_k = \frac{\bar{\Phi}}{N_k}$ for $l \neq k, k \in \Gamma$, where $\bar{\Phi}$ represents the average value of $\Phi(t)$ in [39].

(6) The diffusion rates $d_i, i = 1, 2, \cdots, 7$. From [40], we can obtain the migration index (denoted as $\tilde{d}$) of each patch, $\tilde{d} \in [1, 18]$. Here, one migration index is approximately equal to 44520 [39]. Hence, based on the data in Table 3, we obtain that $d_i \approx 44520 \times 360\tilde{d}/N \in [0.166, 0.92]$ and assume that $d_1 = 0.2, d_2 = 0.2, d_3 = 0.3, d_4 = 0.24, d_5 = 0.18, d_6 = 0.2, d_7 = 0.26$.

(7) The values of $E_k(0), \epsilon_k, \omega_k, \eta_{1k}, \eta_{2k}, \alpha_k, \beta_k, \gamma_k, \sigma_k$, $k \in \Gamma$ are obtained by data fitting. Based on the above model parameter estimation (1)-(6), we fit the cumulative syphilis reported cases (primary, secondary, latent and tertiary stages) from 2004 to 2018 in China by model (5.10), which are shown in Figs. 6.20–6.25. The corresponding fitted curves are given in "Appendix C". These figures show that multi-patch model (5.10) fits the syphilis cumulative cases in 30 provinces/cities reasonably well, so we obtain the estimated values of $E_k(0), \epsilon_k, \omega_k, \eta_{1k}, \eta_{2k}, \alpha_k, \beta_k, \gamma_k$ and σ_k, which are listed in Tables 5 and 6.

5.2.1. The basic reproduction number of system (5.10)

In this subsection, we first derive the expression of the basic reproduction number R_0 of system (5.10). It is easy to obtain that system (5.10) always has a disease-free equilibrium $E_0 = (S_0, 0, 0, 0, 0, 0, 0)$, where $S^0 = (S^0_1, \cdots, S^0_n)$ and S^0_k is the unique positive solution of

$$d_1 \sum_{l \in \Gamma} M^S_{kl} S_l(t) + \lambda_k - \mu_k S_k(t) = 0, \quad k \in \Gamma.$$

Based on the definition of the next generation reproduction number matrix, we obtain the basic reproduction number $R_0 = r(\mathcal{F}\mathcal{V}^{-1})$, where r is the dominant eigenvalue of matrix $(\mathcal{F}\mathcal{V}^{-1})$. The incidence matrix $\mathcal{F}$ and transition matrix $\mathcal{V}$ are given by

$$\mathcal{F} = \begin{pmatrix} 0 & \mathcal{F}_1 & \mathcal{F}_2 & \mathcal{F}_3 \\ 0 & 0 & 0 & 0 \\ 0 & 0 & 0 & 0 \\ 0 & 0 & 0 & 0 \end{pmatrix}, \quad \mathcal{V} = \begin{pmatrix} \mathcal{V}_{11} & 0 & 0 & 0 \\ \mathcal{V}_{21} & \mathcal{V}_{22} & 0 & \mathcal{V}_{24} \\ 0 & \mathcal{V}_{32} & \mathcal{V}_{33} & \mathcal{V}_{34} \\ 0 & 0 & \mathcal{V}_{43} & \mathcal{V}_{44} \end{pmatrix},$$

where

$$\mathcal{F}_1 = \mathrm{diag}\{\alpha_1 S^0_1, \cdots, \alpha_n S^0_n\}, \quad \mathcal{F}_2 = \mathrm{diag}\{\beta_1 S^0_1, \cdots, \beta_n S^0_n\},$$
$$\mathcal{F}_3 = \mathrm{diag}\{\gamma_1 S^0_1, \cdots, \gamma_n S^0_n\},$$
$$\mathcal{V}_{11} = D_E - d_2 M^E, \quad D_E = \mathrm{diag}\{\mu_1 + \delta_1, \cdots, \mu_n + \delta_n\},$$
$$\mathcal{V}_{21} = \mathrm{diag}\{-\delta_1, \cdots, -\delta_n\},$$
$$\mathcal{V}_{22} = D_{I_1} - d_3 M^{I_1}, \quad D_{I_1} = \mathrm{diag}\{\mu_1 + \zeta_{11}, \cdots, \mu_n + \zeta_{1n}\},$$
$$\mathcal{V}_{24} = \mathrm{diag}\{-(1-\epsilon_1)\omega_1, \cdots, -(1-\epsilon_n)\omega_n\}, \mathcal{V}_{32} = \mathrm{diag}\{-\zeta_{11}, \cdots, -\zeta_{1n}\},$$
$$\mathcal{V}_{34} = \mathrm{diag}\{-\omega_1\epsilon_1, \cdots, -\omega_n\epsilon_n\},$$
$$\mathcal{V}_{33} = D_{I_2} - d_4 M^{I_2}, \quad D_{I_2} = \mathrm{diag}\{\mu_1 + \zeta_{21} + \sigma_1, \cdots, \mu_n + \zeta_{2n} + \sigma_n\},$$
$$\mathcal{V}_{43} = \mathrm{diag}\{-\zeta_{21}, \cdots, -\zeta_{2n}\},$$
$$\mathcal{V}_{44} = D_{L_1} - d_5 M^{L_1},$$
$$D_{L_1} = \mathrm{diag}\{\mu_1 + \omega_1 + \eta_{11}, \cdots, \mu_n + \omega_n + \eta_{1n}\}, \quad n = 30.$$

Applying the MCMC method to model (5.10) with multiple patches, we can obtain the estimated values of the parameters (see Table 5). Thus, we can calculate the basic reproduction number $R_0 = 2.1753$ (95% CI: (1.9133, 2.2687)), which is shown in Fig. 5.3. The value of basic reproduction number is close to the numerical result in [21] where the range of the estimated values of the basic reproduction number of syphilis is [1.19, 2.55] and the numerical result in [22] where the estimated value of the basic reproduction number of syphilis is 2.470724.

To better display the difference of syphilis epidemic risk among the 30 provinces/cities in China, we first define the following isolated reproduction number of each patch in model (5.10) ($k = 1, 2, \ldots, 30$) according to [41, Section 3]:

$$R^0_k = r(\mathbf{F}_k \mathbf{V}_k^{-1}),$$

where r is the dominant eigenvalue of matrix $(\mathbf{F}_k \mathbf{V}_k^{-1})$ and

$$\mathbf{F}_k = \begin{pmatrix} 0 & \alpha_k \bar{S}^0_k & \beta_k \bar{S}^0_k & \gamma_k \bar{S}^0_k \\ 0 & 0 & 0 & 0 \\ 0 & 0 & 0 & 0 \\ 0 & 0 & 0 & 0 \end{pmatrix},$$

Table 5
The values of some estimated parameters by the MCMC method.

i	α_i(Std)(e^{-9})	β_i(Std)(e^{-8})	γ_i(Std)(e^{-8})	η_{1i}(Std)	η_{2i}(Std)	σ_i(Std)	ϵ_i(Std)	ω_i(Std)
1	1.20(1.03)	7.54(8.07)	1.29(1.78)	0.125(0.084)	0.493(0.284)	0.699(0.2237)	0.464(0.290)	0.125(0.075)
2	1.362(1.071)	8.310(7.83)	5.763(2.481)	0.439(0.282)	0.463(0.282)	0.752(0.194)	0.497(0.283)	0.411(0.293)
3	2.751(2.453)	7.72(10.30)	10.66(4.924)	0.385(0.260)	0.437(0.289)	0.676(0.251)	0.521(0.288)	0.382(0.269)
4	4.428(5.661)	5.805(5.46)	6.644(7.007)	0.196(0.167)	0.337(0.298)	0.488(0.321)	0.464(0.284)	0.181(0.161)
5	7.172(5.489)	4.732(4.449)	4.81(3.28)	0.321(0.269)	0.535(0.287)	0.747(0.205)	0.493(0.292)	0.321(0.268)
6	5.133(1.730)	5.304(5.491)	7.299(7.094)	0.475(0.196)	0.288(0.202)	0.688(0.179)	0.462(0.266)	0.137(0.097)
7	3.69(12.71)	3.787(3.622)	10.01(9.433)	0.202(0.216)	0.427(0.287)	0.529(0.329)	0.507(0.293)	0.229(0.246)
8	4.69(4.288)	13.313(2.842)	4.102(5.047)	0.415(0.275)	0.530(0.289)	0.699(0.227)	0.478(0.288)	0.361(0.276)
9	5.21(3.58)	4.598(4.671)	1.179(1.671)	0.255(0.271)	0.436(0.310)	0.551(0.300)	0.527(0.287)	0.212(0.242)
10	3.083(2.252)	3.570(3.708)	2.990(1.119)	0.452(0.281)	0.495(0.283)	0.589(0.284)	0.500(0.281)	0.457(0.272)
11	4.951(1.586)	2.820(2.773)	1.631(0.872)	0.158(0.181)	0.446(0.308)	0.553(0.284)	0.502(0.286)	0.161(0.184)
12	3.378(2.805)	2.245(2.208)	1.676(0.721)	0.459(0.295)	0.473(0.287)	0.721(0.204)	0.521(0.294)	0.457(0.288)
13	1.680(1.653)	2.370(2.931)	1.009(3.123)	0.589(0.267)	0.441(0.279)	0.685(0.259)	0.459(0.290)	0.503(0.287)
14	1.458(1.348)	4.296(4.179)	3.319(1.548)	0.362(0.265)	0.473(0.303)	0.648(0.265)	0.483(0.277)	0.357(0.281)
15	3.816(3.382)	11.87(12.14)	1.857(0.920)	0.193(0.213)	0.432(0.308)	0.527(0.327)	0.537(0.274)	0.161(0.181)
16	2.806(0.398)	1.398(1.269)	1.569(3.026)	0.384(0.228)	0.453(0.331)	0.476(0.320)	0.469(0.279)	0.350(0.208)
17	2.901(0.919)	2.694(3.282)	2.046(4.490)	0.149(0.107)	0.382(0.301)	0.681(0.268)	0.517(0.290)	0.162(0.115)
18	2.386(1.693)	3.362(3.014)	5.018(1.057)	0.368(0.259)	0.361(0.291)	0.540(0.272)	0.261(0.217)	0.698(0.195)
19	1.751(0.691)	3.004(2.975)	1.547(5.926)	0.328(0.235)	0.422(0.299)	0.586(0.284)	0.469(0.286)	0.275(0.211)
20	1.879(1.951)	2.877(2.791)	3.932(2.408)	0.399(0.239)	0.456(0.282)	0.732(0.245)	0.543(0.287)	0.335(0.239)
21	1.672(1.671)	2.144(2.283)	3.171(8.582)	0.583(0.259)	0.465(0.299)	0.588(0.299)	0.494(0.288)	0.556(0.274)
22	1.321(1.742)	4.354(4.262)	6.04(5.119)	0.507(0.254)	0.393(0.299)	0.754(0.197)	0.492(0.284)	0.479(0.273)
23	0.93(0.840)	7.029(7.481)	5.546(2.041)	0.425(0.275)	0.469(0.287)	0.687(0.238)	0.509(0.283)	0.464(0.272)
24	1.259(1.420)	7.026(6.667)	7.27(5.437)	0.519(0.285)	0.490(0.297)	0.672(0.256)	0.485(0.289)	0.499(0.288)
25	1.058(1.499)	7.642(7.439)	4.490(6.964)	0.335(0.255)	0.408(0.276)	0.750(0.226)	0.506(0.294)	0.284(0.229)
26	0.969(0.883)	3.469(3.390)	3.365(0.948)	0.529(0.286)	0.371(0.294)	0.612(0.290)	0.450(0.282)	0.565(0.257)
27	1.029(1.210)	3.140(2.777)	2.66(4.153)	0.559(0.271)	0.395(0.303)	0.731(0.222)	0.496(0.290)	0.551(0.281)
28	0.485(0.524)	1.390(1.384)	1.732(5.018)	0.540(0.288)	0.470(0.311)	0.602(0.286)	0.441(0.282)	0.598(0.264)
29	0.182(0.176)	1.309(1.449)	1.866(4.904)	0.643(0.253)	0.485(0.293)	0.464(0.349)	0.495(0.287)	0.665(0.253)
30	0.170(0.199)	3.200(2.732)	3.100(4.521)	0.538(0.287)	0.479(0.291)	0.612(0.261)	0.464(0.283)	0.572(0.272)

Table 6
The values of $E_k(0)$ for model (5.10) by the MCMC method.

$E_k(0)$	$E_1(0)$	$E_2(0)$	$E_3(0)$	$E_4(0)$	$E_5(0)$	$E_6(0)$	$E_7(0)$	$E_8(0)$	$E_9(0)$	$E_{10}(0)$
Value	2100	1342	10 091	4010	3012	1270	1423	3422	1844	1544
$E_k(0)$	$E_{11}(0)$	$E_{12}(0)$	$E_{13}(0)$	$E_{14}(0)$	$E_{15}(0)$	$E_{16}(0)$	$E_{17}(0)$	$E_{18}(0)$	$E_{19}(0)$	$E_{20}(0)$
Value	1370	4703	14 692	4598	39 882	47 000	23 882	38 001	84 789	34 344
$E_k(0)$	$E_{21}(0)$	$E_{22}(0)$	$E_{23}(0)$	$E_{24}(0)$	$E_{25}(0)$	$E_{26}(0)$	$E_{27}(0)$	$E_{28}(0)$	$E_{29}(0)$	$E_{30}(0)$
Value	33 400	43 288	2488	2397	17 174	20 016	9834	16 344	5400	12 780

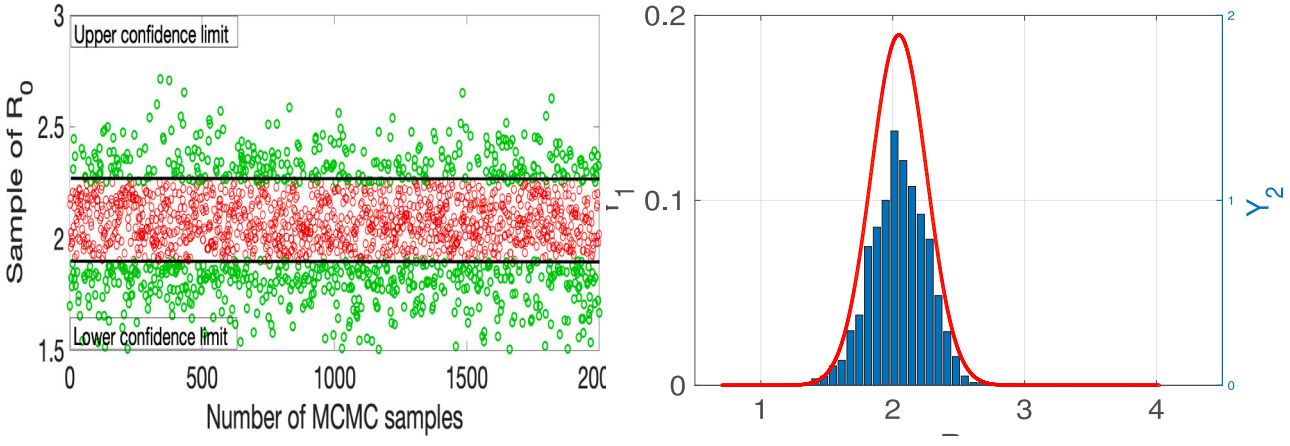

(a) The sample of R_0 (b) The frequency of R_0

Fig. 5.3. (a) The sample of R_0. The green and red points illustrate the value of R_0 outside and within the 95% confidence interval, respectively. The black lines illustrate the lower and upper confidence limits; (b) The frequency of R_0, the red curve is the probability density function (PDF) curve of R_0. Here Y_1 represents the ratio of the number of each column (frequency) to the total number of data and Y_2 represents the value of the probability density function curve.

$$\mathbf{V}_k = \begin{pmatrix} \mu_k+\delta_k & 0 & 0 & 0 \\ -\delta_k & \mu_k+\zeta_{1k} & 0 & -(1-\epsilon_k)\omega_k \\ 0 & -\zeta_{1k} & \mu_k+\zeta_{2k}+\sigma_k & -\omega_k\epsilon_k \\ 0 & 0 & -\zeta_{2k} & \mu_k+\omega_k+\eta_{1k} \end{pmatrix}, \tag{5.11}$$

with $\bar{S}_k^0 = \lambda_k/\mu_k$. We further define $R_k^0 = R_k^{I_1} + R_k^{I_2} + R_k^{L_1}$, where $R_k^{I_1}$, $R_k^{I_2}$ and $R_k^{L_1}$ are the reproduction number through $I_{1k}(t)$, $I_{2k}(t)$ and $L_{1k}(t)$ transmission routes in each patch, respectively (see Box I).

Based on the estimated value of some parameters of model (5.10) in Table 5, we can obtain the value of the basic reproduction numbers

$$R_k^{I_1} = \frac{\alpha_k\lambda_k((\mu_k+\zeta_{2k}+\sigma_k)(\mu_k+\omega_k+\eta_{1k})-\omega_k\epsilon_k\zeta_{2k})\delta_k}{\mu_k(\mu_k+\delta_k)(\zeta_{2k}\omega_k(\mu_k+\zeta_{1k})+(\mu_k+\zeta_{2k}+\sigma_k)(\mu_k+\omega_k+\eta_{1k})+(1-\epsilon_k)\omega_k\zeta_{1k}(\mu_k+\omega_k+\eta_{1k}))},$$

$$R_k^{I_2} = \frac{\beta_k\lambda_k\delta_k\zeta_{1k}(\mu_k+\omega_k+\eta_{1k})}{\mu_k(\mu_k+\delta_k)(\zeta_{2k}\omega_k(\mu_k+\zeta_{1k})+(\mu_k+\zeta_{2k}+\sigma_k)(\mu_k+\omega_k+\eta_{1k})+(1-\epsilon_k)\omega_k\zeta_{1k}(\mu_k+\omega_k+\eta_{1k}))},$$

$$R_k^{L_1} = \frac{\gamma_k\lambda_k\delta_k\zeta_{1k}\zeta_{2k}}{\mu_k(\mu_k+\delta_k)(\zeta_{2k}\omega_k(\mu_k+\zeta_{1k})+(\mu_k+\zeta_{2k}+\sigma_k)(\mu_k+\omega_k+\eta_{1k})+(1-\epsilon_k)\omega_k\zeta_{1k}(\mu_k+\omega_k+\eta_{1k}))}.$$

Box I.

Table 7
The value of the basic reproduction numbers R_k^0, $R_k^{I_1}$, $R_k^{I_2}$ and $R_k^{L_1}$ for each patch.

$\mathbf{R_1^0 = 2.1695}$			$\mathbf{R_2^0 = 3.1479}$			$\mathbf{R_3^0 = 3.2664}$			$\mathbf{R_4^0 = 3.0087}$		
$R_1^{I_1}$	$R_1^{I_2}$	$R_1^{L_1}$	$R_2^{I_1}$	$R_2^{I_2}$	$R_2^{L_1}$	$R_3^{I_1}$	$R_3^{I_2}$	$R_3^{L_1}$	$R_4^{I_1}$	$R_4^{I_2}$	$R_4^{L_1}$
0.0053	0.8164	1.3478	0.0432	0.8302	2.2745	0.0107	0.7464	2.5093	0.0184	0.6290	2.3614
$\mathbf{R_5^0 = 1.9890}$			$\mathbf{R_6^0 = 3.1266}$			$\mathbf{R_7^0 = 2.6072}$			$\mathbf{R_8^0 = 2.3257}$		
$R_5^{I_1}$	$R_5^{I_2}$	$R_5^{L_1}$	$R_6^{I_1}$	$R_6^{I_2}$	$R_6^{L_1}$	$R_7^{I_1}$	$R_7^{I_2}$	$R_7^{L_1}$	$R_8^{I_1}$	$R_8^{I_2}$	$R_8^{L_1}$
0.0292	0.4694	1.4904	0.1022	1.2760	1.748	0.0130	0.3538	2.2405	0.0206	1.0170	1.2881
$\mathbf{R_9^0 = 1.5315}$			$\mathbf{R_{10}^0 = 1.3606}$			$\mathbf{R_{11}^0 = 2.0640}$			$\mathbf{R_{12}^0 = 0.8037}$		
$R_9^{I_1}$	$R_9^{I_2}$	$R_9^{L_1}$	$R_{10}^{I_1}$	$R_{10}^{I_2}$	$R_{10}^{L_1}$	$R_{11}^{I_1}$	$R_{11}^{I_2}$	$R_{11}^{L_1}$	$R_{12}^{I_1}$	$R_{12}^{I_2}$	$R_{12}^{L_1}$
0.0239	0.5319	0.9757	0.0110	0.3293	1.0194	0.0197	0.2910	1.7533	0.0130	0.212	0.5792
$\mathbf{R_{13}^0 = 0.5637}$			$\mathbf{R_{14}^0 = 1.9387}$			$\mathbf{R_{15}^0 = 2.4856}$			$\mathbf{R_{16}^0 = 1.8793}$		
$R_{13}^{I_1}$	$R_{13}^{I_2}$	$R_{13}^{L_1}$	$R_{14}^{I_1}$	$R_{14}^{I_2}$	$R_{14}^{L_1}$	$R_{15}^{I_1}$	$R_{15}^{I_2}$	$R_{15}^{L_1}$	$R_{16}^{I_1}$	$R_{16}^{I_2}$	$R_{16}^{L_1}$
0.0070	0.2409	0.3158	0.0057	0.4198	1.5132	0.0178	0.4034	2.0644	0.0109	0.1417	1.7268
$\mathbf{R_{17}^0 = 2.4714}$			$\mathbf{R_{18}^0 = 1.2256}$			$\mathbf{R_{19}^0 = 1.3068}$			$\mathbf{R_{20}^0 = 2.3161}$		
$R_{17}^{I_1}$	$R_{17}^{I_2}$	$R_{17}^{L_1}$	$R_{18}^{I_1}$	$R_{18}^{I_2}$	$R_{18}^{L_1}$	$R_{19}^{I_1}$	$R_{19}^{I_2}$	$R_{19}^{L_1}$	$R_{20}^{I_1}$	$R_{20}^{I_2}$	$R_{20}^{L_1}$
0.0116	0.2699	2.1898	0.0053	0.2138	1.0065	0.0078	0.3365	0.9625	0.0087	0.3184	1.9890
$\mathbf{R_{21}^0 = 2.0673}$			$\mathbf{R_{22}^0 = 0.8576}$			$\mathbf{R_{23}^0 = 2.4873}$			$\mathbf{R_{24}^0 = 2.9330}$		
$R_{21}^{I_1}$	$R_{21}^{I_2}$	$R_{21}^{L_1}$	$R_{22}^{I_1}$	$R_{22}^{I_2}$	$R_{22}^{L_1}$	$R_{23}^{I_1}$	$R_{23}^{I_2}$	$R_{23}^{L_1}$	$R_{24}^{I_1}$	$R_{24}^{I_2}$	$R_{24}^{L_1}$
0.0061	0.1977	1.8635	0.3800	0.2400	0.2376	0.0032	0.6239	0.1.8600	0.0048	0.6629	2.2653
$\mathbf{R_{25}^0 = 3.089}$			$\mathbf{R_{26}^0 = 1.2089}$			$\mathbf{R_{27}^0 = 1.0234}$			$\mathbf{R_{28}^0 = 1.5638}$		
$R_{25}^{I_1}$	$R_{25}^{I_2}$	$R_{25}^{L_1}$	$R_{26}^{I_1}$	$R_{26}^{I_2}$	$R_{26}^{L_1}$	$R_{27}^{I_1}$	$R_{27}^{I_2}$	$R_{27}^{L_1}$	$R_{28}^{I_1}$	$R_{28}^{I_2}$	$R_{28}^{L_1}$
0.0043	0.8610	2.7380	0.0034	0.3089	0.8966	0.0038	0.2824	0.7372	0.0018	0.1284	1.4337
$\mathbf{R_{29}^0 = 1.007}$			$\mathbf{R_{30}^0 = 1.1301}$								
$R_{29}^{I_1}$	$R_{29}^{I_2}$	$R_{29}^{L_1}$	$R_{30}^{I_1}$	$R_{30}^{I_2}$	$R_{30}^{L_1}$						
0.5067	0.10034	0.4000	0.0652	0.3067	0.8227						

R_k^0, $R_k^{I_1}$, $R_k^{I_2}$ and $R_k^{L_1}$ for each patch, which are listed in Table 7. Furthermore, Based on the value of the basic reproduction numbers R_k^0 ($k = 1, 2, \ldots, 30$) in Table 7, we can display the level of syphilis outbreak for the 30 provinces/cities in Fig. 5.4. This figure shows that (1) There are significant differences in risk indicators for syphilis outbreaks in different regions, which indicates that spatial factors are one of the important factors that cannot be ignored; (2) Compared to the original high incidence areas of syphilis reported in [42,43] (i.e., Qinghai, Beijing, Tianjin, the south and southeast coastal area) (see Fig. 5.5), Xinjiang, Guizhou, Hunan, and Northeast China have become the new high incidence areas of syphilis. This suggests that disease prevention and control departments should promptly pay attention to the changes in high incidence areas of syphilis and take timely and effective prevention and control measures to reduce the risk of syphilis outbreaks in these areas.

5.2.2. Underestimation of the risk of syphilis outbreaks

In this subsection, we explore the underestimation of the risk of syphilis outbreaks. Similar to [41, Section 4], we define the proportions of underestimation of the basic reproduction number R_k^0 for each patch as follows:

$$\mathbb{P}_k^{I_1} = 1 - \frac{R_k^{I_1}}{R_k^0}, \quad \mathbb{P}_k^{I_2} = 1 - \frac{R_k^{I_2}}{R_k^0}, \quad \mathbb{P}_k^{L_1} = 1 - \frac{R_k^{L_1}}{R_k^0}.$$

Based on the values of the basic reproduction numbers R_k^0, $R_k^{I_1}$, $R_k^{I_2}$ and $R_k^{L_1}$ for each patch in Fig. 5.4, we can obtain the value of $\mathbb{P}_k^m, (m = 1, 2, 3, k = 1, 2, \ldots, 30)$ in Table 8. In this table, we can find that in different high and low incidence regions, the main transmission routes of syphilis are the same. For example, in these 30 provinces/cities, the underestimation rate of primary stage syphilis infected individuals is almost more than 90% and the underestimation rate of early latent stage syphilis infected individuals is almost less than 10%. This indicates that among the three stages of syphilis infected individuals, those in the early latent syphilis stage have the highest risk of syphilis transmission, which is in line with [44]. Hence, the disease control department needs to take corresponding prevention and control measures according to this characteristic of syphilis transmission.

5.3. Numerical simulations for model (2.1) in space-continuous environment

In this subsection, we conduct some numerical simulations of model (2.1).

5.3.1. One-dimensional domain

In this subsection, we project 16 discrete patches (i.e., 16 provinces/cites in China) onto a continuous one-dimensional domain $\Omega \in [0, 1]$. We set space step $\Delta x = 0.01$ and $K = 1/\Delta x = 100$. Based on the geographical coordinates of the capital of 30 provinces in China in international standard plane coordinate system (see Table 9), we calculate the plane coordinates of the capital of 30 provinces in China under the new standard plane coordinate system, which takes Heihe-Tengchong Line (Hu-Line) [45] as the horizontal axis and Tengchong city coordinates as the origin coordinates.

Thus, we delineate a four-step process to ascertain the planar coordinates of the capitals for 30 provinces within the newly established coordinate system.

Fig. 5.4. The value of the basic reproduction numbers R_k^0 for each patch.

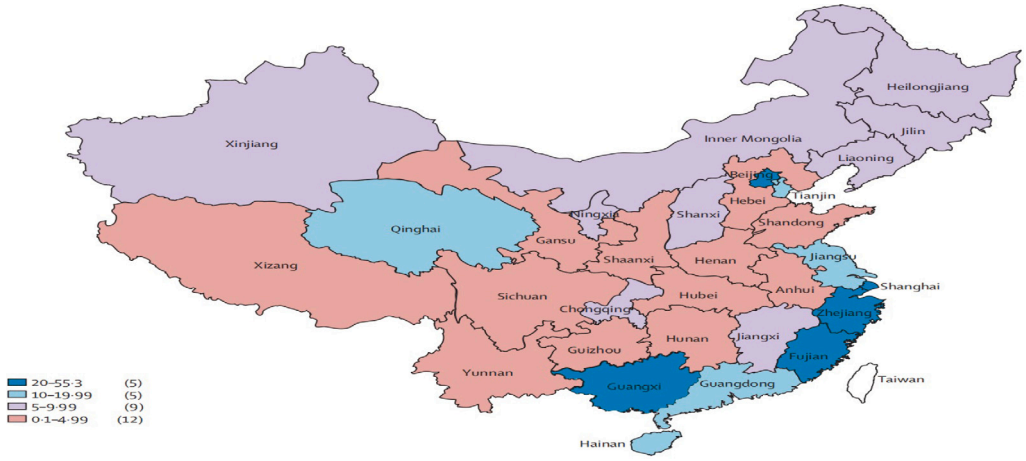

Fig. 5.5. Incidence of total syphilis in 2005 by province from nationwide STD surveillance system.
Source: The figure adapted from [43].

Table 8
The proportions of underestimation (primary, secondary and early latent stages) of the basic reproduction number for each patch.

1			2			3			4		
$\mathbb{P}_1^{I_1}$	$\mathbb{P}_1^{I_2}$	$\mathbb{P}_1^{L_1}$	$\mathbb{P}_2^{I_1}$	$\mathbb{P}_2^{I_2}$	$\mathbb{P}_2^{L_1}$	$\mathbb{P}_3^{I_1}$	$\mathbb{P}_3^{I_2}$	$\mathbb{P}_3^{L_1}$	$\mathbb{P}_4^{I_1}$	$\mathbb{P}_4^{I_2}$	$\mathbb{P}_4^{L_1}$
0.9980	0.6976	0.3155	0.9863	0.7363	0.2775	0.9975	0.8251	0.1775	0.9963	0.8744	0.1292
5			6			7			8		
$\mathbb{P}_5^{I_1}$	$\mathbb{P}_5^{I_2}$	$\mathbb{P}_5^{L_1}$	$\mathbb{P}_6^{I_1}$	$\mathbb{P}_6^{I_2}$	$\mathbb{P}_6^{L_1}$	$\mathbb{P}_7^{I_1}$	$\mathbb{P}_7^{I_2}$	$\mathbb{P}_7^{L_1}$	$\mathbb{P}_8^{I_1}$	$\mathbb{P}_8^{I_2}$	$\mathbb{P}_8^{L_1}$
0.9902	0.8430	0.1668	0.9801	0.5560	0.4640	0.9977	0.9369	0.0654	0.9938	0.5739	0.4323
9			10			11			12		
$\mathbb{P}_9^{I_1}$	$\mathbb{P}_9^{I_2}$	$\mathbb{P}_9^{L_1}$	$\mathbb{P}_{10}^{I_1}$	$\mathbb{P}_{10}^{I_2}$	$\mathbb{P}_{10}^{L_1}$	$\mathbb{P}_{11}^{I_1}$	$\mathbb{P}_{11}^{I_2}$	$\mathbb{P}_{11}^{L_1}$	$\mathbb{P}_{12}^{I_1}$	$\mathbb{P}_{12}^{I_2}$	$\mathbb{P}_{12}^{L_1}$
0.9844	0.6527	0.3629	0.9919	0.7580	0.2508	0.9905	0.8590	0.1505	0.9838	0.7362	0.2793
13			14			15			16		
$\mathbb{P}_{13}^{I_1}$	$\mathbb{P}_{13}^{I_2}$	$\mathbb{P}_{13}^{L_1}$	$\mathbb{P}_{14}^{I_1}$	$\mathbb{P}_{14}^{I_2}$	$\mathbb{P}_{14}^{L_1}$	$\mathbb{P}_{15}^{I_1}$	$\mathbb{P}_{15}^{I_2}$	$\mathbb{P}_{15}^{L_1}$	$\mathbb{P}_{16}^{I_1}$	$\mathbb{P}_{16}^{I_2}$	$\mathbb{P}_{16}^{L_1}$
0.9876	0.5726	0.4398	0.9971	0.7835	0.2963	0.9949	0.5974	0.4077	0.9962	0.9508	0.0530
17			18			19			20		
$\mathbb{P}_{17}^{I_1}$	$\mathbb{P}_{17}^{I_2}$	$\mathbb{P}_{17}^{L_1}$	$\mathbb{P}_{18}^{I_1}$	$\mathbb{P}_{18}^{I_2}$	$\mathbb{P}_{18}^{L_1}$	$\mathbb{P}_{19}^{I_1}$	$\mathbb{P}_{19}^{I_2}$	$\mathbb{P}_{19}^{L_1}$	$\mathbb{P}_{20}^{I_1}$	$\mathbb{P}_{20}^{I_2}$	$\mathbb{P}_{20}^{L_1}$
0.9953	0.8908	0.1139	0.9957	0.8256	0.1788	0.9940	0.7425	0.2635	0.9962	0.8625	0.1412
21			22			23			24		
$\mathbb{P}_{21}^{I_1}$	$\mathbb{P}_{21}^{I_2}$	$\mathbb{P}_{21}^{L_1}$	$\mathbb{P}_{22}^{I_1}$	$\mathbb{P}_{22}^{I_2}$	$\mathbb{P}_{22}^{L_1}$	$\mathbb{P}_{23}^{I_1}$	$\mathbb{P}_{23}^{I_2}$	$\mathbb{P}_{23}^{L_1}$	$\mathbb{P}_{24}^{I_1}$	$\mathbb{P}_{24}^{I_2}$	$\mathbb{P}_{24}^{L_1}$
0.9970	0.9044	0.0986	0.5569	0.7201	0.7229	0.9987	0.7492	0.9252	0.9984	0.7740	0.9095
25			26			27			28		
$\mathbb{P}_{25}^{I_1}$	$\mathbb{P}_{25}^{I_2}$	$\mathbb{P}_{25}^{L_1}$	$\mathbb{P}_{26}^{I_1}$	$\mathbb{P}_{26}^{I_2}$	$\mathbb{P}_{26}^{L_1}$	$\mathbb{P}_{27}^{I_1}$	$\mathbb{P}_{27}^{I_2}$	$\mathbb{P}_{27}^{L_1}$	$\mathbb{P}_{28}^{I_1}$	$\mathbb{P}_{28}^{I_2}$	$R_{28}^{L_1}$
0.9986	0.7213	0.1136	0.9972	0.7445	0.2583	0.9963	0.7241	0.2797	0.9988	0.9179	0.0832
29			30								
$\mathbb{P}_{29}^{I_1}$	$\mathbb{P}_{29}^{I_2}$	$\mathbb{P}_{29}^{L_1}$	$\mathbb{P}_{30}^{I_1}$	$\mathbb{P}_{30}^{I_2}$	$\mathbb{P}_{30}^{L_1}$						
0.5381	0.9085	0.6354	0.9423	0.7286	0.2720						

Table 9
The geographical coordinates of the capital of 30 provinces in China in international standard plane coordinate system.

City	Latitude	Longitude	City	Latitude	Longitude
Beijing	39.92	116.46	Tianjin	39.13	117.2
Shanghai	31.22	121.48	Chongqing	29.59	106.54
Urumchi	43.77	87.68	Yinchuan	38.47	106.27
Hohhot	40.82	111.65	Nanning	22.84	108.33
Harbin	45.75	126.63	Changchun	43.88	125.35
Shenyang	41.8	123.38	Shijiazhuang	38.03	114.48
Taiyuan	37.87	112.53	Xining	36.56	101.74
Jinan	36.65	117	Zhengzhou	34.76	113.6
Nanjing	32.04	118.78	Hefei	31.86	117.27
Hangzhou	30.26	120.19	Fuzhou	26.08	119.3
Nanchang	28.68	115.89	Changsha	28.21	113
Wuhan	30.52	114.31	Guangzhou	23.16	113.23
Lanzhou	36.03	103.73	Xi'an	34.27	108.95
Chengdu	30.67	104.06	Guiyang	26.57	106.71
Kunming	25.04	102.73	Haikou	20.02	110.35

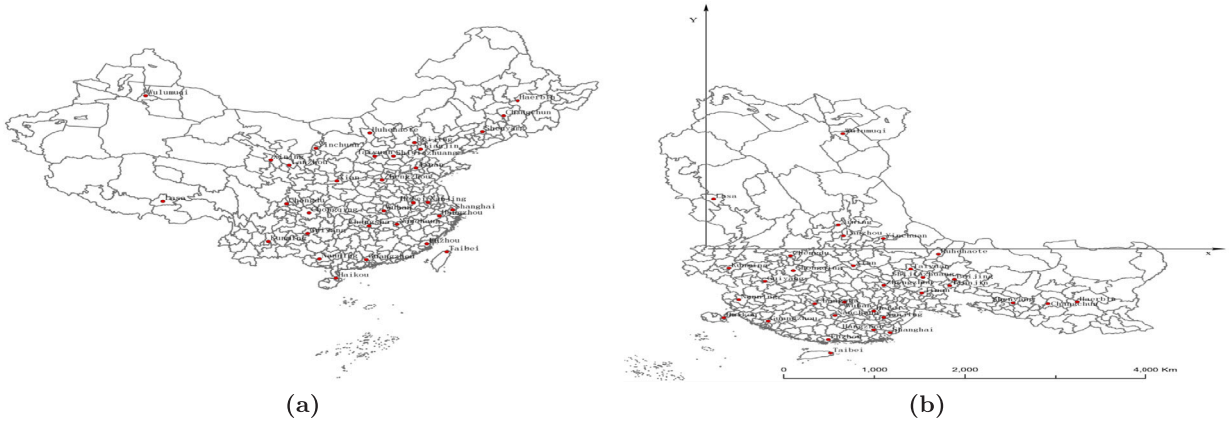

Fig. 5.6. (a) Map of China in international standard plane coordinate system; (b) Map of China in new standard plane coordinate system, which takes Heihe-Tengchong Line (Hu-Line) [45] as the horizontal axis and Tengchong city coordinates as the origin coordinates. The map was created in ArcGIS 9.2 software (ESRIInc.,Redlands, CA, USA).

Step 1. Drawing the Heihe-Tengchong Line, also known as the Hu-Line, according to the existing coordinates. We add the longitude and latitude values in the table to the points, generate Tengchong and Mohe points, create a new line layer, connect Tengchong and Mohe points, and form the Hu-Line (see Fig. 5.6(a));

Step 2. Drawing the coordinates of the provincial capital city into provincial capital city points. Adding the values in the provincial capital city table as points in ArcGIS;

Step 3. Projecting the provincial capital city and the Hu-Line. Projecting two layers into the WGS 1984 Web Mercator (auxiliary sphere) coordinate system in ArcGIS, then we calculate the projection coordinate values of points and lines using the calculation set tool (see Fig. 5.6(a));

Step 4. Using Tengchong city as the coordinate origin and the Hu-Line as the x-axis, construct a planar coordinate system to calculate the angle between the existing Hu-Line and the equator, which is 57.6197201 degrees. Rotate the existing coordinate system clockwise at this angle. Based on the original projected coordinate values, we calculate the relative coordinate systems of each provincial capital city point with Tengchong as the origin coordinates, and we obtain the final plane coordinates of each provincial capital, as shown in the Table 10.

Finally, we project the plane coordinates of 30 provinces/cites in Table 10 onto the X-axis (denoted by $x_k(k = 1, 2, \cdots, 30)$) and normalize them to a range between 0 and 1 after dimensionless transformation (i.e. $\bar{x}_k = x_k/\bar{x}, \bar{x} = \max\{x_k, k = 1, 2, \cdots, 30\}$), which shown in Table 11.

5.3.2. The initial values and some space-dependent parameters of system (2.1) estimations

In fact, model (5.10) is transformed from Model (2.1) in the discrete environment. Hence, we try to use the fitting results of the model (2.1) in Table 5 to estimate some space-dependent parameters in the model (2.1). Therefore, by using the least squares method, we can use MATLAB software to perform function fitting on discrete points to obtain the function expression of the parameters in the model (2.1) with respect to location x, which are shown in (5.12) and Fig. 5.7.

$$
\begin{aligned}
\eta_1(x) =& 0.416 + 9.12\times 10^{-9}\sin(\frac{15.923\pi x}{2}) + 0.097\cos(\frac{15.923\pi x}{2}),\\
\eta_2(x) =& 0.36021 - 0.285\sin(\frac{24.85\pi x}{2}) + 3.54\times 10^{-12}\cos(\frac{24.85\pi x}{2}),\\
\epsilon(x) =& 0.52, \omega(x) = -38.95 + 20.425e^{-0.1123x} + 18.755e^{0.1123x},\\
\alpha(x) =& 1.99\mathbf{B}(x|2,5) + 0.1, \mathbf{B}(x|2,5) \text{ is Beta distribution function},\\
\sigma(x) =& -0.439(-0.027\sin(0.3988\pi x + 0.4971) - 0.4412\sin(2\pi x + 0.8177)\\
&+ 0.3782\cos(4\pi x + 0.3771)\\
&+ 0.5651\sin(-0.3691\pi x + 0.211))e^{-0.05474x} + 0.4352,\\
\beta(x) =& -5.68\times 10^{-8}(-0.103 + 0.181\cos(\pi x - 0.35) + 0.2348\cos(3\pi x + 1.22)\\
&+ 0.203\cos(5\pi x - 0.35) + 0.152\sin(6\pi x + 0.867))e^{0.203x} + 4.5\times 10^{-8},\\
\gamma(x) =& 0.01126(5.39\times 10^{-5} - 8.07\times 10^{-6}\sin(0.08\pi x) - 8.07\times 10^{-6}\sin(2\pi x)\\
&+ 1.126\times 10^{-6}\cos(4\pi x))e^{0.7144x} - 1.1\times 10^{-8}.
\end{aligned}
\tag{5.12}
$$

In addition, we choose $d(x) = \bar{d}$, $\mu(x) = \bar{\mu}$, $\Lambda(x) = \bar{\mu}\sum_{k=1}^{30} N_k$, where $\bar{\mu}$ and $\bar{d}$ are the average values of μ_k and d_k, respectively, $k = 1, 2, \ldots, 30$.

Table 10
The plane coordinates of the capital of 30 provinces in China in the new plane coordinate system.

City	Y-axis(meter)	X-axis(meter)	City	Y-axis(meter)	X-axis(meter)
Beijing	−632194.2691	2738240.241	Tianjin	−762820.5759	2686069.91
Shanghai	−1743006.606	2030032.54	Chongqing	−451162.3325	961 692.3256
Urumchi	2381684.561	1508599.259	Yinchuan	214 228.6723	1954855.18
Hohhot	−109577.6762	2562546.015	Nanning	−1068368.296	360 470.2974
Harbin	−1113769.473	4092813.641	Changchun	−1150608.174	3768653.115
Shenyang	−1134541.941	3384493.687	Shijiazhuang	−591000.8203	2391626.453
Taiyuan	−419776.2903	2256300.791	Xining	496 528.9935	1458397.201
Jinan	−931390.3117	2378671.223	Zhengzhou	−755222.2373	1960129.572
Nanjing	−1431763.485	1959609.691	Hefei	−1302454.018	1849647.003
Hangzhou	−1688320.872	1848122.568	Fuzhou	−1887426.096	1349143.832
Nanchang	−1392271.724	1421154.829	Changsha	−1152447.423	1198613.821
Wuhan	−1117569.096	1525918.906	Guangzhou	−1508296.093	685 268.2906
Haikou	−1438895.732	196 056.3683	Lanzhou	270 245.1428	1515211.837
Xi'an	−348824.2408	1624029.951	Chengdu	−143571.0605	931 241.113
Guiyang	−671239.8721	649 978.7818	Kunming	−398396.7214	252 933.3667

Table 11
The X-axis of 30 provinces/cites (denoted by $x_k, k = 1, 2, \ldots, 30$) under dimensionless transformation.

$\tilde{x}_k$	$\tilde{x}_1$	$\tilde{x}_2$	$\tilde{x}_3$	$\tilde{x}_4$	$\tilde{x}_5$	$\tilde{x}_6$	$\tilde{x}_7$	$\tilde{x}_8$	$\tilde{x}_9$	$\tilde{x}_{10}$
Value	1.00	0.92	0.83	0.67	0.66	0.63	0.58	0.57	0.55	0.50
$\tilde{x}_k$	$\tilde{x}_{11}$	$\tilde{x}_{12}$	$\tilde{x}_{13}$	$\tilde{x}_{14}$	$\tilde{x}_{15}$	$\tilde{x}_{16}$	$\tilde{x}_{17}$	$\tilde{x}_{18}$	$\tilde{x}_{19}$	$\tilde{x}_{20}$
Value	0.48	0.47	0.46	0.45	0.43	0.40	0.39	0.38	0.36	0.34
$\tilde{x}_k$	$\tilde{x}_{21}$	$\tilde{x}_{22}$	$\tilde{x}_{23}$	$\tilde{x}_{24}$	$\tilde{x}_{25}$	$\tilde{x}_{26}$	$\tilde{x}_{27}$	$\tilde{x}_{28}$	$\tilde{x}_{29}$	$\tilde{x}_{30}$
Value	0.33	0.29	0.24	0.23	0.17	0.16	0.09	0.06	0.05	0.02

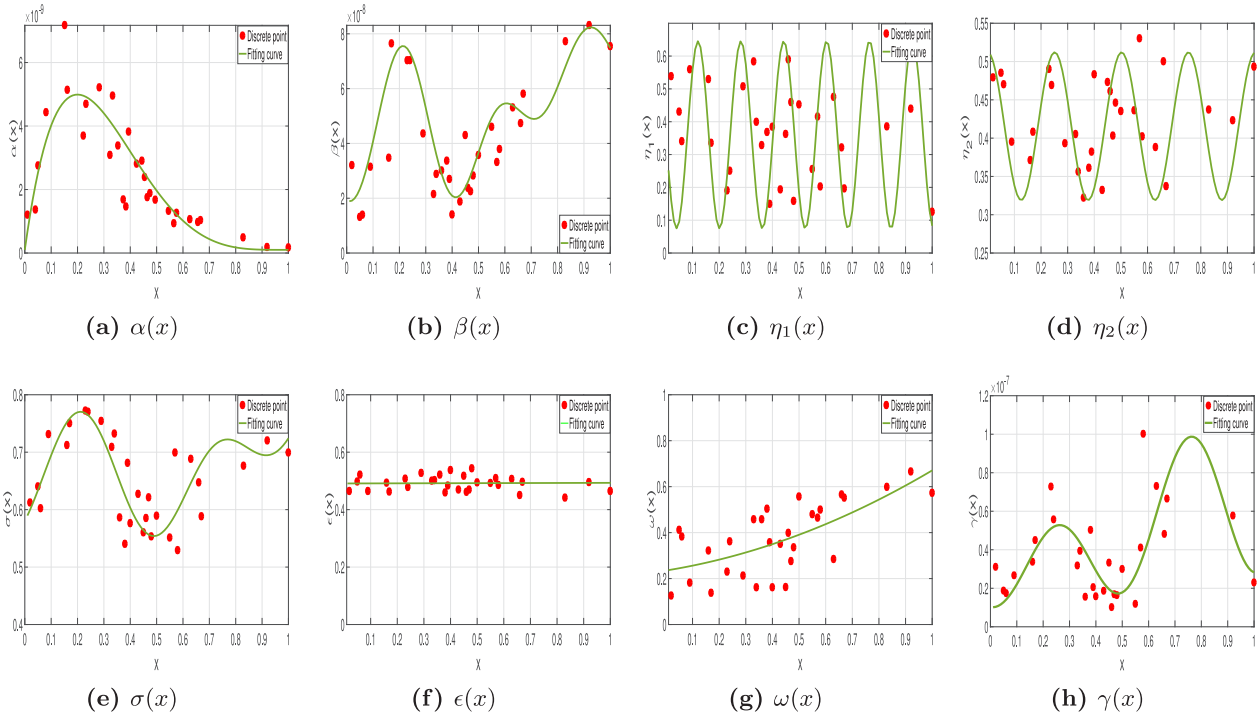

Fig. 5.7. The fitting curves of some estimated parameters of system (2.1) by using the values of parameters in Table 5 and the plane coordinates of 30 provinces/cites in Table 11.

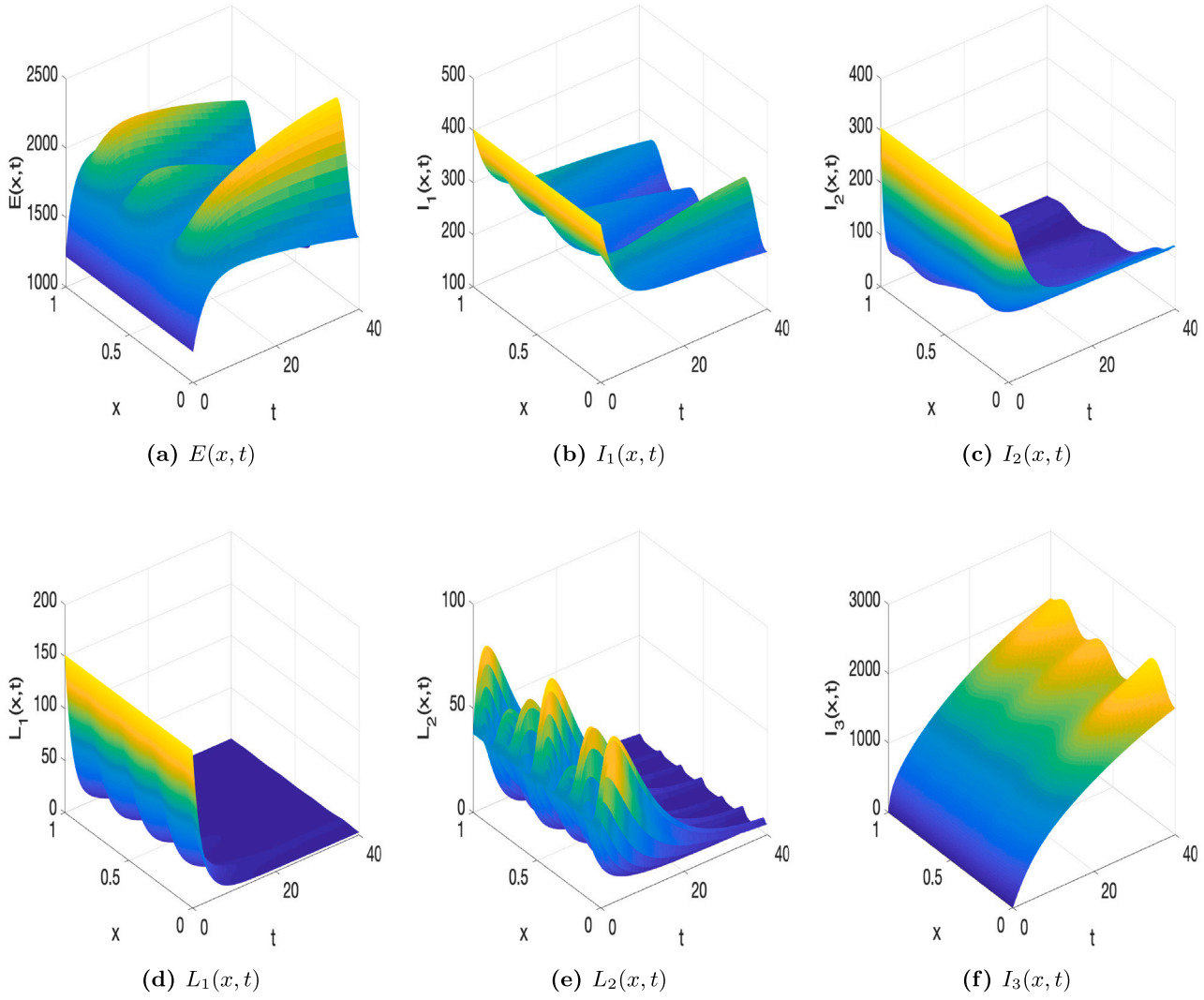

(a) $E(x,t)$ (b) $I_1(x,t)$ (c) $I_2(x,t)$

(d) $L_1(x,t)$ (e) $L_2(x,t)$ (f) $I_3(x,t)$

Fig. 5.8. The spatial distribution of $E(x,t), I_m(x,t), L_k(x,t), m = 1,2,3, k = 1,2$ when $R_0 > 1$. The value of model parameters are the same as in Eqs. (5.12).

Moreover, we can obtain the following initial values of model (2.1) from Tables 1 and 6.

$$\phi_1(x) = \sum_{k=1}^{30} S_k(0)/100,\ \phi_2(x) = \sum_{k=1}^{30} E_k(0)/100,\ \phi_3(x) = \sum_{k=1}^{30} I_{1k}(0)/100,$$
$$\phi_4(x) = \sum_{k=1}^{30} I_{2k}(0)/100,$$
$$\phi_5(x) = \sum_{k=1}^{30} L_{1k}(0)/100,\ \phi_6(x) = \sum_{k=1}^{30} L_{2k}(0)/100,\ \phi_7(x) = \sum_{k=1}^{30} I_{3k}(0)/100, \tag{5.13}$$

Applying the calculation method of the basic reproduction number for reaction–diffusion epidemic model, as mentioned in [24], we can obtain the value of the basic reproduction number of model (2.1) with the parameters given in Eqs. (5.12), $\mathcal{R}_0 \approx 2.2572$. This numerical result is within the estimation range of the basic reproduction number of the corresponding discrete space dispersal model (5.10) (see Fig. 5.3). In Fig. 5.8, we display the spatial distribution of $E(x,t), I_m(x,t), L_k(x,t), m = 1,2,3, k = 1,2$ when $R_0 > 1$. In this figure, we can see that the distribution of the infected compartments is far from the zero plane as t increases. This implies that the disease will be uniformly persistent, which is in line with the theoretical result in Theorem 4.4. Furthermore, from Fig. 5.9, we can see that the spatially continuous heterogeneous reaction–diffusion model (2.1) fits the actual reported cases very well. This indicates that it is very reasonable to obtain the parameter values of the model by fitting the actual cases of different regions to model (5.10) in discrete space and then estimate the functional form of the space-dependent parameters of model (2.1) in Eqs. (5.12). This is also a problem ignored in previous related work: how to apply real data to perform a space-structured compartmental epidemic model that can reflect the actual syphilis transmission situation. This numerical scheme can also be extended to other epidemic models.

5.3.3. *Contribution to cumulative four-stage cases*

In this subsection, we study the contributions to cumulative primary, secondary, latent and tertiary stage syphilis cases from the four-stage syphilis cases, which are defined as $\frac{\bar{I}_1(t)}{\bar{I}_1(t)+\bar{I}_2(t)+\bar{L}(t)+\bar{I}_3(t)}$, $\frac{\bar{I}_2(t)}{\bar{I}_1(t)+\bar{I}_2(t)+\bar{L}(t)+\bar{I}_3(t)}$, $\frac{\bar{L}(t)}{\bar{I}_1(t)+\bar{I}_2(t)+\bar{L}(t)+\bar{I}_3(t)}$ and $\frac{\bar{I}_3(t)}{\bar{I}_1(t)+\bar{I}_2(t)+\bar{L}(t)+\bar{I}_3(t)}$, respectively. Here $\bar{I}_m(t) = \int_\Omega I_m(x,t)dx$, $\bar{L}(t) = \int_\Omega (L_1(x,t) + L_2(x,t))dx, m = 1,2,3$. In Fig. 5.10, we set the parameter values the same as given in Eqs. (5.12) expect for $\zeta_k(x), k = 1,2$. Then we observe that the contributions to cumulative syphilis latent infected cases are 90.28%, 80.8%, 63.97%, 32.97% when the progression rates ζ_1 and ζ_2 are fixed as $364/46$, $365/(46 \times 3), 365/(46 \times 4), 365/(46 \times 6)$ and $365/108, 365/(108 \times 2)$, $365/(108 \times 2.5), 365/(108 \times 4)$, respectively. That is, the smaller the

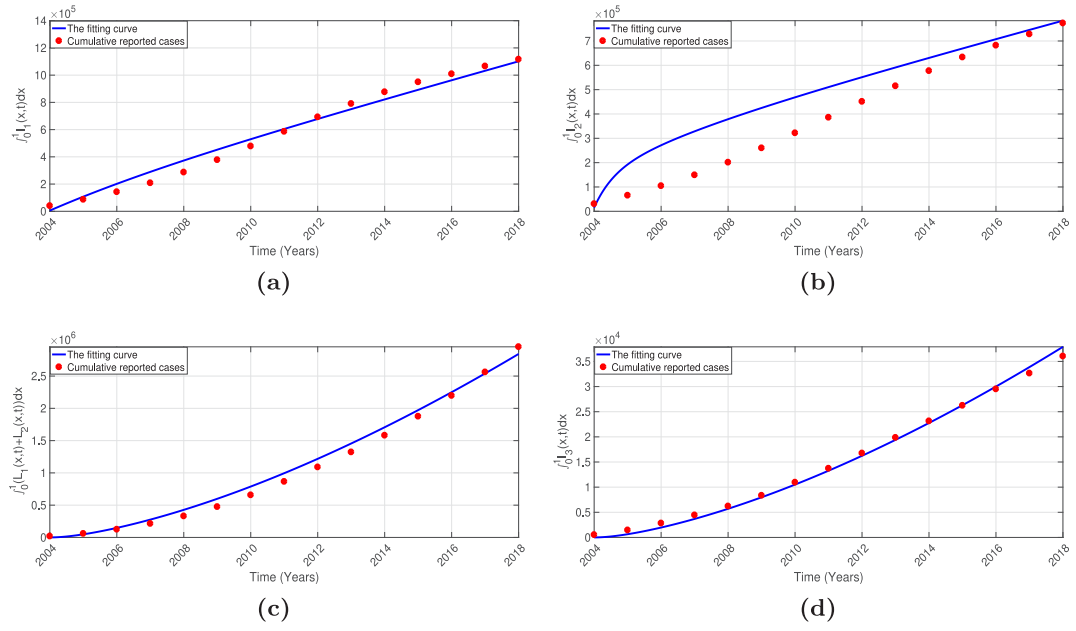

Fig. 5.9. Fitting cures of the total cumulative primary, secondary, latent and tertiary stage syphilis reported cases from 2004 to 2018 by model (2.1) under the initial condition (5.13) and with model parameters given in Eqs. (5.12).

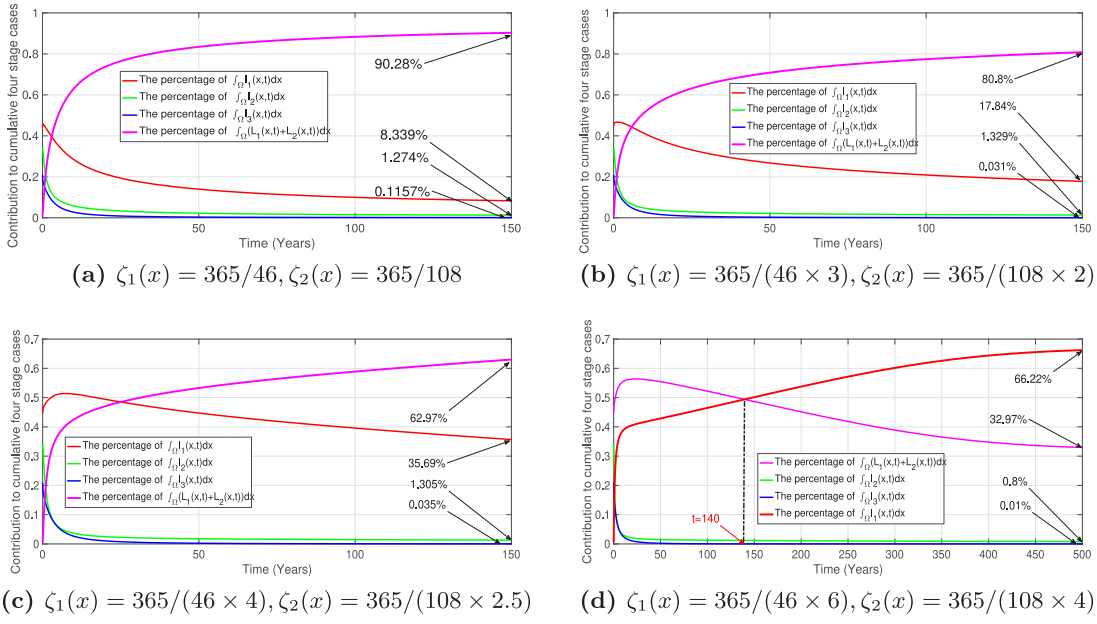

Fig. 5.10. The contribution to cumulative primary, secondary, latent and tertiary stage cases with all the other parameters being the same as given in Eqs. (5.12).

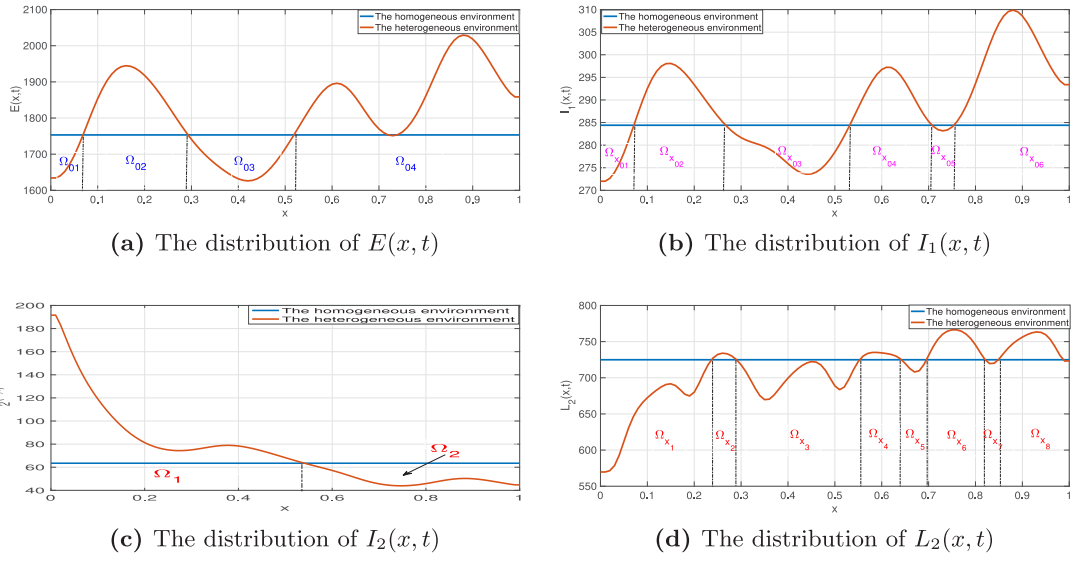

(a) The distribution of $E(x,t)$ (b) The distribution of $I_1(x,t)$

(c) The distribution of $I_2(x,t)$ (d) The distribution of $L_2(x,t)$

Fig. 5.11. Distribution of exposed, primary, secondary and latent stages infected individuals for homogeneous model (5.14) and heterogeneous model (2.1) at time $t = 40$, respectively.

progression rate is, the lower the percentage of $\bar{L}(t)$ among the total cumulative syphilis reported cases is. This implies that the intensive treatment of latent syphilis infected individuals can effectively reduce the proportion of these infected individuals, thereby effectively reduce the syphilis infection risk among population, which is in line with the conclusion of Section 5.2.2.

5.3.4. The influence of the spatial heterogeneity on the transmission of syphilis

To study the influence of the spatial heterogeneity on the transmission of syphilis, we first give the following model with constant diffusion coefficients and parameters:

$$\begin{cases} \dfrac{\partial S(x,t)}{\partial t} = d_1 \Delta S(x,t) + \lambda S(x,t) - \hat{\alpha} I_1(x,t) S(x,t) - \hat{\beta} I_2(x,t) S(x,t) \\ \qquad - \hat{\gamma} L_1(x,t) S(x,t) - \mu S(x,t), \\ \dfrac{\partial E(x,t)}{\partial t} = d_2 \Delta E(x,t) + \hat{\alpha} I_1(x,t) S(x,t) + \hat{\beta} I_2(x,t) S(x,t) \\ \qquad + \hat{\gamma} L_1(x,t) S(x,t) - (\mu + \delta) E(x,t), \\ \dfrac{\partial I_1(x,t)}{\partial t} = d_3 \Delta I_1(x,t) + \delta E(x,t) + (1-\epsilon)\hat{\omega} L_1(x,t) - (\mu + \zeta_1) I_1(x,t), \\ \dfrac{\partial I_2(x,t)}{\partial t} = d_4 \Delta I_2(x,t) + \zeta_1 I_1(x,t) + \epsilon \hat{\omega} L_1(x,t) - (\mu + \zeta_2 + \sigma) I_2(x,t), \\ \dfrac{\partial L_1(x,t)}{\partial t} = d_5 \Delta L_1(x,t) + \zeta_2 I_2(x,t) - (\mu + \omega + \hat{\eta}_1) L_1(x,t), \\ \dfrac{\partial L_2(x,t)}{\partial t} = d_6 \Delta L_2(x,t) + \hat{\eta}_1 L_1(x,t) - (\mu + \hat{\eta}_2) L_2(x,t), \\ \dfrac{\partial I_3(x,t)}{\partial t} = d_7 \Delta I_3(x,t) + \hat{\eta}_2 L_2(x,t) + \hat{\sigma} I_2(x,t) - (\mu + d) I_3(x,t), \\ \partial_\nu S = \partial_\nu I_m = \partial_\nu L_k = 0, \quad m = 1,2,3, \quad k = 1,2, \end{cases} \tag{5.14}$$

where $\hat{\eta}_k, \hat{\alpha}, \hat{\beta}, \hat{\gamma}, \hat{\sigma}, \hat{\gamma}$ represent the average of $\eta_1(x), \eta_2(x), \omega(x), \alpha(x), \sigma(x), \beta(x), \gamma(x)$, which defined as $\hat{\eta}_k = \frac{\int_\Omega \eta_k(x)dx}{|\Omega|}, k = 1,2, \hat{\omega} = \frac{\int_\Omega \omega_{(x)}dx}{|\Omega|}, \hat{\beta} = \frac{\int_\Omega \beta_{(x)}dx}{|\Omega|}, \hat{\alpha} = \frac{\int_\Omega \alpha_{(x)}dx}{|\Omega|}, \hat{\beta} = \frac{\int_\Omega \beta_{(x)}dx}{|\Omega|}, \hat{\gamma} = \frac{\int_\Omega \gamma_{(x)}dx}{|\Omega|}$.

The density distribution of infected individuals (exposed, primary, secondary and latent stages) in homogeneous and heterogeneous environments at time $t = 40$ and $x = 0.5$ are shown in Figs. 5.11 and 5.12, respectively. On the one hand, as can be seen from Fig. 5.11(a)–(b), in regions $\Omega_{02}, \Omega_{04}, \Omega_{x_{02}}, \Omega_{x_{04}}, \Omega_{x_{06}}, \Omega_1, \Omega_{x_2}, \Omega_{x_4}, \Omega_{x_6}, \Omega_{x_8}$, the densities of syphilis infected individuals (exposed, primary, secondary and latent stages) in model (2.1) are higher than that in model (5.14). In regions $\Omega_{01}, \Omega_{03}, \Omega_{x_{01}}, \Omega_{x_{03}}, \Omega_{x_{05}}, \Omega_2, \Omega_{x_1}, \Omega_{x_3}, \Omega_{x_5}, \Omega_{x_7}$, the densities of syphilis infected individuals (exposed, primary, secondary and latent stages) in model (2.1) are less than that in model (5.14). Obviously, if we use the spatially homogeneous model to describe the situation of the syphilis disease, we will be unable to describe the regional differences caused by spatial heterogeneity. On the other hand, in Figs. 5.12 (b)–(d), we can see that the densities of infectious individuals in model (2.1) are more than that in model (5.14) at position $x = 0.5$. This means that if we ignore spatial heterogeneity, we will underestimate the prevalence of the disease and the number of infected individuals.

Next, we study dynamics of system (5.14) for the case of heterogeneous diffusion (high-low diffusion) which can be used as a benchmark and may facilitate to identify the factor determining whether traveling waves can be observed. To this end, we consider the following high-low diffusion mentioned in [25]

$$d_i(x) = d_i D(x), \quad D(x) = \frac{13}{6}\arctan(x - 0.5) + \frac{15}{4}, \quad x \in [0,1], \ i = 1,2,\dots,7. \tag{5.15}$$

In this case, we divide the spatial domain $\Omega = [0,1]$ into two subintervals letting $[0, 0.5]$ represent the low diffusion region and $(0.5, 1]$ the high diffusion region. Moreover, we give the following stepwise initial conditions

$$\phi(x) = (\phi_1(x), \cdots, \phi_7(x)) = \begin{cases} (\tilde{S}, \tilde{E}, \tilde{I}_1, \tilde{I}_2, \tilde{L}_1, \tilde{L}_2, \tilde{I}_3), x \in [0, 0.3], \\ (\dfrac{\lambda}{\mu}, 0, 0, 0, 0, 0, 0), x \in (0.3, 1], \end{cases} \tag{5.16}$$

$$\phi(x) = (\phi_1(x), \cdots, \phi_7(x)) = \begin{cases} (\tilde{S}, \tilde{E}, \tilde{I}_1, \tilde{I}_2, \tilde{L}_1, \tilde{L}_2, \tilde{I}_3), x \in [0.2, 0.8], \\ (\dfrac{\lambda}{\mu}, 0, 0, 0, 0, 0, 0), x \in [0, 0.2) \cup (0.8, 1], \end{cases} \tag{5.17}$$

$$\phi(x) = (\phi_1(x), \cdots, \phi_7(x)) = \begin{cases} (\tilde{S}, \tilde{E}, \tilde{I}_1, \tilde{I}_2, \tilde{L}_1, \tilde{L}_2, \tilde{I}_3), x \in [0, 0.2) \cup (0.8, 1], \\ (\dfrac{\lambda}{\mu}, 0, 0, 0, 0, 0, 0), x \in [0.2, 0.8], \end{cases} \tag{5.18}$$

where $(\tilde{S}, \tilde{E}, \tilde{I}_1, \tilde{I}_2, \tilde{L}_1, \tilde{L}_2, \tilde{I}_3)$ is the positive equilibrium of system (5.14).

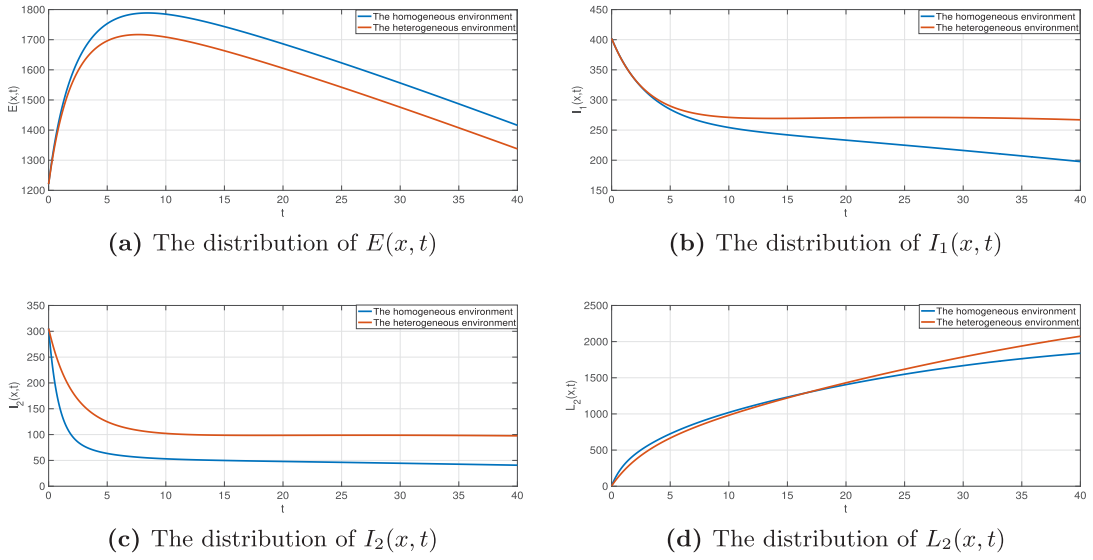

(a) The distribution of $E(x,t)$ (b) The distribution of $I_1(x,t)$

(c) The distribution of $I_2(x,t)$ (d) The distribution of $L_2(x,t)$

Fig. 5.12. Distribution of exposed, primary, secondary and latent stages infected individuals for homogeneous model (5.14) and heterogeneous model (2.1) at location $x = 0.5$, respectively.

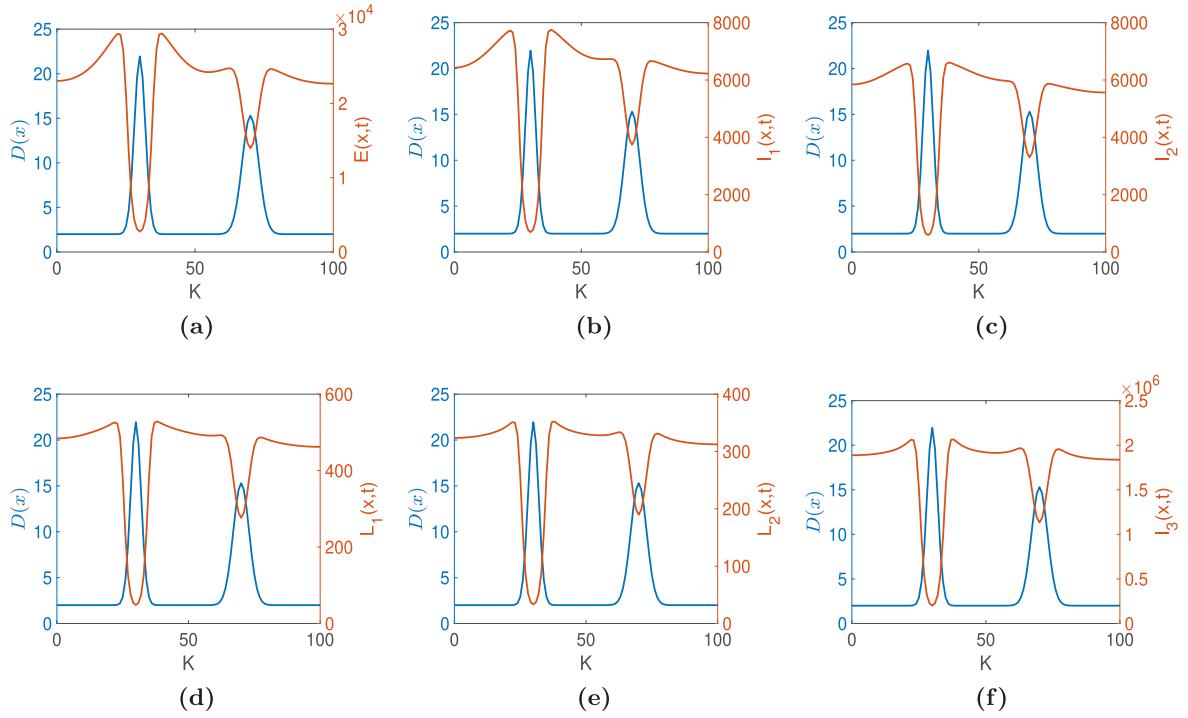

Fig. 5.13. Red curve: steady state of infected individuals with the initial condition and diffusion rate given in (5.13) and (5.19), respectively; Blue curve: diffusion rate $D(x)$. The value of the other parameters are the same as in system (5.14).

The long-term spatial diffusion of infected individuals under the three different initial conditions (5.16)–(5.18) are displayed in Figs. 5.14–5.16, respectively. In these figures, we can see that there is little difference among steady states, which indicates that the initial conditions exert a limited influence on the long-term spatial distribution of syphilis-infected individuals in the high-low diffusion case.

Motivated by [25], we introduce the following Gaussian-type diffusion rate:

$$d_i(x) = d_i D(x), \quad D(x) = 2 + \frac{50}{\sqrt{2\pi}} \exp\left(-\frac{(x-0.3)^2}{8}\right) + \frac{100}{3\sqrt{2\pi}} \exp\left(-\frac{(x-0.7)^2}{18}\right). \tag{5.19}$$

The spatial distribution of infected individuals with Gaussian diffusion under the initial condition (5.13) is shown in Fig. 5.13. The diffusion rate is a function with respect to two Gaussian distributions (see blue curves in Fig. 5.13) and it has two peaks. From these figures, we can see that a local minimum of the steady state distribution of infected individuals corresponds to a local maximum of the diffusion rate. This means that the number of infected individuals at the steady state is small at a location where the diffusion rate is large. In fact, this seems reasonable since the infected individuals with a large diffusion rate tend to disperse far away so that the infected population at the original location becomes smaller and hence the infection risk of syphilis will decrease for the susceptible individuals at that location leading to fewer

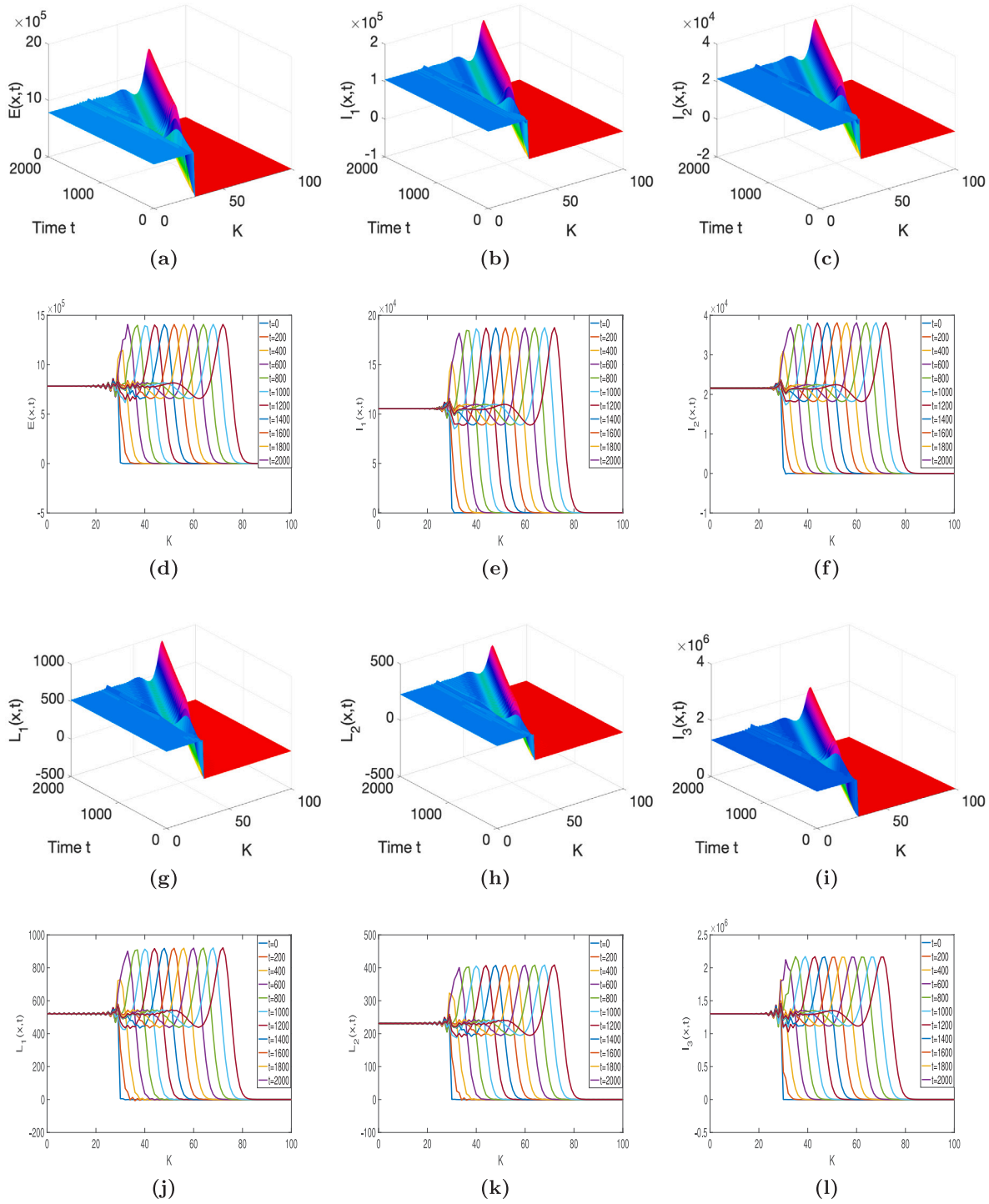

Fig. 5.14. The spatial distribution of exposed, primary, secondary, late latent and tertiary stages of infected individuals with the initial condition and diffusion rate given in (5.15) and (5.16), respectively. The value of the other parameters are the same as in system (5.14).

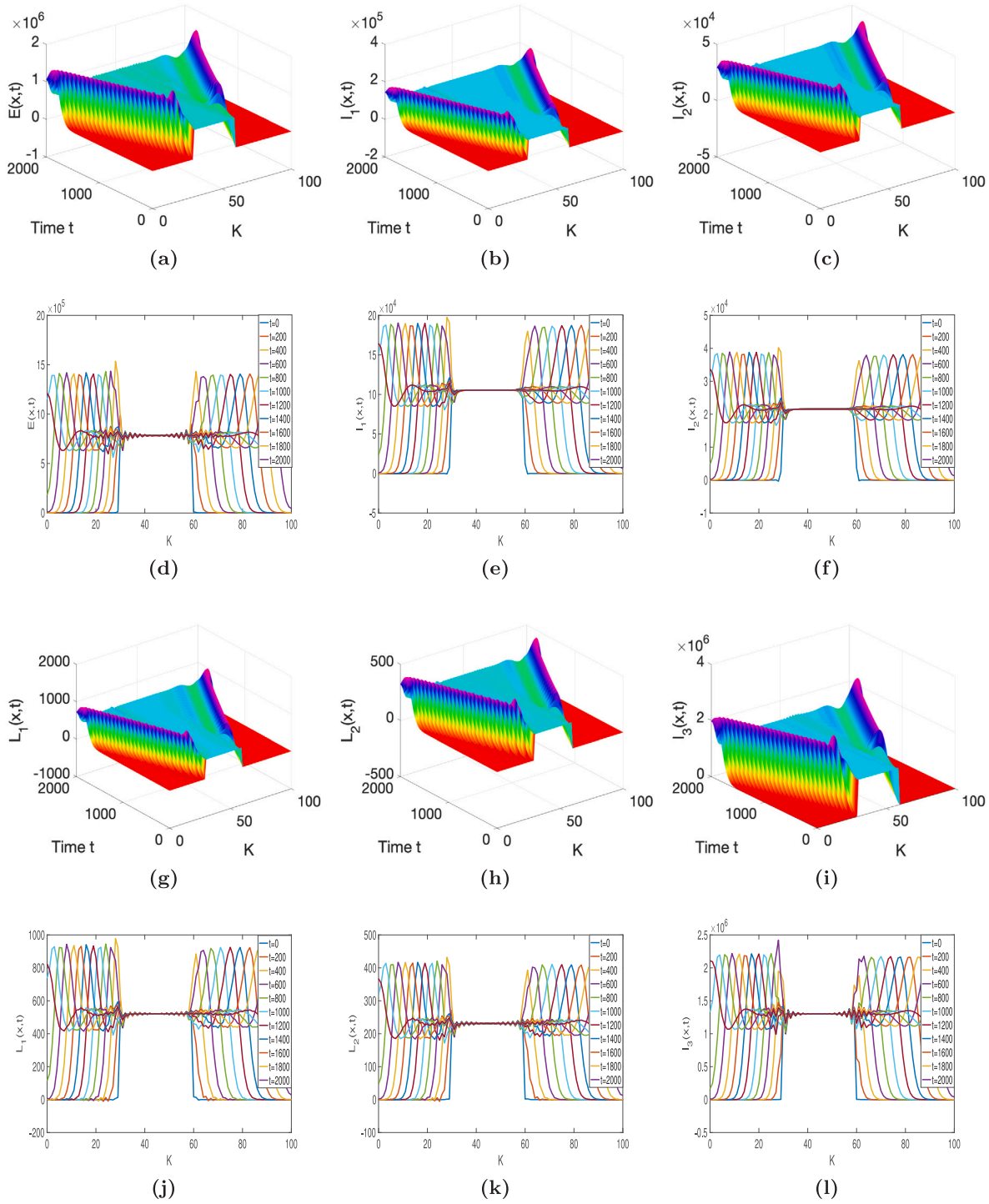

Fig. 5.15. The spatial distribution of exposed, primary, secondary, late latent and tertiary stages of infected individuals with the initial condition and diffusion rate given in (5.15) and (5.17), respectively. The value of the other parameters are the same as in system (5.14).

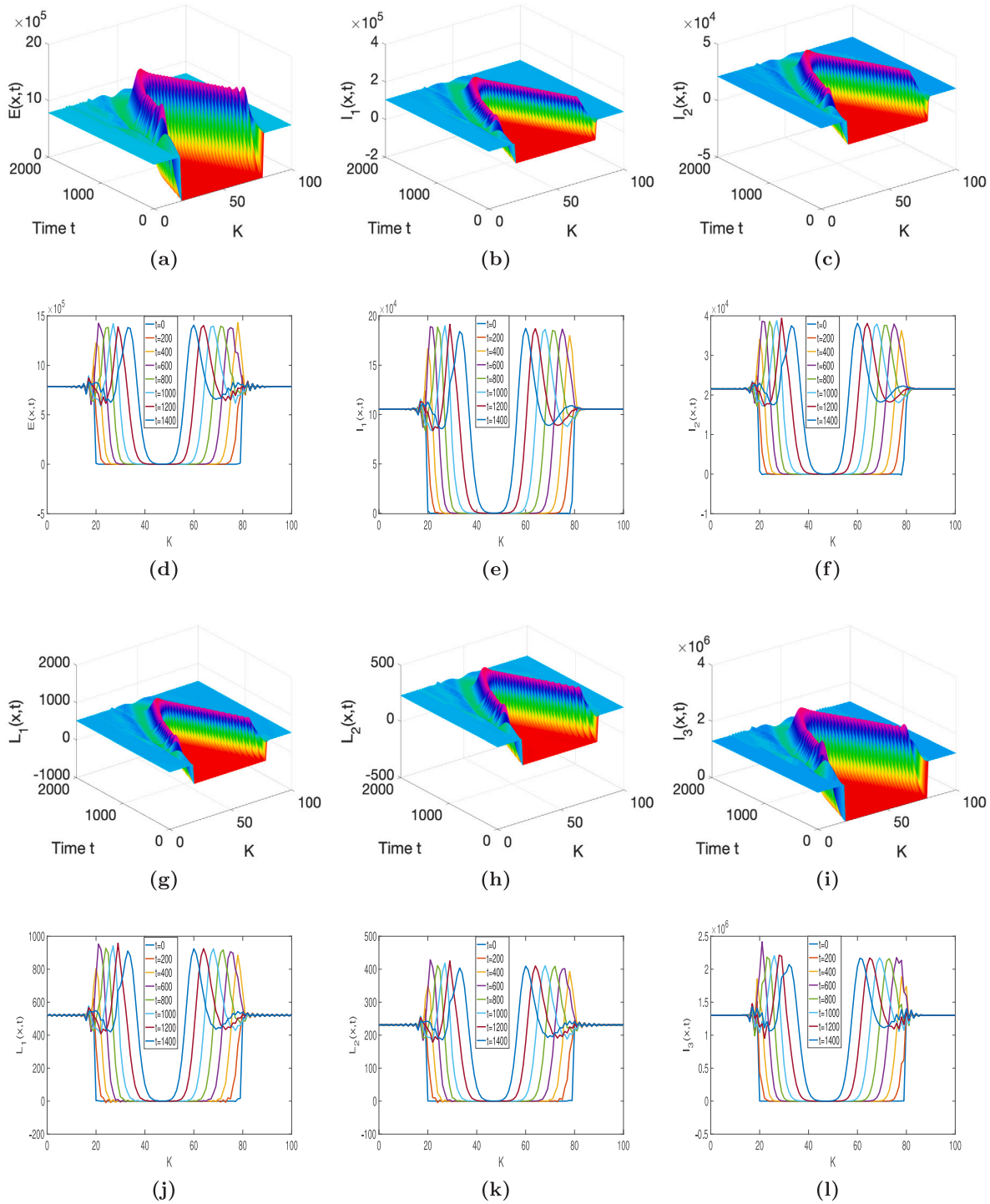

Fig. 5.16. The spatial distribution of exposed, primary, secondary, late latent and tertiary stages of infected individuals with the initial condition and diffusion rate given in (5.15) and (5.18), respectively. The value of the other parameters are the same as in system (5.14).

infected individuals there. On the contrary, at the location where the diffusion rate is small, the infection risk will increase for the susceptible individuals at that location leading to more infected individuals there (i.e., the effective contact rate between susceptible and infected individuals is high due to the low diffusion rate at the location).

6. Discussion

Our study addresses a notable research gap in the field of disease modeling, specifically concerning the often overlooked aspect of spatial diffusion in disease spread. While some studies have underscored the impact of spatial heterogeneity on syphilis transmission in China, the effects of spatial diffusion in a heterogeneous environment have received limited attention within the realm of mathematical modeling. This gap is particularly challenging to bridge due to the inherent difficulties in incorporating real reported data into numerical simulations of reaction–diffusion models, especially when dealing with diverse data from various regions within a country. To tackle this challenge, our paper introduces an innovative approach that transforms the reaction–diffusion model into a patch model within a discrete space framework. Leveraging a multi-objective Markov Chain Monte Carlo (MCMC) method, we successfully fit the model with actual case data, overcoming the hurdles associated with diverse and complex datasets. The parameter values obtained from the patch model inform the space-dependent parameter values of the continuous space reaction–diffusion model, ensuring the model's validity. This methodological innovation not only contributes to the refinement of our understanding of syphilis transmission dynamics but also provides a robust framework for addressing similar challenges in modeling the spread of infectious diseases in heterogeneous environments.

We have contributed to the understanding of syphilis transmission dynamics by developing a spatially continuous reaction–diffusion model that incorporates general incidences within a heterogeneous environment. The primary objective was to explore the nuanced impact of spatial heterogeneity and assess the effectiveness of intervention strategies in eradicating syphilis transmission within a population. Our theoretical analysis commenced with the derivation of the functional expression for the basic reproduction number. This key epidemiological metric serves as a fundamental threshold for disease dynamics. Subsequently, we demonstrated the global stability of the disease-free steady state and the uniform persistence of the disease, providing essential insights into the long-term behavior of syphilis transmission in spatially diverse populations.

For the numerical simulation, we transitioned from the spatially continuous reaction–diffusion model to a spatially discrete dispersal multi-patch model. This model was parameterized using reported syphilis cases spanning 30 provinces and cities in China from 2004 to 2018. The multi-objective Markov Chain Monte Carlo (MCMC) method facilitated the estimation of crucial parameters, resulting in the computation of the basic reproduction number (R_0) at 2.1753, with a 95% confidence interval of (1.9133, 2.2687). The utilization of MCMC in fitting a multi-patch model to real-world data underscores the robustness and reliability of our approach.

Beyond these foundational analyses, we delved into the challenges and complexities of fitting a multi-patch model to actual reported data, highlighting the intricacies involved in this process. Under certain assumptions, we translated the estimated parameters of the patch model into the functional form of space-dependent parameters in the reaction–diffusion model. This allowed us to calculate an approximate R_0 of 2.2572 for the reaction–diffusion model, aligning closely with the R_0 value derived from the patch model. The successful fitting of cumulative syphilis reported cases using the reaction–diffusion model further affirms its credibility and utility in capturing real-world transmission dynamics.

Our numerical simulations provided a detailed examination of both the reaction–diffusion model and the corresponding patch model. By calculating the isolated reproduction number of the patch model and quantifying the underestimation proportions of each syphilis-infected stage (primary, secondary, latent, and tertiary), we identified additional high-incidence regions for syphilis in China, namely Xinjiang, Guizhou, Hunan, and Northeast China, in addition to the original high-incidence regions. Significantly, our findings underscore the critical role of accounting for the transmission of latent stage syphilis-infected individuals, as neglecting this aspect leads to substantial underestimation of syphilis outbreaks.

Furthermore, our comprehensive discussion of the impacts of spatial heterogeneity, including considerations of initial conditions and space-dependent diffusion rates, on syphilis transmission emphasizes the resilience of long-term spatial distribution patterns against variations in initial conditions. Neglecting spatial heterogeneity could result in a systematic underestimation of syphilis prevalence and the number of infected individuals, highlighting the importance of integrating spatial dynamics into public health strategies aimed at controlling and preventing syphilis transmission in China. In summary, our study provides crucial insights into the nuanced interplay of spatial factors in syphilis transmission dynamics, emphasizing the indispensability of considering these factors for effective public health measures and policy implementation.

While our study makes significant strides in advancing the understanding of syphilis transmission dynamics within a spatially heterogeneous environment, it is imperative to acknowledge certain limitations inherent in our approach. Firstly, our model relies on reported syphilis cases from 2004 to 2018 in China, and the accuracy of these data is subject to variations in reporting practices and healthcare-seeking behavior. Additionally, the spatial distribution of reported cases may be influenced by factors such as healthcare infrastructure, testing accessibility, and public awareness, potentially introducing biases into our model. Furthermore, the simplifying assumptions made to facilitate the numerical simulations, such as uniform diffusivity and homogeneous mixing within patches, may not fully capture the intricate real-world dynamics of syphilis transmission. Moreover, our study focuses on the spatial dynamics within China, and the applicability of our findings to other regions or countries may require careful consideration of contextual differences. Despite these limitations, our work lays the groundwork for future refinements and extensions of spatially explicit disease models, contributing to the ongoing discourse on effective strategies for preventing and controlling syphilis transmission.

Our current study opens avenues for several promising directions in future research that can enhance our understanding of syphilis transmission dynamics and contribute to more effective public health interventions. Firstly, refining our model by incorporating additional socio-demographic [46,47] and behavioral factors [48] can provide a more subtle representation of syphilis dynamics, enabling a comprehensive understanding of the intricate interplay between various influencing factors. This refinement sets the stage for exploring the impact of temporal changes in spatial patterns and population mobility on disease transmission, offering the potential to yield insights into the evolving nature of syphilis outbreaks. Additionally, recent progress in data science, particularly the integration of machine learning techniques (see, e.g., [49,50]), offers exciting opportunities for improving the accuracy of disease forecasting. Moreover, investigating the sensitivity of the basic reproduction number to various parameters through advanced sensitivity analysis methods [51] can provide a more comprehensive understanding of the factors influencing syphilis transmission. Besides, integrating real-time data sources, such as social media or mobile health applications, could enhance the accuracy and timeliness of model predictions, offering a dynamic and adaptive approach to monitoring and controlling syphilis spread. Furthermore, extending our approach to consider other sexually transmitted infectious diseases with similar spatial characteristics would broaden the applicability of our findings. Collaborative efforts between mathematical modelers

Table 12
The reported primary stage syphilis cases for 30 provinces/cities in China from 2004 to 2018.
Source: Data from [33].

Cases	2004	2005	2006	2007	2008	2009	2010	2011	2012	2013	2014	2015	2016	2017	2018
Beijing	510	601	737	950	690	829	930	808	760	773	742	550	506	510	471
Tianjin	281	282	896	308	492	609	663	596	595	560	470	392	257	311	282
Hebei	186	260	303	345	461	593	811	1297	1709	1888	1976	2096	1850	1898	1844
Shanxi	622	686	904	972	1093	1056	1120	1129	1642	1562	1682	1068	959	1007	967
InnerMongolia	365	707	961	1107	1318	1436	1721	1950	2548	3068	3022	2588	2218	2247	2092
Liaoning	939	1075	1488	1860	2274	2942	4308	5064	5175	5393	4953	4019	3178	3296	2864
Jilin	701	688	831	1279	1830	1931	2317	3338	2980	2638	2065	1645	1354	1095	1127
Heilongjiang	973	976	1100	1653	2040	2294	2621	2990	3184	3344	3397	2921	2657	2280	2184
Shanghai	2459	2675	3039	3588	4011	3769	3723	3535	3242	3063	2923	2998	3086	2628	2167
Jiangsu	2918	3215	4416	5817	7441	8432	7524	6616	5844	5663	5674	4825	4275	4252	4059
Zhejiang	6162	6952	8843	10 690	13 412	14 973	17 009	14 675	9969	8132	6573	4689	4309	4032	2964
Anhui	1285	1178	1762	1994	2067	2793	3151	3963	4253	4024	3805	3832	3293	3315	2766
Fujian	3508	2873	2854	3257	3993	3987	3841	3819	3809	4001	4049	3197	1832	1700	1454
Jiangxi	787	895	910	1070	1196	1445	1382	1667	1494	1630	1996	1484	1217	1337	632
Shandong	805	744	783	936	1203	1665	1896	2189	2570	3201	3563	3332	2984	3024	2595
Henan	837	971	1229	1646	2178	2729	3547	4553	6137	5644	4051	3177	2372	2511	2766
Hubei	632	830	1004	1292	2070	2496	2639	2671	2590	1862	1683	1665	1326	1151	1054
Hunan	699	1041	1434	1833	2540	3547	4502	5263	6441	5365	3324	2104	1487	1717	1243
Guangdong	3833	5922	6297	6422	6803	7418	8180	8853	8445	7736	7145	5268	4065	3795	3182
Guangxi	5070	5783	6853	6802	6993	7312	7594	6947	4057	1738	1161	801	564	462	450
Hainan	259	329	261	316	275	360	387	387	515	405	323	295	245	248	288
Chongqing	1370	1754	1736	1936	2648	2601	2938	3093	2897	2584	2035	1974	1497	1239	850
Sichuan	2040	2016	2199	2496	2814	4053	5167	5865	5650	4662	3940	3781	3236	3185	3183
Guizhou	483	536	662	1005	1245	1730	2234	2351	2345	2607	2299	2097	1223	1414	1260
Yunnan	431	548	715	893	1007	1338	1337	1555	2005	1089	578	388	235	241	238
Shaanxi	351	311	473	524	724	1022	1144	1244	1357	1692	1837	1721	1729	1466	1047
Gansu	686	813	640	867	906	1267	1219	1228	1234	623	521	534	496	604	488
Qinghai	233	292	289	452	442	646	622	653	1057	1456	1219	883	757	636	674
Ningxia	131	168	199	340	418	504	529	669	824	863	810	517	547	379	350
Xinjiang	654	1163	2105	2943	4154	5131	5524	8606	11 220	10 645	8421	8229	5541	4982	4558

Table 13
The secondary stage syphilis cases for 30 provinces/cities in China from 2012 to 2018.
Source: Data from [33].

Cases	2004	2005	2006	2007	2008	2009	2010	2011	2012	2013	2014	2015	2016	2017	2018
Beijing	612	723	765	821	825	974	994	1169	1134	1216	1317	1110	851	944	860
Tianjin	340	433	326	1336	1898	1631	1302	1385	1528	1584	1352	1077	772	599	527
Hebei	157	223	182	219	260	298	655	1000	1444	1488	1551	1685	1463	1468	1625
Shanxi	189	301	239	264	354	360	424	580	741	932	816	650	596	688	623
InnerMongolia	187	275	275	318	367	330	648	1061	1293	1652	1689	1401	1251	1342	1145
Liaoning	1060	1077	1379	1682	2152	2944	4035	5626	5960	6227	5706	4445	3408	3321	3010
Jilin	550	579	681	1175	1415	1464	1960	2596	2754	2669	2360	2144	1518	1327	1416
Heilongjiang	622	623	810	1004	1251	1539	1609	1895	2040	2249	2074	1890	1531	1479	1242
Shanghai	2776	3183	3558	4107	5043	5283	4405	3857	3521	3550	3476	3258	3003	2674	2267
Jiangsu	2716	3214	4213	5446	7498	8859	8507	7905	7494	6831	6478	5592	5110	4567	5547
Zhejiang	4344	5304	6600	7432	8379	9625	9963	8680	7341	6461	6616	5564	4892	4497	3612
Anhui	1351	1555	1445	1732	2339	2879	3234	3288	3772	4163	4267	4193	3676	3362	3067
Fujian	2718	2331	2142	2354	2443	2661	2591	2469	2535	2850	2824	2148	1745	1508	1511
Jiangxi	708	724	635	567	824	722	710	834	844	977	1049	1078	1130	1174	1052
Shandong	751	868	860	978	1477	2041	2351	2584	3433	3484	3329	2919	2821	2859	2757
Henan	482	613	714	778	856	1146	1438	1591	1793	1764	1398	1458	1265	1578	1722
Hubei	487	500	642	717	1332	1484	1821	2308	2333	1516	1756	1758	1235	1026	1008
Hunan	414	735	1340	1517	1390	2046	2108	2038	2115	1672	2050	1828	1405	1319	1276
Guangdong	3522	4262	4641	4325	4541	4812	4560	4637	4663	4327	4199	3711	3286	3394	3159
Guangxi	3045	3098	3249	2939	2501	2210	2246	1954	1248	834	819	679	622	568	502
Hainan	303	302	220	300	200	247	308	358	388	422	532	457	334	343	452
Chongqing	763	837	921	861	919	1012	1044	1105	1050	1163	953	1276	1083	1021	936
Sichuan	1288	1591	1767	1892	1842	2408	2603	2284	2404	2401	2254	2180	1991	2038	2128
Guizhou	159	181	190	158	208	301	342	375	472	409	563	616	522	563	632
Yunnan	128	193	178	194	194	205	215	237	308	430	373	375	287	294	333
Shaanxi	242	262	260	290	314	307	447	477	627	681	680	885	1083	897	855
Gansu	106	95	150	120	146	145	153	274	295	185	199	169	249	217	178
Qinghai	57	101	63	75	97	112	228	213	199	219	267	114	197	143	226
Ningxia	57	75	75	87	66	74	105	227	276	321	274	192	216	152	147
Xinjiang	403	512	652	885	875	782	762	961	1264	1245	933	1213	958	964	1092

and public health practitioners are crucial to bridge the gap between theoretical research and practical implementation, ensuring that the insights gained from our study contribute tangibly to syphilis prevention and control strategies. As a novel avenue, employing the discrete inverse method [52] to estimate time-varying transmission rates of syphilis could provide a valuable tool for extracting information from available incidence data, offering additional depth and precision to future modeling endeavors. Future research endeavors in these directions, coupled with the integration of cutting-edge data science methodologies, have the potential to refine and expand upon our current findings,

Table 14
The latent stage syphilis cases for 30 provinces/cities in China from 2012 to 2018.
Source: Data from [33].

Cases	2004	2005	2006	2007	2008	2009	2010	2011	2012	2013	2014	2015	2016	2017	2018
Beijing	648	1296	2003	2116	2221	2148	2396	2621	2488	3106	3545	3601	3576	3699	4187
Tianjin	216	322	450	649	786	905	986	928	962	1168	1342	1456	1527	2223	2000
Hebei	200	305	553	698	942	1288	1660	2163	2866	3834	4669	5875	5914	6429	7098
Shanxi	441	1101	1878	2928	3391	4365	5207	6237	7777	7474	7403	7813	7518	9114	10 614
InnerMongolia	85	407	1030	1620	2069	2546	3337	3944	5045	5915	6376	6655	5903	6778	7727
Liaoning	1105	1252	1703	2512	3036	3265	3986	5033	5895	7594	8603	9009	9516	9861	9917
Jinlin	185	340	620	904	1231	1277	1266	1947	1537	1607	1661	1893	2000	1876	2056
Heilongjiang	771	1062	1572	2001	2529	3016	3449	3622	3804	3956	4188	4660	4870	5274	5291
Shanghai	1917	2634	3797	4018	4921	5683	6145	6312	6625	6140	6417	7145	7514	7926	7397
Jiangsu	1895	2535	3373	4741	5812	6663	7890	8331	8817	8646	11 148	12 587	13 745	15 675	17 201
Zhejiang	3573	7280	10 199	12 557	15 269	17 186	20 685	19 166	16 268	16 903	19 783	22 198	24 911	26 985	24 237
Anhui	365	604	1032	1549	1736	2317	3434	4456	5690	7433	9286	12 271	15 434	18 925	19 396
Fujian	1473	2906	4356	6247	8481	9094	10 516	11 382	12 801	14 030	15 819	17 821	18 232	20 173	20 940
Jiangxi	193	890	1587	2045	2779	2962	3399	3617	4526	5841	6565	8608	10 522	13 434	15 509
Shandong	176	480	622	816	1116	1541	2018	2552	4241	5684	6935	8059	9177	11 619	13 239
Henan	271	911	1467	2416	3483	5383	8013	11 533	15 415	15 487	11 984	11 105	10 765	10 861	12 658
Hubei	137	366	908	1340	2614	3609	4385	4005	4284	5795	6679	8357	9887	11 382	13 006
Hunan	135	379	1259	2235	3074	4488	7910	10 245	11 277	12 903	14 664	16 438	19 544	24 220	29 308
Guangdong	2483	6580	10 966	14 878	18 575	21 423	25 670	31 082	33 091	34 545	38 098	40 071	44 850	48 068	49 338
Guangxi	626	3365	6843	10 002	13 890	18 886	25 299	29 048	21 337	9514	7551	6482	5984	5048	8916
Hainan	125	416	717	975	1136	1323	1557	1538	2050	2589	2528	3591	3985	4828	5006
Chongqing	330	714	1270	2375	3558	3164	3916	5081	6391	7200	8639	11 032	13 674	16 812	16 311
Sichuan	778	2027	2818	3585	4627	7844	11 291	12 155	13 470	11 999	12 538	16 201	17 490	21 506	23 339
Guizhou	74	318	471	813	1292	2406	3190	3173	4549	4958	6307	8241	8650	10 787	12 845
Yunan	81	299	659	1096	1765	2601	3319	4108	6200	7927	11 969	14 762	16 499	16 267	16 060
Shaanxi	258	479	740	1094	1456	2169	2856	3634	4616	4887	5676	6454	6754	8069	8708
Gansu	166	319	561	683	1051	1526	2597	3353	2994	2651	2888	3594	4032	4985	5782
Qinghai	23	275	184	285	234	482	622	687	1118	1303	1569	1249	1793	2537	2948
Ningxia	24	204	268	388	482	477	796	1307	1560	2304	2410	2505	2986	3148	3103
Xinjiang	142	407	1087	1844	2868	4359	4220	5363	6313	9375	11 368	14 826	14 247	15 810	17 761

Table 15
The tertiary syphilis cases for 30 provinces/cities in China from 2012 to 2018.
Source: Data from [33].

Cases	2004	2005	2006	2007	2008	2009	2010	2011	2012	2013	2014	2015	2016	2017	2018
Beijing	22	51	41	47	20	35	35	47	36	33	26	28	29	29	31
Tianjin	12	4	6	11	9	18	16	16	27	23	14	8	5	25	40
Hebei	2	6	9	6	16	24	22	18	37	39	36	53	100	73	57
Shanxi	18	12	16	12	26	42	24	24	37	62	120	24	30	35	29
InnerMongolia	3	7	20	21	19	20	20	31	38	26	38	34	34	34	38
Liaoning	13	19	21	22	28	35	59	60	54	54	66	79	63	86	77
Jinlin	8	17	79	22	18	28	19	32	55	29	35	39	69	38	41
Heilongjiang	5	10	23	28	36	24	32	46	52	71	49	53	73	38	37
Shanghai	22	28	50	58	53	48	64	95	125	140	237	202	172	156	168
Jiangsu	41	60	81	106	145	150	149	128	188	195	241	249	325	339	338
Zhejiang	79	99	111	139	149	185	250	204	191	159	198	204	272	271	228
Anhui	24	17	26	33	37	49	67	92	148	127	197	186	206	212	293
Fujian	48	104	147	210	206	250	302	310	293	316	303	354	349	317	356
Jiangxi	7	20	19	24	39	43	45	55	60	84	87	90	105	129	125
Shandong	6	16	16	21	27	39	367	46	54	77	79	101	124	88	117
Henan	18	16	47	33	46	54	123	149	168	199	156	84	67	100	102
Hubei	10	24	21	33	51	62	83	56	60	73	54	83	93	717	73
Hunan	43	78	77	38	49	73	88	114	114	153	122	156	110	106	142
Guangdong	63	171	216	318	329	452	591	608	612	562	575	433	341	315	360
Guangxi	25	64	88	134	139	157	193	236	157	114	138	154	171	138	164
Hainan	6	11	18	8	17	24	22	11	27	21	20	30	29	21	22
Chongqing	20	19	23	32	40	34	56	53	58	71	83	68	92	71	62
Sichuan	21	24	48	68	72	95	121	135	163	164	191	178	198	238	288
Guizhou	0	3	15	8	18	33	33	30	45	47	72	49	36	46	79
Yunan	17	22	57	41	28	26	23	25	34	30	9	12	12	13	8
Shanxi	8	13	10	21	20	15	10	16	26	37	29	21	38	50	28
Gansu	2	9	12	40	28	23	21	20	23	17	12	6	18	9	6
Qinghai	1	1	4	2	11	6	13	8	11	11	11	16	8	20	7
Ningxia	0	11	10	10	8	5	7	9	13	21	9	9	14	14	8
Xinjiang	18	34	54	66	88	84	82	96	121	152	77	91	84	62	70

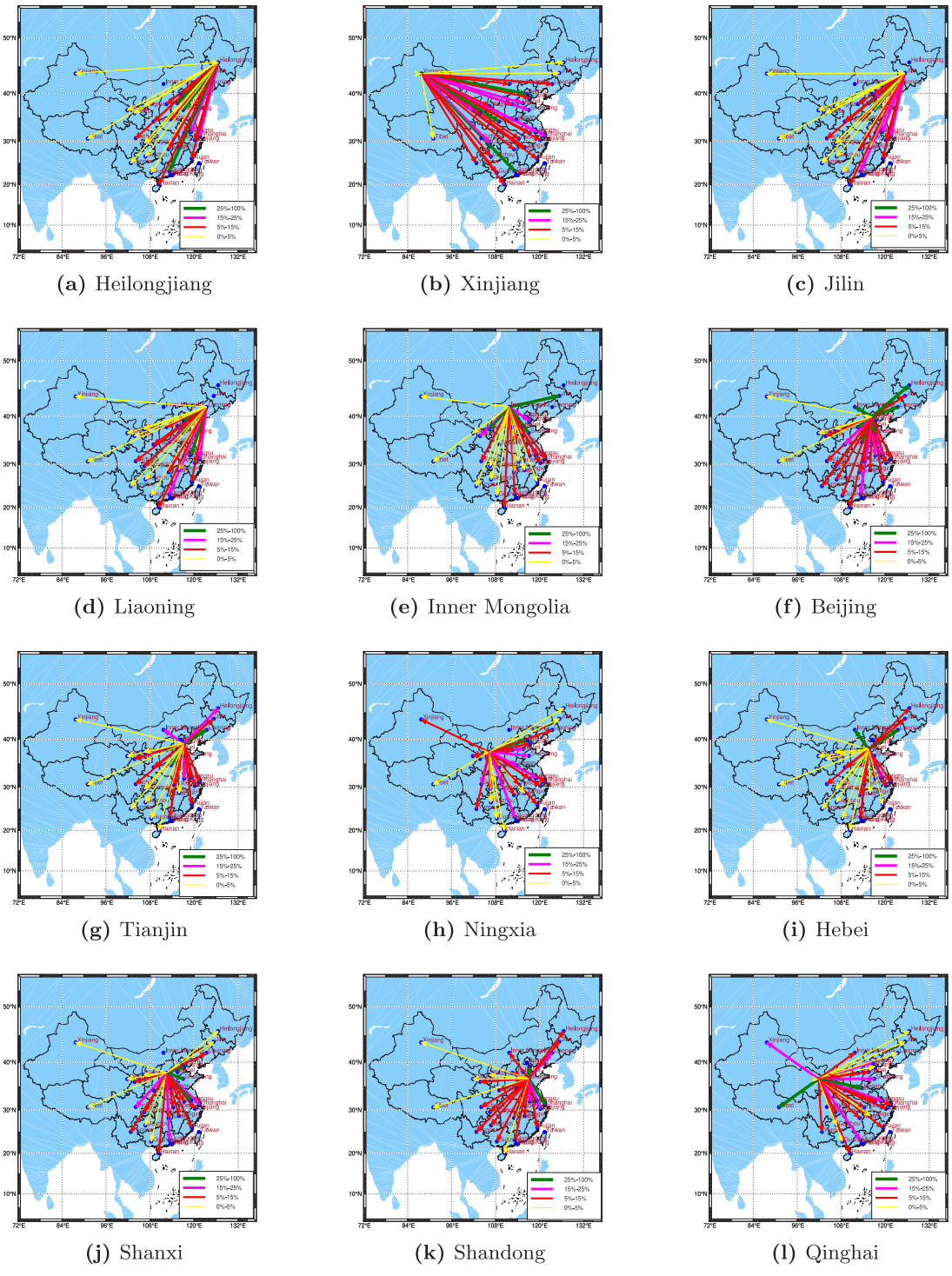

Fig. 6.17. The migration rates of the 12 provinces: Heilongjiang, Xinjiang, Jilin, Liaoning, Inner Mongolia, Beijing, Tianjin, Ningxia, Hebei, Shanxi, Shandong, Qinghai. The real-time travel data were collected by using the Baidu Migration server (2020a) [53].

fostering a comprehensive understanding of the spatial dynamics of syphilis transmission.

CRediT authorship contribution statement

Peng Wu: Writing – original draft, Visualization, Methodology, Investigation, Funding acquisition, Formal analysis, Data curation, Conceptualization. **Xiunan Wang:** Writing – review & editing, Validation, Project administration, Methodology, Investigation. **Hao Wang:** Writing – review & editing, Validation, Supervision, Project administration, Investigation, Funding acquisition, Data curation, Conceptualization.

Declaration of competing interest

The authors declare that they have no conflict of interest.

Data availability

All used data are public and have been listed in the paper.

Acknowledgments

Research of PW is partially supported by the National Natural Science Foundation of China (No. 12201557), the Foundation of Zhejiang Provincial Education Department, China (No. Y202249921). Research of XW is partially supported by the Faculty Graduate Engagement Award from College of Arts and Sciences at the University of Tennessee at Chattanooga, USA. Research of HW is partially supported by the Natural Sciences and Engineering Research Council of Canada (Individual Discovery Grant RGPIN-2020-03911 and Discovery Accelerator Supplement Award RGPAS-2020-00090) and the Canada Research Chairs program (Tier 1 Canada Research Chair Award).

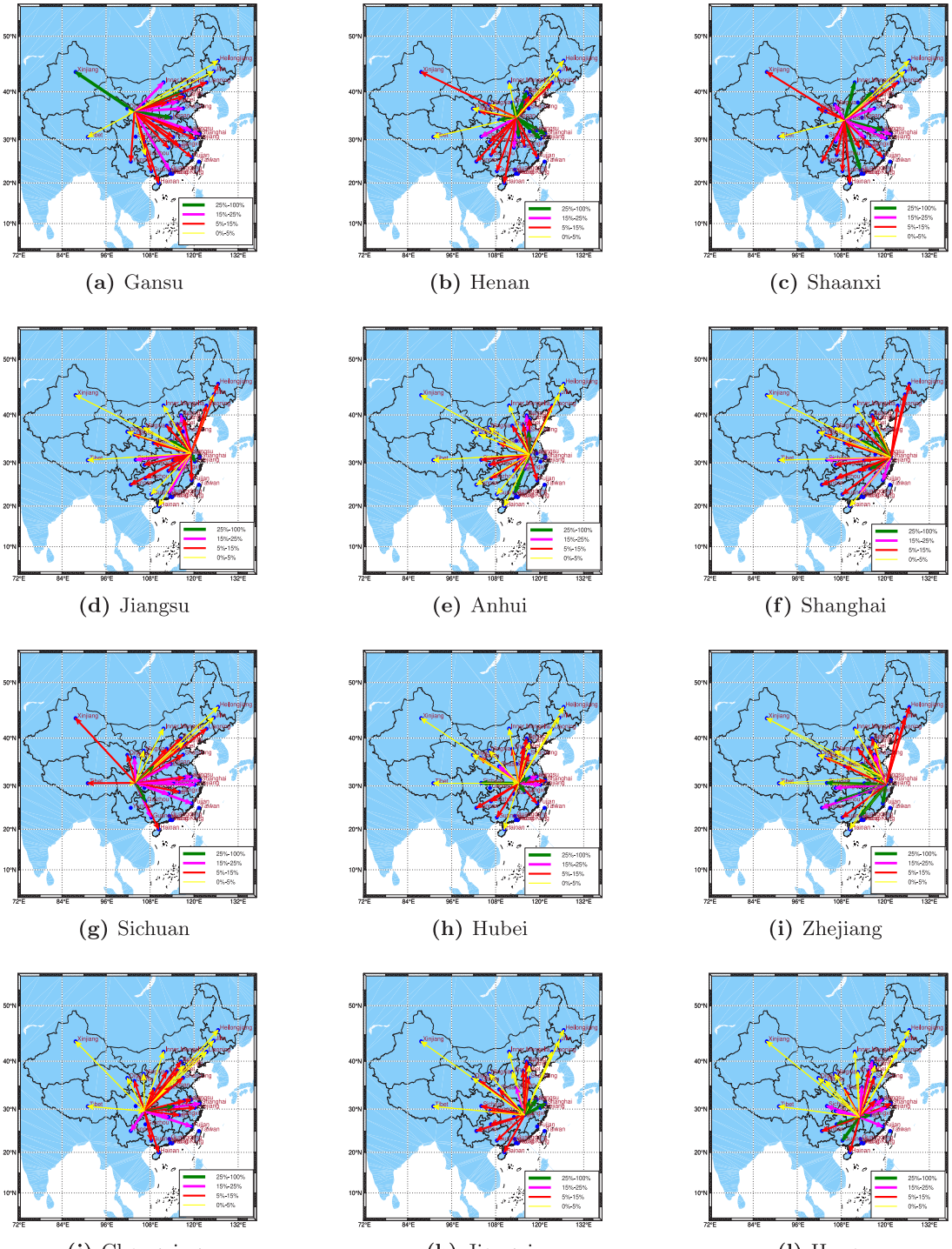

Fig. 6.18. The migration rates of 12 provinces: Gansu, Henan, Shaanxi, Jiangsu, Anhui, Shanghai, Sichuan, Hubei, Zhejiang, Chongqing, Jiangxi, Hunan. The real-time travel data were collected by using the Baidu Migration server (2020a) [53].

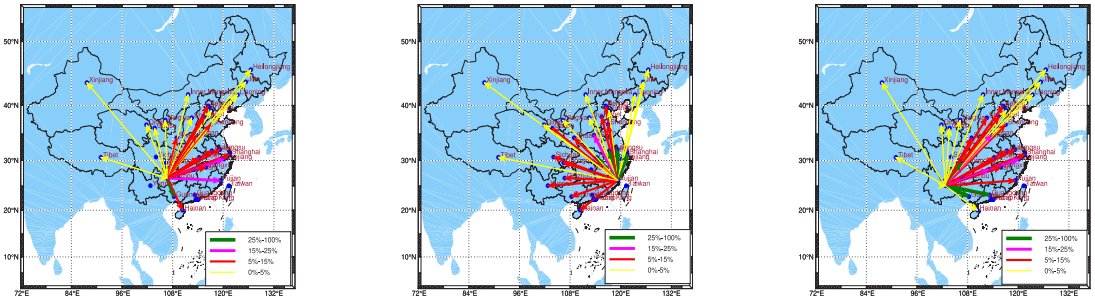

(a) Guizhou (b) Fujian (c) Yunnan

(d) Guangdong (e) Guangxi (f) Hainan

Fig. 6.19. The migration rates of the 6 provinces: Guizhou, Fujian, Yunnan, Guangdong, Guangxi, Hainan. The real-time travel data were collected by using the Baidu Migration server (2020a) [53].

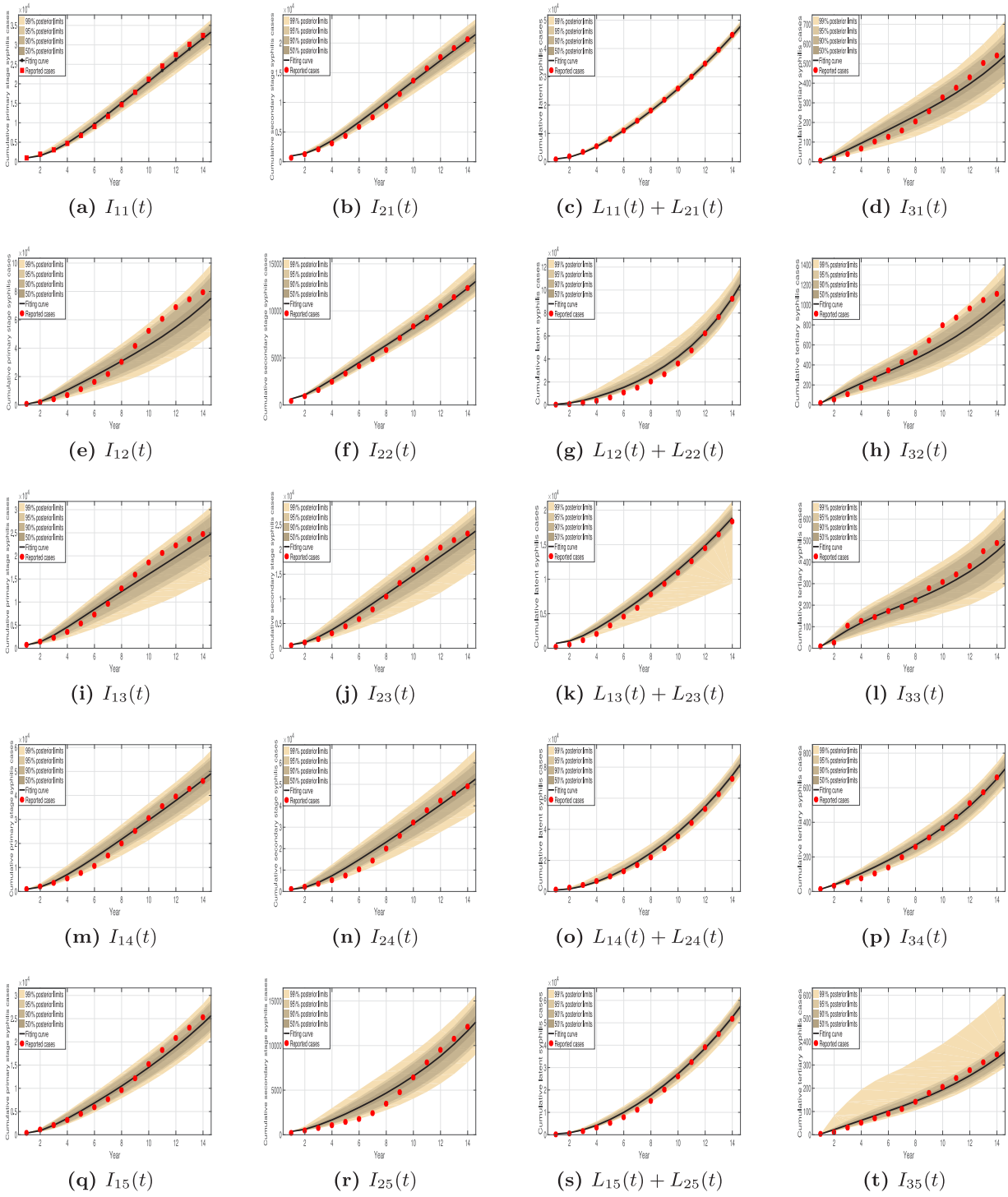

(a) $I_{11}(t)$ (b) $I_{21}(t)$ (c) $L_{11}(t) + L_{21}(t)$ (d) $I_{31}(t)$

(e) $I_{12}(t)$ (f) $I_{22}(t)$ (g) $L_{12}(t) + L_{22}(t)$ (h) $I_{32}(t)$

(i) $I_{13}(t)$ (j) $I_{23}(t)$ (k) $L_{13}(t) + L_{23}(t)$ (l) $I_{33}(t)$

(m) $I_{14}(t)$ (n) $I_{24}(t)$ (o) $L_{14}(t) + L_{24}(t)$ (p) $I_{34}(t)$

(q) $I_{15}(t)$ (r) $I_{25}(t)$ (s) $L_{15}(t) + L_{25}(t)$ (t) $I_{35}(t)$

Fig. 6.20. (a)–(d) The fitting curves of the cumulative syphilis reported cases in Heilongjiang Province; (e)–(h) The fitting curves of the cumulative syphilis reported cases in Xinjiang Province; (i)–(l) The fitting curves of the cumulative syphilis reported cases in Jilin Province; (m)–(p) The fitting curves of the cumulative syphilis reported cases in Liaoning Province; (q)–(t) The fitting curves of the cumulative syphilis reported cases in Inner Mongolia.

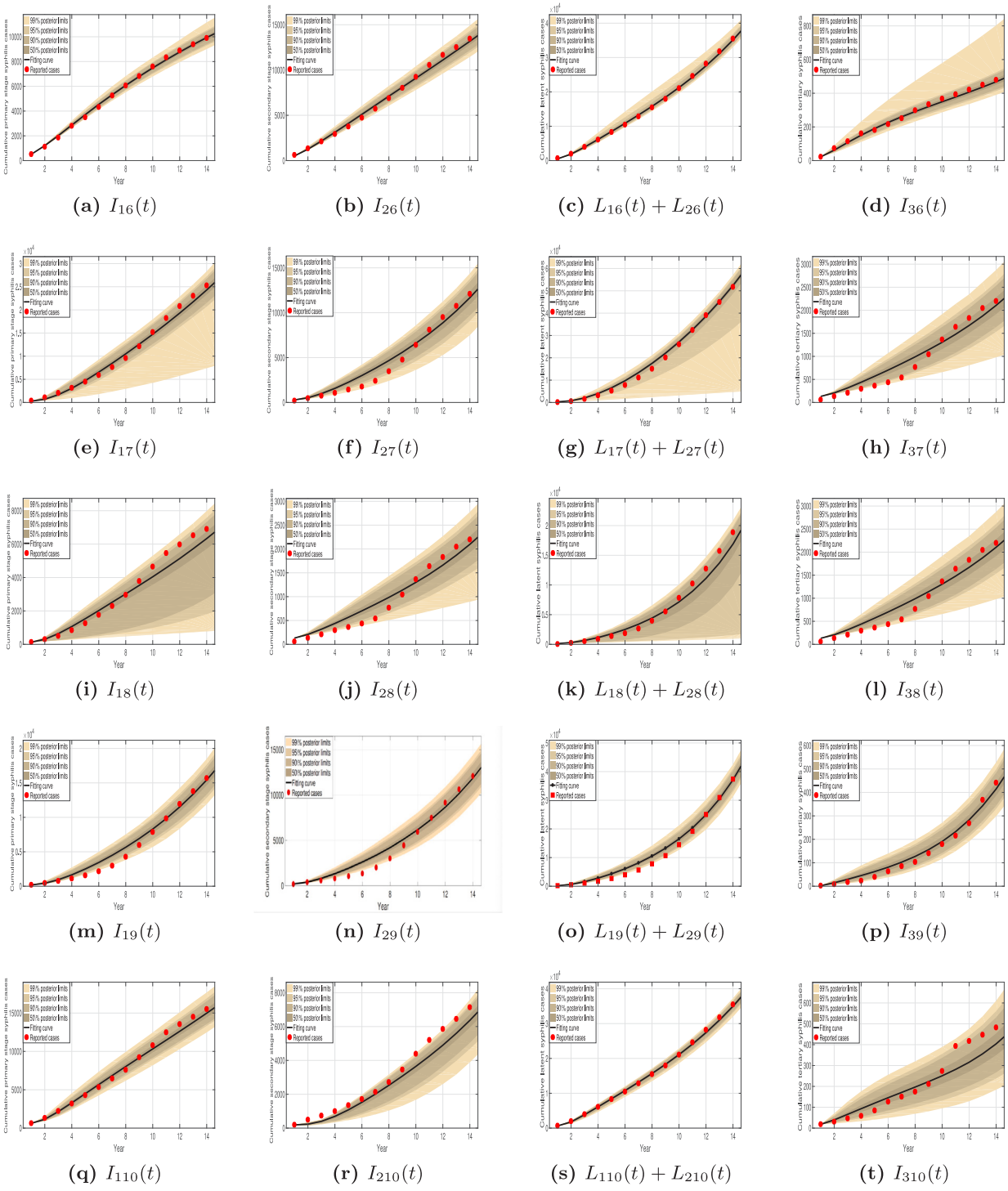

(a) $I_{16}(t)$ (b) $I_{26}(t)$ (c) $L_{16}(t) + L_{26}(t)$ (d) $I_{36}(t)$

(e) $I_{17}(t)$ (f) $I_{27}(t)$ (g) $L_{17}(t) + L_{27}(t)$ (h) $I_{37}(t)$

(i) $I_{18}(t)$ (j) $I_{28}(t)$ (k) $L_{18}(t) + L_{28}(t)$ (l) $I_{38}(t)$

(m) $I_{19}(t)$ (n) $I_{29}(t)$ (o) $L_{19}(t) + L_{29}(t)$ (p) $I_{39}(t)$

(q) $I_{110}(t)$ (r) $I_{210}(t)$ (s) $L_{110}(t) + L_{210}(t)$ (t) $I_{310}(t)$

Fig. 6.21. (a)–(d) The fitting curves of the cumulative syphilis reported cases in Beijing; (e)–(h) The fitting curves of the cumulative syphilis reported cases in Tianjin; (i)–(l) The fitting curves of the cumulative syphilis reported cases in Ningxia; (m)–(p) The fitting curves of the cumulative syphilis reported cases in Hebei Province; (q)–(t) The fitting curves of the cumulative syphilis reported cases in Shanxi Province.

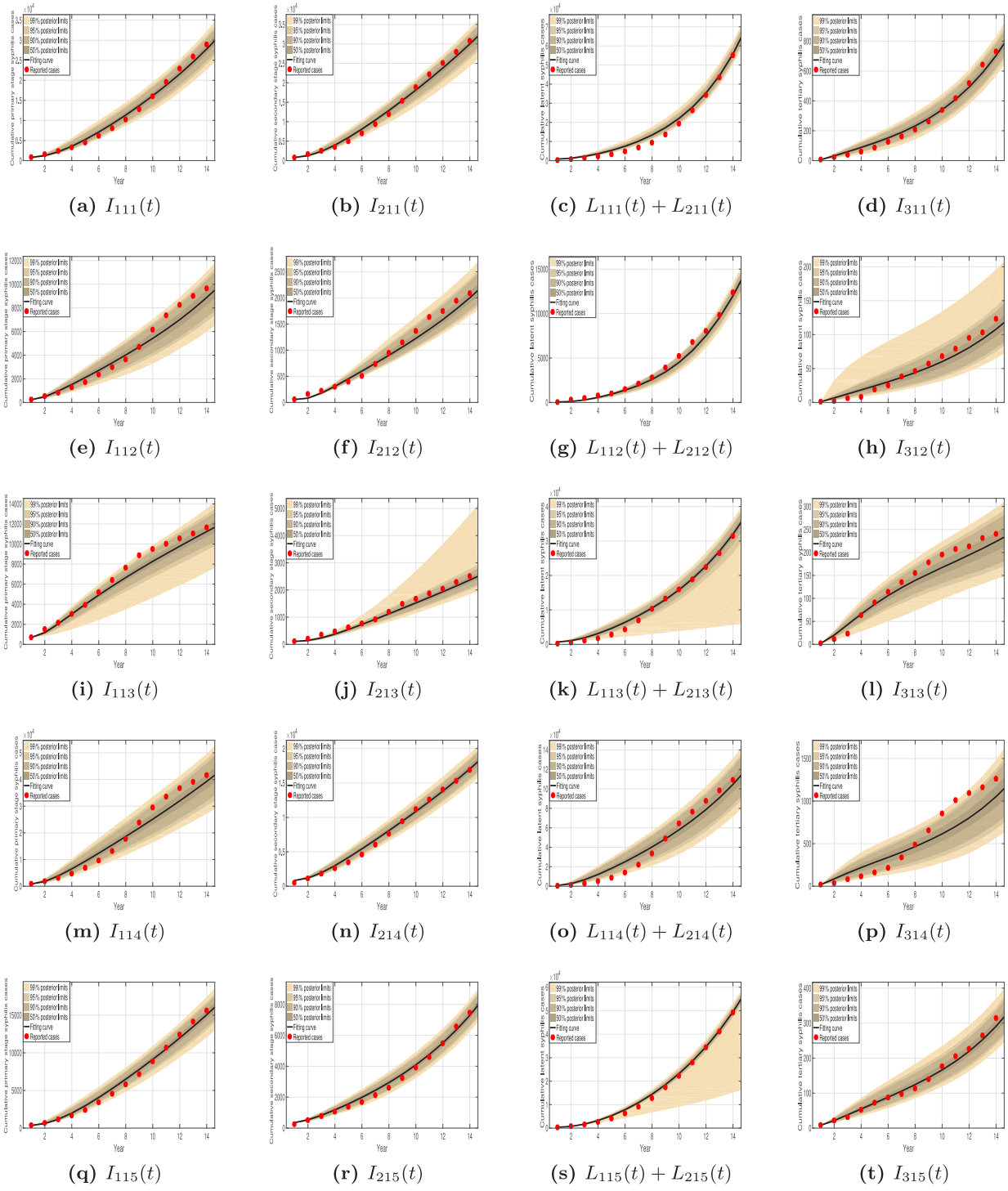

(a) $I_{111}(t)$ (b) $I_{211}(t)$ (c) $L_{111}(t) + L_{211}(t)$ (d) $I_{311}(t)$

(e) $I_{112}(t)$ (f) $I_{212}(t)$ (g) $L_{112}(t) + L_{212}(t)$ (h) $I_{312}(t)$

(i) $I_{113}(t)$ (j) $I_{213}(t)$ (k) $L_{113}(t) + L_{213}(t)$ (l) $I_{313}(t)$

(m) $I_{114}(t)$ (n) $I_{214}(t)$ (o) $L_{114}(t) + L_{214}(t)$ (p) $I_{314}(t)$

(q) $I_{115}(t)$ (r) $I_{215}(t)$ (s) $L_{115}(t) + L_{215}(t)$ (t) $I_{315}(t)$

Fig. 6.22. (a)–(d) The fitting curves of the cumulative syphilis reported cases in Shandong Province; (e)–(h) The fitting curves of the cumulative syphilis reported cases in Qinghai Province; (i)–(l) The fitting curves of the cumulative syphilis reported cases in Gansu Province; (m)–(p) The fitting curves of the cumulative syphilis reported cases in Henan Province; (q)–(t) The fitting curves of the cumulative syphilis reported cases in Shaanxi Province.

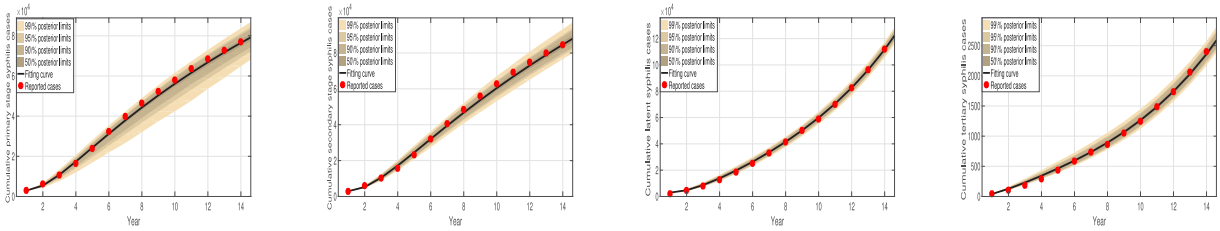

(a) $I_{116}(t)$ (b) $I_{216}(t)$ (c) $L_{116}(t) + L_{216}(t)$ (d) $I_{316}(t)$

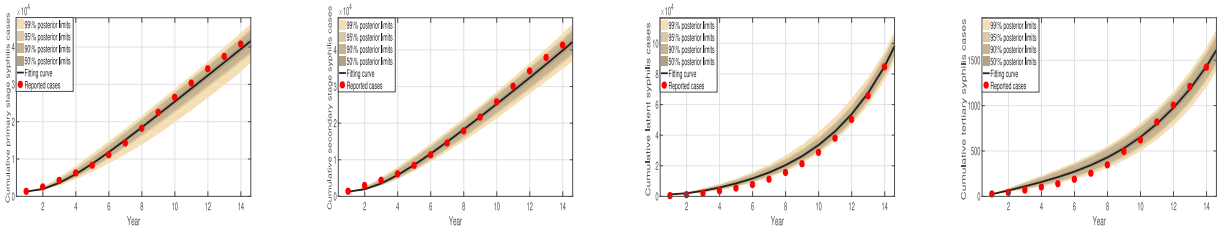

(e) $I_{117}(t)$ (f) $I_{217}(t)$ (g) $L_{117}(t) + L_{217}(t)$ (h) $I_{317}(t)$

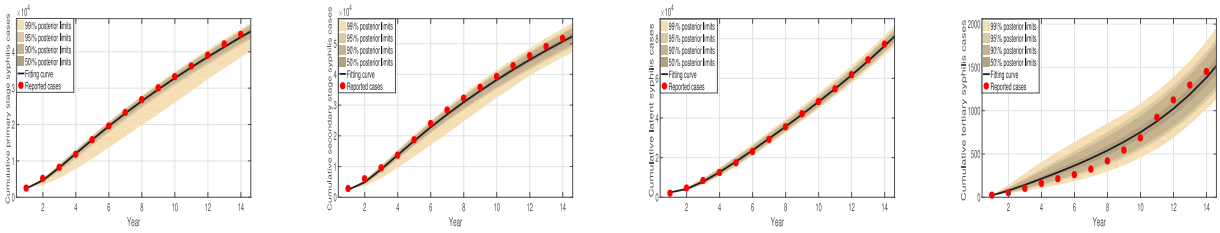

(i) $I_{118}(t)$ (j) $I_{218}(t)$ (k) $L_{118}(t) + L_{218}(t)$ (l) $I_{318}(t)$

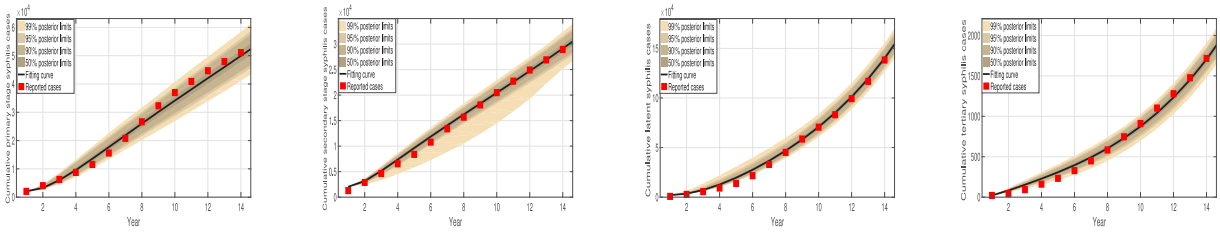

(m) $I_{119}(t)$ (n) $I_{219}(t)$ (o) $L_{119}(t) + L_{219}(t)$ (p) $I_{319}(t)$

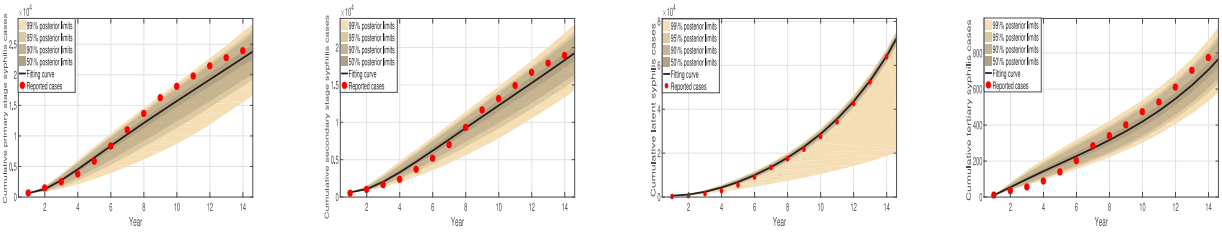

(q) $I_{120}(t)$ (r) $I_{220}(t)$ (s) $L_{120}(t) + L_{220}(t)$ (t) $I_{320}(t)$

Fig. 6.23. (a)–(d) The fitting curves of the cumulative syphilis reported cases in Jiangsu Province; (e)–(h) The fitting curves of the cumulative syphilis reported cases in Anhui Province; (i)–(l) The fitting curves of the cumulative syphilis reported cases in Shanghai; (m)–(p) The fitting curves of the cumulative syphilis reported cases in Sichuan Province; (q)–(t) The fitting curves of the cumulative syphilis reported cases in Hubei Province.

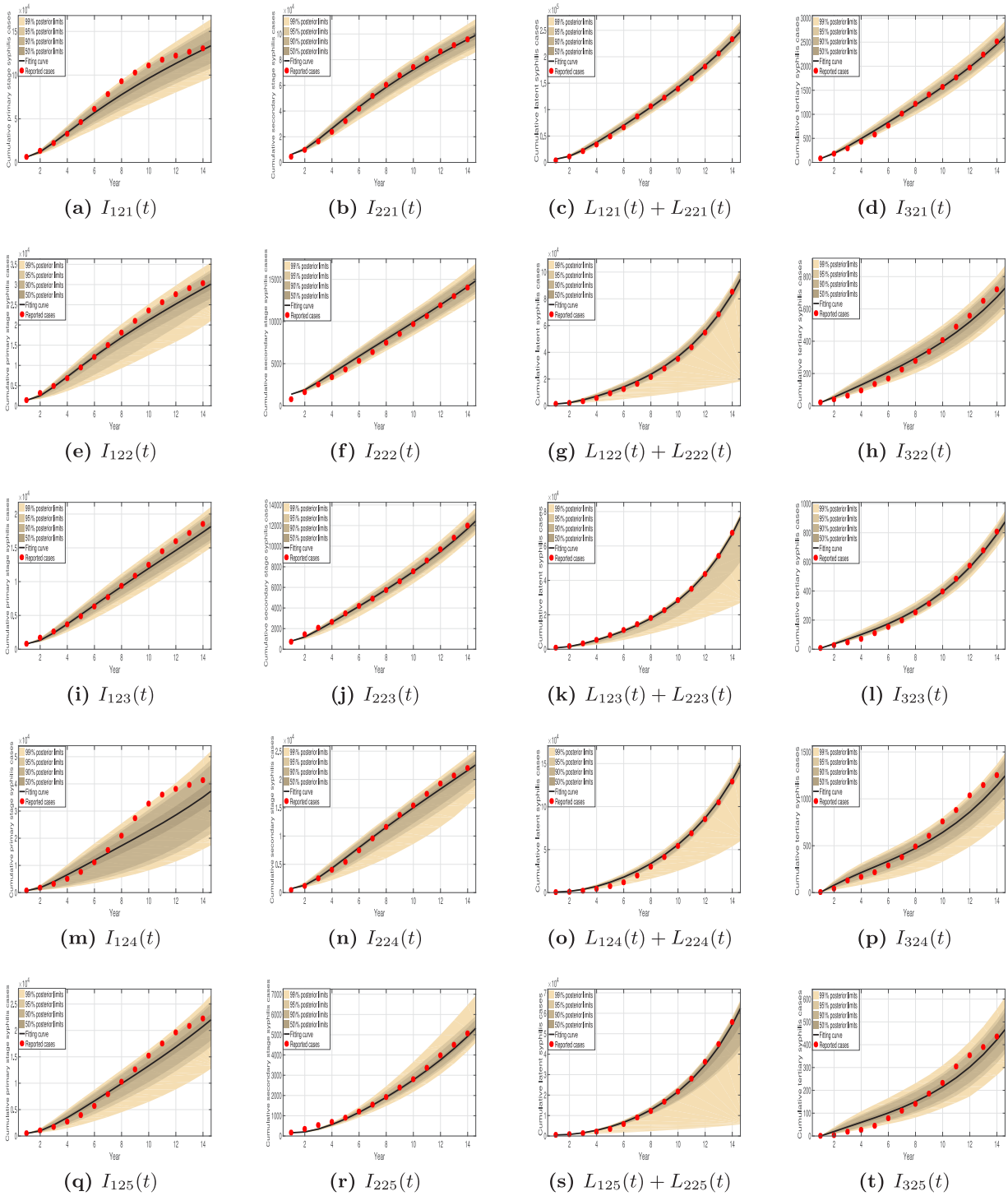

(a) $I_{121}(t)$ (b) $I_{221}(t)$ (c) $L_{121}(t) + L_{221}(t)$ (d) $I_{321}(t)$

(e) $I_{122}(t)$ (f) $I_{222}(t)$ (g) $L_{122}(t) + L_{222}(t)$ (h) $I_{322}(t)$

(i) $I_{123}(t)$ (j) $I_{223}(t)$ (k) $L_{123}(t) + L_{223}(t)$ (l) $I_{323}(t)$

(m) $I_{124}(t)$ (n) $I_{224}(t)$ (o) $L_{124}(t) + L_{224}(t)$ (p) $I_{324}(t)$

(q) $I_{125}(t)$ (r) $I_{225}(t)$ (s) $L_{125}(t) + L_{225}(t)$ (t) $I_{325}(t)$

Fig. 6.24. (a)–(d) The fitting curves of the cumulative syphilis reported cases in Zhejiang Province; (e)–(h) The fitting curves of the cumulative syphilis reported cases in Chongqing; (i)–(l) The fitting curves of the cumulative syphilis reported cases in Jiangxi Province; (m)–(p) The fitting curves of the cumulative syphilis reported cases in Hunan Province; (q)–(t) The fitting curves of the cumulative syphilis reported cases in Guizhou Province.

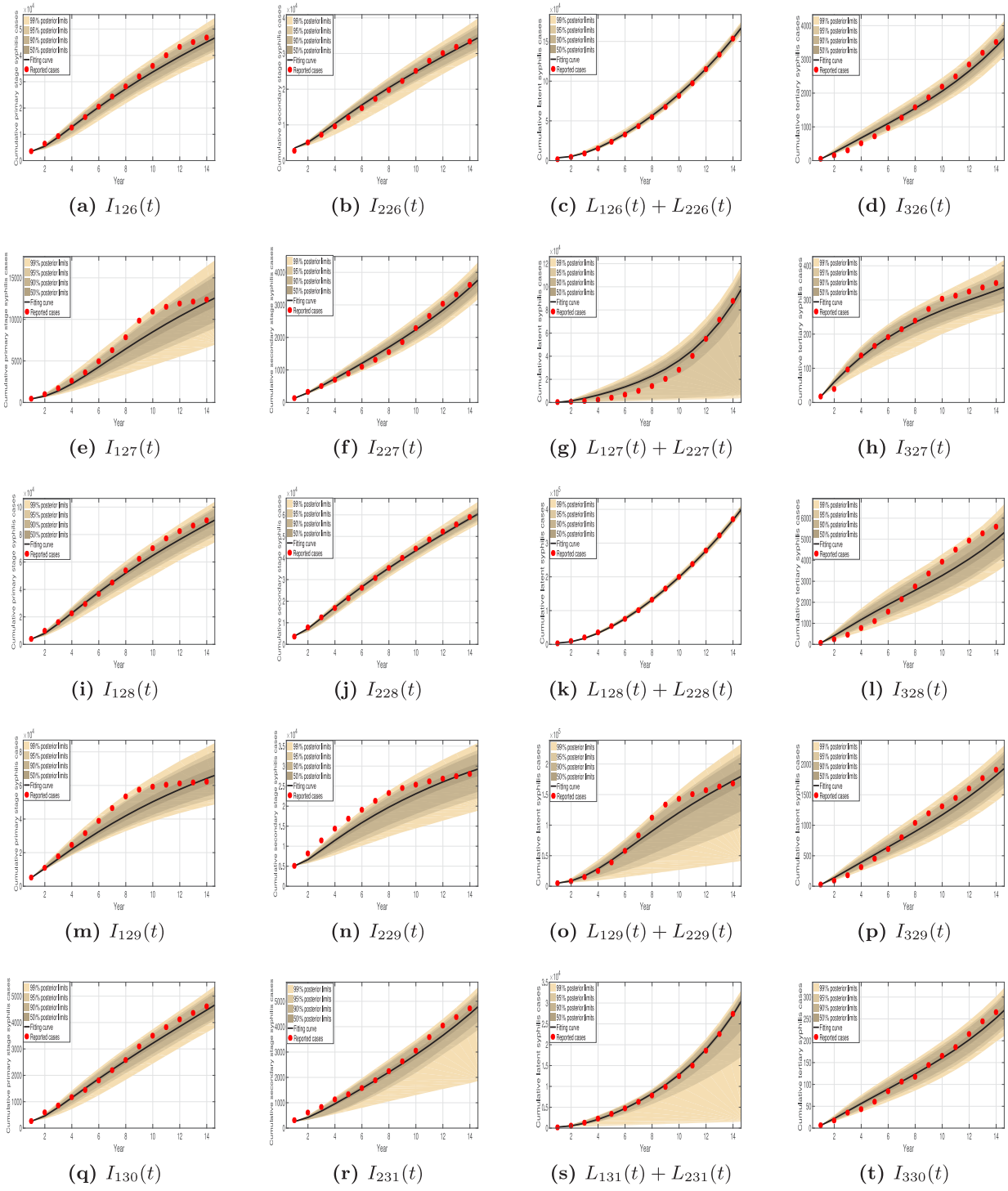

(a) $I_{126}(t)$ (b) $I_{226}(t)$ (c) $L_{126}(t) + L_{226}(t)$ (d) $I_{326}(t)$

(e) $I_{127}(t)$ (f) $I_{227}(t)$ (g) $L_{127}(t) + L_{227}(t)$ (h) $I_{327}(t)$

(i) $I_{128}(t)$ (j) $I_{228}(t)$ (k) $L_{128}(t) + L_{228}(t)$ (l) $I_{328}(t)$

(m) $I_{129}(t)$ (n) $I_{229}(t)$ (o) $L_{129}(t) + L_{229}(t)$ (p) $I_{329}(t)$

(q) $I_{130}(t)$ (r) $I_{231}(t)$ (s) $L_{131}(t) + L_{231}(t)$ (t) $I_{330}(t)$

Fig. 6.25. (a)–(d) The fitting curves of the cumulative syphilis reported cases in Fujian Province; (e)–(h) The fitting curves of the cumulative syphilis reported cases in Yunnan Province; (i)–(l) The fitting curves of the cumulative syphilis reported cases in Guangdong Province; (m)–(p) The fitting curves of the cumulative syphilis reported cases in Guangxi Province; (q)–(t) The fitting curves of the cumulative syphilis reported cases in Hainan Province.

Appendix A. Reported cases of syphilis

The reported cases of syphilis (primary, secondary, latent and tertiary infection stages) from 2004 to 2018 in China are given in Tables 12–15.

Appendix B. Human migration rates in 30 provinces of China

The migration rates of people in the 30 provinces of China are shown in Figs. 6.17–6.19.

Appendix C. The fitting curves

The fitting curves of the cumulative four stages of syphilis infected cases are presented in Figs. 6.20–6.25

References

[1] T.F. Sparling, Natural History of Syphilis, STD, McGrans-Hill Book co., 1981, pp. 298–299,

[2] A.B. Mathew, M. Michael, et al., Global phylogeny of treponema pallidum lineages reveals recent expansion and spread of contemporary syphilis, Nature Microbiol. 12 (2021) 1549–1560.

[3] National Institute of Infectious Diseases, Infectious agents surveillance report, 2020, https://www.niid.go.jp/niid/en/iasr-e.html.

[4] Data-Center of China Public Health Science, Data directory, 2021, Available from: https://www.phsciencedata.cn/Share/en/index.jsp. (Accessed 15 March 2021).

[5] R.R. Willcox, J.R. Willcox, Pocket Consultant of Vererollogi Medicine, Chicargo year book publishers inc, Chicargo, 1981, pp. 161–162.

[6] R.B. Odom, et al., Andrew's Disease of the Skin, ninth ed., WB Saundersco, London, 2000.

[7] N.J. Fiumara, S. Lessell, Manifestations of late congeital syphilis, Arch. Dermatol. 102 (1970) 78–83.

[8] T.A. Peterman, R.H. Kahn, C.A. Ciesielski, et al., Misclassification of the stages of syphilis: implications for surveillance, Sex. Transm. Dis. 32 (2005) 144.

[9] R. Pinto, L. Silva, R. Valentim, et al., Assessing the impact of public health campaigns through epidemiological, communication and education indicators, in: 2020 IEEE 20th International Conference on Advanced Learning Technologies, ICALT, Tartu, Estonia, 2020, pp. 147–149.

[10] S. Hawkes, N. Matin, N. Broutet, N. Low, Effectiveness of interventions to improve screening for syphilis in pregnancy: a systematic review and meta-analysis, Lancet Infect. Dis. 11 (9) (2011) 684–691.

[11] S.W. Dooley, O.T. Dubose, J.F. Fletcher, Recommendations for partner services programs for HIV infection, syphilis, gonorrhea, and chlamydial infection, 2008, Series: MMWR. Recommendations and reports: Morbidity and mortality weekly report. Recommendations and reports, 57, RR-9.

[12] C.A. Koss, E.F. Dunne, L. Warner, A systematic review of epidemiologic studies assessing condom use and risk of syphilis, Sex. Transm. Dis. 36 (2009) 7, 401-405.

[13] P.J. Kissinger, L.M. Niccolai, M. Magnus, Partner notification for HIV and syphilis: Effects on sexual behaviors and relationship stability, Sex. Transm. Dis. 30 (2003) 1, 75-82.

[14] B.T. Goh, A.C. Thornton, Antenatal screening for syphilis, Sex. Transm. Infect. 83 (2007) 345–346.

[15] J.J. Ong, H. Fu, M.K. Smith, J.D. Tucker, Expanding syphilis testing: a scoping review of syphilis testing interventions among key populations, Expert Rev. Anti-Infect. Ther. 16 (2018) 5, 423-432.

[16] G.P. Garnett, S.O. Aral, D.V. Hoyle, W. Cates, R.M. Anderson, The natural history of syphilis: implications for the transmission dynamics and control of infection, Sex. Transm. Dis. 24 (1997) 185–200.

[17] K.A. Fenton, R. Breban, R. Vardavas, J.T. Okano, T. Martin, S. Aral, S. Blower, Infectious syphilis in high-income settings in the 21st century, Lancet Infect. Dis. 8 (2008) 244–253.

[18] C. Grassly, C. Fraser, G.P. Garnett, Host immunity and synchronized epidemics of syphilis across the United States, Nature 433 (2005) 417–421.

[19] E. Iboi, D. Okuonghae, Population dynamics of a mathematical model for syphilis, Appl. Math. Model. 40 (2016) 3573–3590.

[20] C.M. Saad-Roy, Z. Shuai, P. van den Driessche, A mathematical model of syphilis transmission in an MSM population, Math. Biosci. 277 (2016) 59–70.

[21] A.B. Gumel, J.M.-S. Lubuma, O. Sharomi, Y.A. Terefe, Mathematics of a sex-structured model for syphilis transmission dynamics, Math. Methods Appl. Sci. 23 (2017) 1–26.

[22] A. Nwankwo, D. Okuonghae, Mathematical analysis of the transmission dynamics of HIV syphilis co-infection in the presence of treatment for syphilis, Bull. Math. Biol. 80 (2018) 437–492.

[23] A. Omame, D. Okuonghae, U.E. Nwafor, et al., A co-infection model for HPV and syphilis with optimal control and cost-effectiveness analysis, Int. J. Biomath. 14 (2021) 2150050.

[24] X. Ren, Y. Tian, L. Liu, X. Liu, A reaction–diffusion within-host HIV model with cell-to-cell transmission, J. Math. Biol. 76 (2018) 1831–1872.

[25] X. Wang, H. Wang, M.Y. Li, Modeling rabies transmission in spatially heterogeneous environments via θ-diffusion, Bull. Math. Biol. 83 (2021) 16.

[26] Y. Youm, B. Lee, J. Kim, A measure of centrality in cyclic diffusion processes: Walk-betweenness, PLoS One (2021) e0245476.

[27] H.L. Smith, Monotone Dynamical Systems: An Introduction to the Theory of Competitive and Cooperative Systems, American Mathematical Society, Providence, 1995.

[28] R.H. Martin Jr., H.L. Smith, Abstract functional differential equations and reaction–diffusion systems, Trans. Amer. Math. Soc. 321 (1990) 1–44.

[29] J. Wu, Theory and Applications of Partial Functional-Differential Equations, in: Applied Mathematical Sciences, vol. 119, Springer, New York, 1996.

[30] J. Hale, Asymptotic Behavior of Dissipative Systems, American Mathematical Society, Province, RI, 1988.

[31] H.R. Thieme, Convergence results and a Poincaré–Bendixson trichotomy for asymptotically autonomous differential equations, J. Math. Biol. 30 (1992) 755–763.

[32] A. Pazy, Semigroups of Linear Operators and Applications to Partial Differential Equations, Applied Mathematical Science, Springer-Verlag, New York, 1983.

[33] L.J.S. Allen, B.M. Bolker, Y. Lou, A.L. Nevai, Asymptotic profiles of the steady states for an SIS epidemic patch model, SIAM J. Appl. Math. 67 (2007) 1283–1309.

[34] D.L. DeAngelis, W. Ni, B. Zhang, Effects of diffusion on total biomass in heterogeneous continuous and discrete-patch systems, Theor. Ecol. 9 (2016) 443–453.

[35] National Population and Health Science Data Sharing Platform, The Data-center of China Public Health Science, 2022, Available from: https://www.phsciencedata.cn/Share/en/index.jsp. (Accessed 18 January 2022).

[36] L. Xue, S. Jing, H. Wang, Evaluating strategies for tuberculosis to achieve the goals of WHO in China: a seasonal age-structured model study, Bull. Math. Biol. 84 (2022) 1–50.

[37] C.M. Saad-Roya, Z. Shuai, P. van den Driessche, A mathematical model of syphilis transmission in an MSM population, Math. Biosci. 277 (2016) 59–70.

[38] National Bureau of Statistics, China statistical yearbook, 2014, Available from: http://www.stats.gov.cn/tjsj/ndsj/2014/indexch.htm. (Accessed 18 January 2014).

[39] L. Xue, S. Jing, W. Sun, M. Liu, Z. Peng, H. Zhu, Evaluating the impact of the travel ban within mainland China on the epidemic of the COVID-19, Int. J. Infect. Dis. 107 (2021) 278–283.

[40] Baidu Migration Server, Available from: https://qianxi.baidu.com/2020/. (Accessed 17 March 2020).

[41] D. Gao, M.W. Munganga, P. Van Den Driessche, L. Zhang, Effects of asymptomatic infections on the spatial spreed of infectious diseases, SIAM J. Appl. Math. 82 (2022) 899–923.

[42] X. Gong, W. Jiang, Q. Wang, J. Zhang, Epidemiological analysis of syphilis in China from 1979 to 1998, China Public Health 11 (2000) 1020–1022.

[43] Z.Q. Chen, G.C. Zhang, et al., Syphilis in China: results of a national surveillance programme, Lancet 369 (2007) 132–138.

[44] T. Tian, Y. Hou, et al., Spatio-temporal analysis of incidence rate of syphilis in China, J. Shanghai Jiao Tong Univ. (Med. Sci.) 41 (2007) 648–652.

[45] Huan Yong Hu, The distribution of population in China, with statistics and maps, Acta Geogr. Sinica 2 (1935) 33–74.

[46] S. Sangar, R. Thakur, Infectious diseases in India: assessing the role of household amenities and socio-demographic determinants, J. Public Health (Berl.) 30 (2022) 2809–2817.

[47] B. Ram, R. Thakur, Epidemiology and economic burden of continuing challenge of infectious diseases in India: Analysis of socio-demographic differentials, Front. Public Health, Sec. Infect. Dis. – Surv. Prev. Treat. 10 (2022).

[48] N. Bharti, Linking human behaviors and infectious diseases, Proc. Natl. Acad. Sci. USA 118 (2021) 11.

[49] X. Wang, H. Wang, P. Ramazi, K. Nah, M. Lewis, A hypothesis-free bridging of disease dynamics and non-pharmaceutical policies, Bull. Math. Biol. 84 (2022) 5.

[50] X. Wang, H. Wang, P. Ramazi, K. Nah, M. Lewis, From policy to prediction: Forecasting COVID-19 dynamics under imperfect vaccination, Bull. Math. Biol. 84 (2022) 9.

[51] X. Wang, H. Wang, M.Y. Li, R_0 And sensitivity analysis of a predator–prey model with seasonality and maturation delay, Math. BioSci. 315 (2019) 108225.

[52] X. Wang, H. Wang, Discrete inverse method for extracting disease transmission rates from accessible infection data, SIAM J. Appl. Math. (Spec. Sect. Life Sci.) (2023) S336–S361.

[53] Baidu Migration Server, Available from: https://qianxi.baidu.com/2020/. (Accessed 17 March 2020).